$5

QEX

INCLUDING: COMMUNICATIONS QUARTERLY

Forum for Communications Experimenters

September/October 2003

Issue No. 220

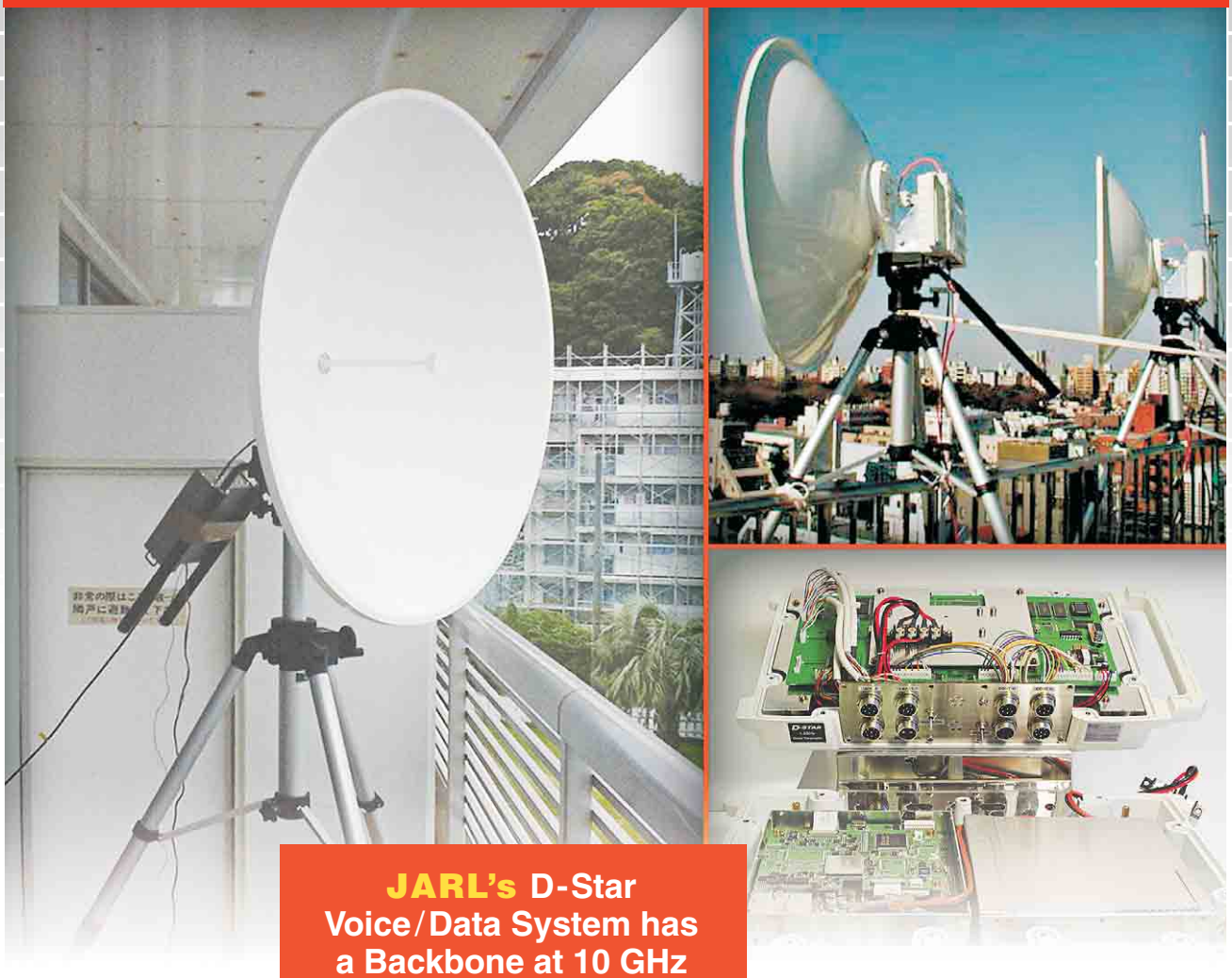

JARL's D-Star Voice/Data System has a Backbone at 10 GHz

ARRL The national association for AMATEUR RADIO

225 Main Street
Newington, CT USA 06111-1494

RSGB PRODUCTS

Imported by ARRL — from the Radio Society of Great Britain

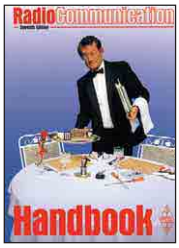

Radio Communication Handbook

One of the most comprehensive guides to the theory and practice of Amateur Radio communication. Find the latest technical innovations and techniques, from LF (including a new chapter for LowFERS!) to the GHz bands. For professionals and students alike. 820 pages.

ARRL Order No. 5234—**$53**

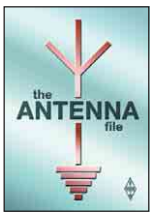

The Antenna File

The best work from the last ten years of RSGB's *RadCom* magazine. 50 HF antennas, 14 VHF/UHF/SHF, 3 on receiving, 6 articles on masts and supports, 9 on tuning and measuring, 4 on antenna construction, 5 on design and theory. Beams, wire antennas, verticals, loops, mobile whips and more. 288 pages.

ARRL Order No. 8558—**$34.95**

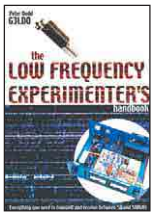

The Low Frequency Experimenter's Handbook

Invaluable reference and techniques for transmitting and receiving between 50 and 500 kHz. 112 pages.

ARRL Order No. RLFS—**$32**

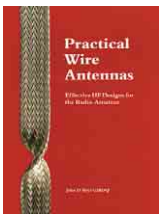

Practical Wire Antennas

The practical aspects of HF wire antennas: how the various types work, and how to buy or build one that's right for you. Marconis, Windoms, loops, dipoles and even underground antennas! The final chapter covers matching systems. 100 pages.

Order No. R878—**$17**

Antenna Toolkit 2

The complete solution for understanding and designing antennas. Book includes a powerful suite of antenna design software (CD-ROM requires *Windows*). Select antenna type and frequency for quick calculations. 256 pages.

ARRL Order No. 8547—**$43.95**

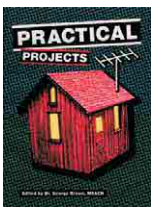

Practical Projects

Packed with 50 simple "weekend projects." A wide variety of radio and electronic ideas are covered, including an 80-m transceiver, antennas, ATUs and simple keyers.

ARRL Order No. 8971—**$24.95**

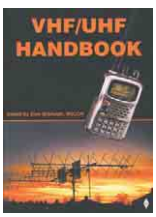

VHF/UHF Handbook

The theory and practice of VHF/UHF operating and transmission lines. Background on antennas, EMC, propagation, receivers and transmitters, and construction details for many projects. Plus, specialized modes such as data and TV. 317 pages.

ARRL Order No. 6559—**$35**

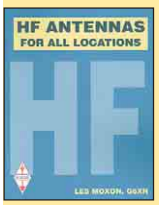

HF Antennas for All Locations

Design and construction details for hundreds of antennas, including some unusual designs. Don't let a lack of real estate keep you off the air! 322 pages.

ARRL Order No. 4300—**$34.95**

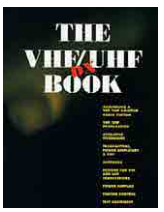

The VHF/UHF DX Book

Assemble a VHF/UHF station, and learn about VHF/UHF propagation, operating techniques, transmitters, power amplifiers and EMC. Includes designs for VHF and UHF transverters, power supplies, test equipment and much more. 448 pages.

Order No. 5668—**$35**

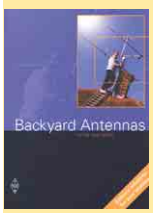

Backyard Antennas

With a variety of simple techniques, you can build high performance antennas. Create compact multi-band antennas, end-fed and center-fed antennas, rotary beams, loops, tuning units, VHF/UHF antennas, and more! 208 pages.

ARRL Order No. RBYA—**$32**

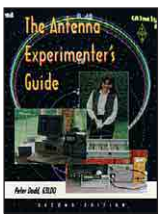

The Antenna Experimenter's Guide

Build and use simple RF equipment to measure antenna impedance, resonance and performance. General antenna construction methods, how to test theories, and using a computer to model antennas. 158 pages.

ARRL Order No. 6087—**$30**

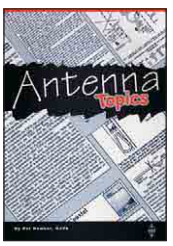

Antenna Topics

A goldmine of information and ideas! This book follows the writings of Pat Hawker, G3VA and his "Technical Topics" column, published in *Radcom*. Forty years of antenna design.

ARRL Order No. 8963—**$34.95**

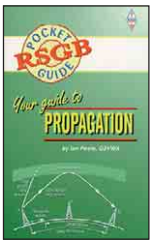

Your Guide to Propagation

This handy, easy-to-read guide takes the mystery out of radio wave propagation. It will benefit anyone who wants to understand how to get better results from their station.

ARRL Order No. 7296—**$17**

- **Guide to EMC** #7350 **$34**
- **IOTA Directory—11th Edition** #8745 **$16**
- **NEW! Microwave Projects** #9022 **$26**
- **NEW! QRP Basics** #9031 **$26**
- **Radio & Electronics Cookbook** #RREC **$28**
- **NEW! RSGB Prefix Guide —6th Edition** #9046 **$16**
- **Technical Compendium** #RTCP **$30**
- **Technical Topics Scrapbook**
  1985-1989 edition #RT85 **$18**
  1990-1994 edition #7423 **$25**
  1995-1999 edition #RT95 **$25**

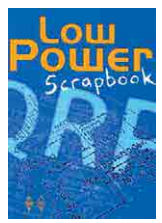

Low Power Scrapbook

Build it yourself! Low power transmitters, simple receivers, accessories, circuit and construction hints and antennas. Projects from the G-QRP Club's magazine Sprat. 320 pages.

ARRL Order No. LPSB—**$19.95**

HF Antenna Collection

Articles from RSGB's *RadCom* magazine. Single- and multi-element horizontal and vertical antennas, very small transmitting and receiving antennas, feeders, tuners and more. 240 pages.

ARRL Order No. 3770—**$34.95**

Order Toll-Free
1-888-277-5289
www.arrl.org/shop

Shipping: US orders add $5 for one item, plus $1 for each additional item ($10 max.). International orders add $2.00 to US rate ($12.00 max.). US orders shipped via UPS

ARRL The national association for AMATEUR RADIO

225 Main Street • Newington, CT 06111-1494 USA

tel: 860-594-0355 fax: 860-594-0303
e-mail: pubsales@arrl.org
www.arrl.org/

QEX

INCLUDING: COMMUNICATIONS QUARTERLY

QEX (ISSN: 0886-8093) is published bimonthly in January, March, May, July, September, and November by the American Radio Relay League, 225 Main Street, Newington CT 06111-1494. Periodicals postage paid at Hartford, CT and at additional mailing offices.

POSTMASTER: Send address changes to: QEX, 225 Main St, Newington, CT 06111-1494 Issue No 220

Offices

225 Main St, Newington, CT 06111-1494 USA
Telephone: 860-594-0200
Telex: 650215-5052 MCI
Fax: 860-594-0259 (24 hour direct line)
e-mail: **qex@arrl.org**

Subscription rate for 6 issues:

In the US: ARRL Member $24, nonmember $36;

US by First Class Mail: ARRL member $37, nonmember $49;

Elsewhere by Surface Mail (4-8 week delivery): ARRL member $31, nonmember $43;

Canada by Airmail: ARRL member $40, nonmember $52;

Elsewhere by Airmail: ARRL member $59, nonmember $71.

Members are asked to include their membership control number or a label from their *QST* when applying.

In order to ensure prompt delivery, we ask that you periodically check the address information on your mailing label. If you find any inaccuracies, please contact the Circulation Department immediately. Thank you for your assistance.

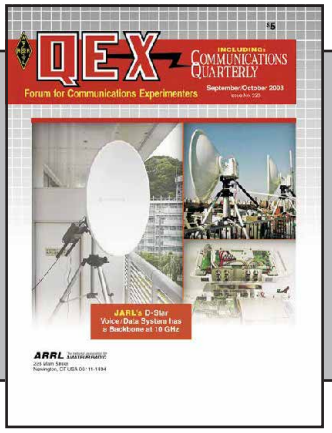

About the Cover

Dishes for D-Star's backbone at 10 GHz and an open receiver; Part 2 of KC7YXD's series begins on p 22.

Features

Columns

Sept/Oct 2003 *QEX* Advertising Index

THE AMERICAN RADIO RELAY LEAGUE

The American Radio Relay League, Inc, is a noncommercial association of radio amateurs, organized for the promotion of interests in Amateur Radio communication and experimentation, for the establishment of networks to provide communications in the event of disasters or other emergencies, for the advancement of radio art and of the public welfare, for the representation of the radio amateur in legislative matters, and for the maintenance of fraternalism and a high standard of conduct.

ARRL is an incorporated association without capital stock chartered under the laws of the state of Connecticut, and is an exempt organization under Section 501(c)(3) of the Internal Revenue Code of 1986. Its affairs are governed by a Board of Directors, whose voting members are elected every two years by the general membership. The officers are elected or appointed by the Directors. The League is noncommercial, and no one who could gain financially from the shaping of its affairs is eligible for membership on its Board.

"Of, by, and for the radio amateur, "ARRL numbers within its ranks the vast majority of active amateurs in the nation and has a proud history of achievement as the standard-bearer in amateur affairs.

A bona fide interest in Amateur Radio is the only essential qualification of membership; an Amateur Radio license is not a prerequisite, although full voting membership is granted only to licensed amateurs in the US.

Membership inquiries and general correspondence should be addressed to the administrative headquarters at 225 Main Street, Newington, CT 06111 USA.

Telephone: 860-594-0200
Telex: 650215-5052 MCI
MCIMAIL (electronic mail system) ID: 215-5052
FAX: 860-594-0259 (24-hour direct line)

Officers

President: JIM D. HAYNIE, W5JBP
3226 Newcastle Dr, Dallas, TX 75220-1640
Executive Vice President: DAVID SUMNER, K1ZZ

The purpose of *QEX* is to:
1) provide a medium for the exchange of ideas and information among Amateur Radio experimenters,
2) document advanced technical work in the Amateur Radio field, and
3) support efforts to advance the state of the Amateur Radio art.

All correspondence concerning *QEX* should be addressed to the American Radio Relay League, 225 Main Street, Newington, CT 06111 USA. Envelopes containing manuscripts and letters for publication in *QEX* should be marked Editor, *QEX*.

Both theoretical and practical technical articles are welcomed. Manuscripts should be submitted on IBM or Mac format 3.5-inch diskette in word-processor format, if possible. We can redraw any figures as long as their content is clear. Photos should be glossy, color or black-and-white prints of at least the size they are to appear in *QEX*. Further information for authors can be found on the Web at **www.arrl.org/qex/** or by e-mail to **qex@arrl.org**.

Any opinions expressed in *QEX* are those of the authors, not necessarily those of the Editor or the League. While we strive to ensure all material is technically correct, authors are expected to defend their own assertions. Products mentioned are included for your information only; no endorsement is implied. Readers are cautioned to verify the availability of products before sending money to vendors.

Empirical Outlook

Forward into the Past

During every project, it seems I spend half my time looking for the information I need. It continually amazes me how much of it is on the worldwide Web. Since the early '90s, that resource has expanded by many orders of magnitude. At least one search engine states that they are indexing over 3×10^9 sites now!

Electronic mail has put us in closer touch with each other than ever before. It is tempting to vow that it is the thing facilitating my editing job more than any other. Computers themselves have changed almost every facet of how we live and work, sometimes even without our awareness. What did we do before we had all this fancy stuff?

Well, we sharpened our pencils and sat down at the drafting board, slide rules at the ready. We wrote letters and placed a two- or three-cent stamp on the envelope. The only Spam we had to worry about was lunch. Each letter got a salutation, a formal or friendly closing and a handwritten signature. Did more thought go into those processes than into what we do now?

With a slide rule, you had to think about the number of significant figures in your result. Getting more than three or four took a lot of extra work. These days, it is a cinch to get 20 at the click of a button for every calculation.

All that brings me to recall what I wrote five years ago as I came to this fine magazine: Many small improvements eventually add to significance. Whether or not that has occurred, we propose to pay closer attention to the implied accuracy of data on our pages. It is no reference to any specific article or articles; but if I print that a power is +50.13 dBm, I should be ready to justify it with an extraordinary claim about my instrumentation. What do *you* think?

My comments about hydrogen fuel cells were not well received by one reader, who informed me about certain hydrocarbons you can put into a "stripper" to run the cell. As it turns out, the trouble is that it generates CO_2 or CO as well as H_2. The reactions are:

$$C_nH_{2n+2} + nH_2O \rightarrow nCO + (2n+1)H_2 \quad \text{(Eq 1)}$$

and

$$C_nH_{2n+2} + 2nH_2O \rightarrow nCO_2 + (3n+1)H_2 \quad \text{(Eq 2)}$$

Those reactions are endothermic but there is one that is exothermic:

$$C_nH_{2n+2} + (n/2)O_2 \rightarrow nCO + (n+1)H_2 \quad \text{(Eq 3)}$$

That is a reaction that takes oxygen out of the atmosphere and replaces it with CO!

David Keith of Carnegie Mellon University and Keith Farrell of UC Berkeley evidently agreed in a recent issue of *Science*. They wrote in a statement, "…we need to think carefully before we invest all this money [$1.5 billion of your taxes] and all this public effort in one area."

In This Issue

Frank Witt, AI1H, presents an analysis of his indirect method for measuring an antenna-matching-network loss with the MFJ-259B and similar instruments. Ralph Crumrine, NØKC, presents his method for stabilization of grounded-grid amplifiers. Ralph dissects his circuit and nails all the stray impedances in a thorough analysis.

John Gibbs, KC7YXD, continues his series on D-Star, the evolving JARL system for multimedia communications over microwave. You have read the introduction; now, dive into the details with John's second segment. Leif Åsbrink, SM5BSZ, brings us his Part 4. Among other things, Leif goes into how *Linrad* improves the communications equation through some rather sophisticated signal processing. He also addresses dynamic-range issues.

Randy Evans, KJ6PO, contributes a piece on crystal measurements and specifications. He shows how to build ladder filters using your new knowledge. It makes one want to get to the network analyzer! Chris Trask, N7ZWY, concludes his two-part series on active loop antennas with a discussion of the active part: low-noise preamplifier design. Chris relates "augmented linearization," a new and apparently promising technique.

Bob Kopski, K3NHI, presents a modification for his "Advanced VHF Wattmeter" from the May/June 2002 *QEX*. In RF, Zack Lau, W1VT, describes design procedures for multiconversion UHF and microwave transverters.—*73, Doug Smith, KF6DX;* **kf6dx@arrl.org.** □□

Evaluation of Antenna Tuners and Baluns–An Update

How to have high confidence in your measurements.

By Frank Witt, AI1H

In a two-part article in April and May 1995 *QST*,[1] I described a simple method for evaluating antenna tuners. Application to the evaluation of baluns was described the following year.[2] The method involves a resistance-load box and a low-power analyzer, and it works equally well for evaluating the performance of equipment with balanced as well as unbalanced loads. A simple extension was described that allows the equipment evaluation with complex-impedance loads as well.

Amateurs around the world have since used the method, which has been dubbed the "indirect method," the "AI1H method" and the "Witt method." It provides—at moderate cost—a simple means for evaluating antenna tuners and baluns. The method was used to evaluate four antenna tuners for a Product Review in March 1997 *QST*.[3]

Most hams had been ignorant about the performance of their antenna tuners. They only knew the circuits were lossy when they got very hot or when a component failed (if running high power). QRPers had no way of knowing whether or not their antenna tuners handicapped them. Some manufacturers' claims for their antenna tuners were (and still are) unreliable, and that is being kind. Much light was shed on this matter by the programs written by Dean Straw, N6BV, *TLA* and its successor *TLW*,[4] which compute antenna-tuner performance. The indirect method complements this analysis tool by providing a very accessible measurement tool.

From the source in Note 1 (May 1995, page 37): "This new application of low-power SWR testers is a demanding one, since the accuracy must be excellent for valid results. Perhaps we will see even more accurate SWR testers in the future, and maybe antenna tuner manufacturers will be inspired to improve their designs." That day has arrived. Improved SWR analyzers and antenna tuners[5] are now available.

The purpose of this article is to show how measurement instruments that are now available provide improved accuracy for the simple characterization of antenna tuners and baluns. It summarizes a better understanding of any inherent limitations of the evaluation method. Finally, it provides a comparison with other measurement methods.

[1]Notes appear on page 14.

ARRL Technical Advisor
41 Glenwood Rd
Andover, MA 01810-6250
ai1h@arrl.net

SWR, Reflection-Coefficient Magnitude and Return Loss

Before getting into the subject of improving the measurement accuracy, it is appropriate to discuss the quantities to be measured. The relationship between reflection coefficient, ρ, the impedance of the device to be tested, Z_L, and the reference resistance of the analyzer, R_{REF}, is as follows:

$$\rho = \frac{Z_L - R_{REF}}{Z_L + R_{REF}} \quad \text{(Eq 1)}$$

The value of R_{REF} for the analyzers we consider here is around 50 Ω. For our purposes in this application, *SWR*, reflection-coefficient magnitude ($|\rho|$) and return loss (*RL*, in decibels) are equivalent in the sense that we can measure any of them and find the antenna-tuner loss. The relationships between them are:

$$SWR = \frac{1+|\rho|}{1-|\rho|} \quad \text{(Eq 2)}$$

$$|\rho| = \frac{SWR-1}{SWR+1} \quad \text{(Eq 3)}$$

$$RL = -20\log|\rho| \quad \text{(Eq 4)}$$

For a discussion of the nature of *SWR*, $|\rho|$ and *return loss* and how *SWR* is sloppily used, see my discussion of "SWR Bandwidth."[6]

I've included these relations because some instruments measure $|\rho|$ more accurately than *SWR*, whereas others might measure return loss more accurately. So, to achieve the highest accuracy, the correct parameter must be used.

The Indirect Method

The indirect method involves connecting a resistance load box with switchable resistors to the output terminals of the antenna tuner. The load box has been named the "geometric resistance box," because the values of resistance follow a geometric progression. For each load, the resistances of the adjacent loads are twice and half the load resistance.

The input of the antenna tuner is connected to a meter that measures *SWR*, reflection coefficient magnitude, $|\rho|$, or return loss, *RL*, in decibels. The measurement is carried out as follows:

1. Set the geometric resistance box to the desired load resistance, R_L.
2. Adjust the antenna tuner so that *SWR* = 1:1, $|\rho| = 0$ or *RL* is maximized.
3. Switch to the next lower load resistance, $R_L/2$, and record the *SWR*, S_1, or $|\rho_1|$ or RL_1.
4. Switch to the next higher load resistance, $2R_L$, and record the *SWR*, S_2, or $|\rho_2|$ or RL_2.
5. Calculate the antenna-tuner loss, *L*, in decibels and percentage of power lost, P_{LOST}, from:

$$L = 5\log\frac{(S_1+1)(S_2+1)}{9(S_1-1)(S_2-1)} = -5\log\left(9|\rho_1\|\rho_2|\right) = \frac{RL_1+RL_2}{4} - 4.77\ \text{dB} \quad \text{(Eq 5)}$$

$$\begin{aligned} P_{LOST} &= 100\left(1-10^{\frac{-L}{10}}\right) \\ &= 100\left(1-3\sqrt{\frac{(S_1-1)(S_2-1)}{(S_1+1)(S_2+1)}}\right) \\ &= 100\left(1-3\sqrt{|\rho_1\|\rho_2|}\right) \\ &= 100\left(1-3\cdot 10^{-\frac{RL_1+RL_2}{40}}\right) \end{aligned} \quad \text{(Eq 6)}$$

These measurements are carried out the same way for unbalanced and balanced loads.

Antenna-Tuner Loss in Decibels versus Percentage of Power Lost

The loss of an antenna tuner is presented above in two ways: as power loss, *L*, in decibels, and percentage of power lost, P_{LOST}. P_{LOST} has an advantage in the antenna-tuner loss application. We all know approximately how much power our transmitter delivers when it is feeding a 50-Ω

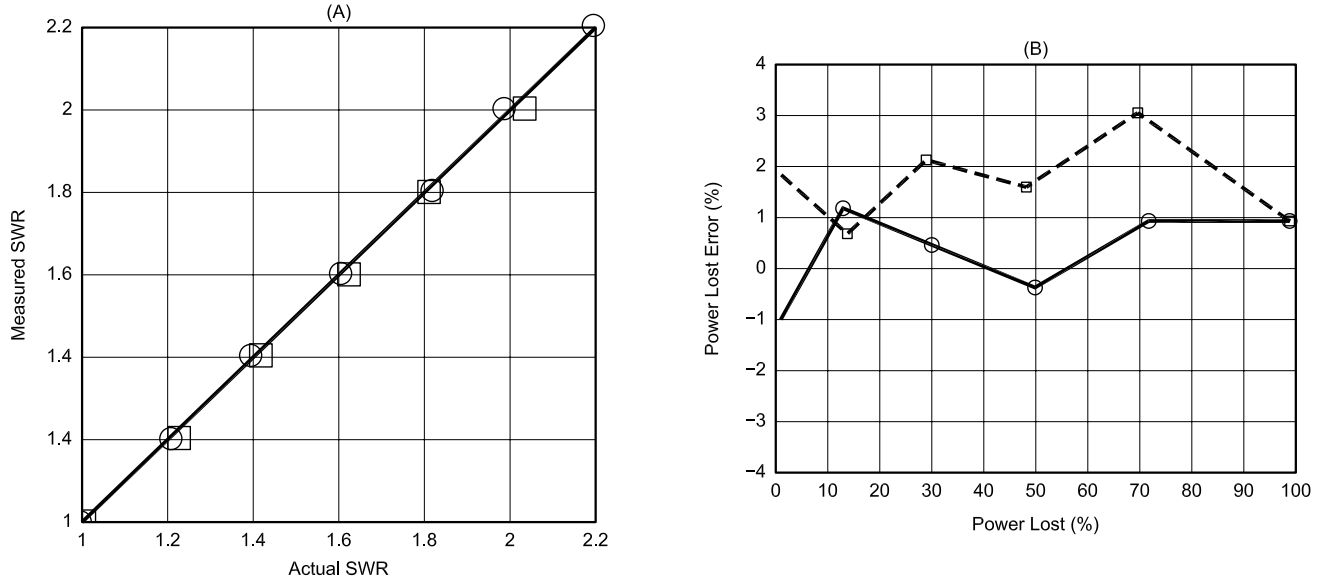

Fig 1—In A: Measured *SWR* for resistive loads using a calibrated MFJ-259B. The circles are for R_L > 50 Ω and the squares are for R_L < 50 Ω. In B: Error in percentage of power lost. The solid trace is for R_L > 50 Ω and the dashed trace is for R_L < 50 Ω. These measurements apply over the entire HF band.

load. What we want to know is how much of that power is being absorbed or radiated by the antenna tuner and not reaching the antenna system. Percentage of power lost tells us this directly. For example, a kilowatt transmitter feeding an antenna tuner with a 20% of power lost figure means that 200 W are lost in the antenna tuner. Most of that power is usually heating components in the tuner.

On the other hand, if the loss is expressed in decibels, we must make a mental translation to percentage of power lost in order to know what is happening. Some familiar decibel-loss quantities are 0, 1, 3 and 10 dB, which equate to 0%, 21%, 50% and 90% of the power lost in the antenna tuner, respectively. Other quantities of decibel loss are far less familiar to most of us. So, the preferred loss-characterization method is percentage of power lost. It is interesting to notice from Eq 6 that percentage of power lost is linearly related to the geometric mean of the reflection-coefficient magnitude readings.

Accuracy of the Analyzers

MFJ-259B

When I first discovered the indirect method, I used low-power SWR testers. These were the Autek Research Model RA1 and the MFJ Model MFJ-259. These units displayed *SWR*, so the *SWR* reading was used for loss calculations using Eqs 5 and 6. These instruments do not display $|\rho|$, although it is the basic quantity measured. *SWR* is calculated internally from the value of $|\rho|$. This calculation is a source of error. Fortunately, some newer instruments

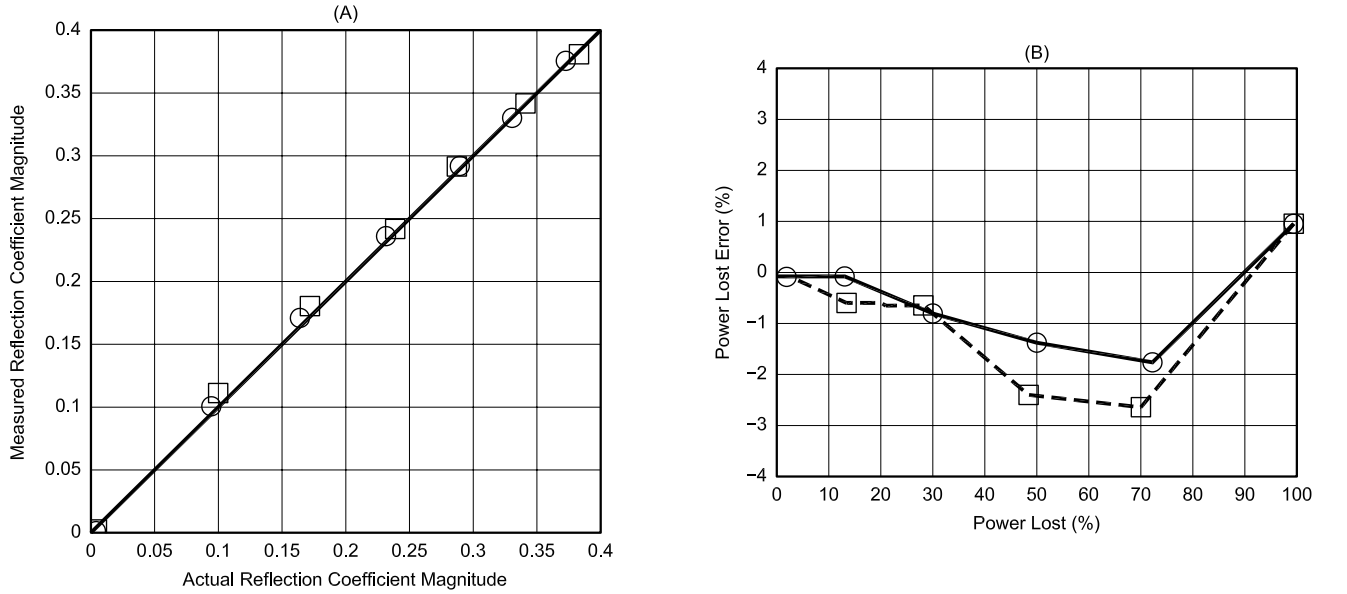

Fig 2 — In A: Measured reflection-coefficient magnitude for resistive loads using a calibrated MFJ-259B. The circles are for R_L > 50 Ω and the squares are for R_L < 50 Ω. In B: Error in percentage of power lost. The solid trace is for R_L > 50 Ω and the dashed trace is for R_L < 50 Ω. These measurements apply over the entire HF band.

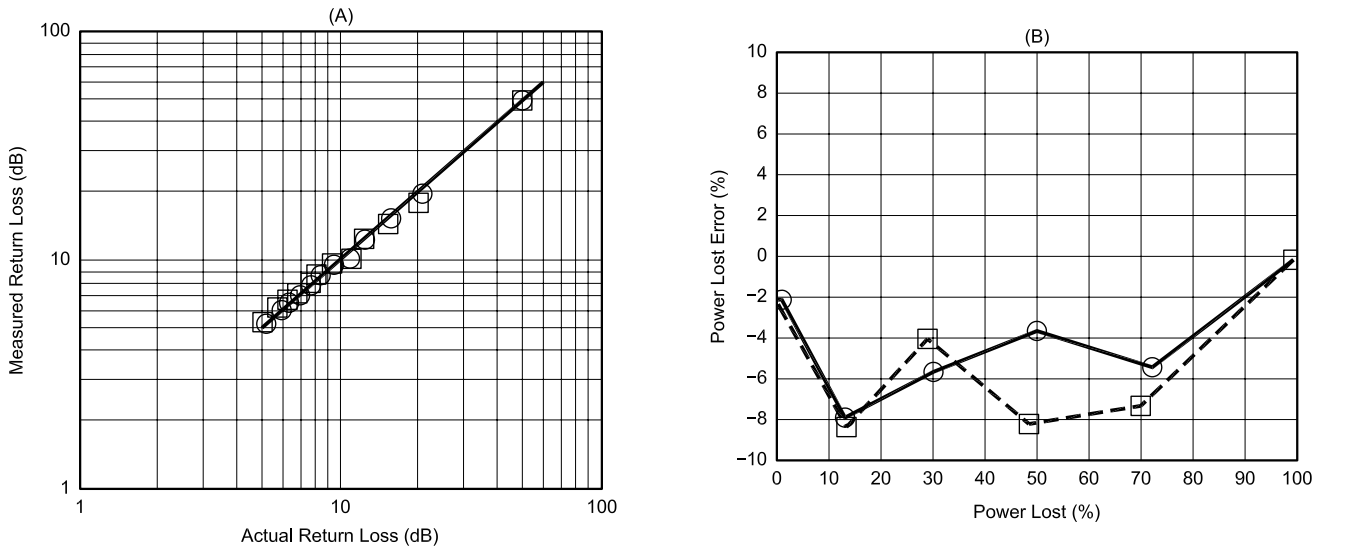

Fig 3 — In A: Measured *return loss* for resistive loads using a calibrated MFJ-259B. The circles are for R_L > 50 Ω and the squares are for R_L < 50 Ω. In B: Error in percentage of power lost. The solid trace is for R_L > 50 Ω and the dashed trace is for R_L < 50 Ω. These measurements apply over the entire HF band.

display $|\rho|$ and *return loss* directly. Further, *SWR*, $|\rho|$ and *return loss* are displayed on a LCD, which is easier to read reliably than an analog meter. An instrument for measuring the loss of antenna tuners is the MFJ-259B, the successor to the MFJ-259. Some features of other candidates for this application are discussed later in the article, but here we will primarily answer the question of whether or not the MFJ-259B will perform adequately in this application.

Although the MFJ-259B impedance analyzer measures many properties of the unknown connected to its terminals, we will focus here on the antenna-tuner evaluation application. It fared well compared with similar units in a recent review.[7] As indicated above, antenna-tuner loss can be determined from *SWR*, $|\rho|$ or *return loss*. The accuracy of the MFJ-259B can be improved through a calibration procedure, which is described below. *SWR*, $|\rho|$ and *return loss* were measured. The date on the unit tested is 1998 and the software version is 2.02. The measurement frequency was 1.8 MHz and the load resistors were 1/4-W, 1% metal-film resistors with very short leads. These resistors are the "standard" for the evaluation of the analyzer. Tests confirmed that the 1.8-MHz data applies over the entire HF band. The dc values for the load resistors were measured with a digital multimeter. I have made measurements using complex-impedance loads that show similar accuracy. This is important, because the impedances seen by the MFJ-259B in this application are complex.

The results are shown in Figs 1, 2 and 3 for *SWR*, $|\rho|$ and *return loss*, respectively.[8] Notice that separate data points and traces are obtained for load resistances above and below R_{REF}. Although the "measured versus actual" plots are interesting, the useful information is contained in the graphs. They show the error in percentage of power lost versus the actual percentage of power lost. These graphs use Eq 6 to find the percentage of power lost, but make the assumption that $|\rho_1|$ and $|\rho_2|$ are the same. The "true" percentage of power lost is assumed to be that calculated from the measured dc resistance values. The error is found by subtracting this true percentage of power lost from that calculated using measurements from the MFJ-259B. For both *SWR* and $|\rho|$, the errors are less than about 3% for percentage of power losses from 0 to 100%. The error for *return loss* is around 8%, however. These differences arise from deficiencies in the algorithm that converts the basic $|\rho|$ measurement into *return loss* and the poor resolution of return-loss measurements in part of the desired region, which is discussed later.

For all calculations, it was assumed that the reference resistance, R_{REF}, for this particular MFJ-259B is 50.1 Ω. This is the value of R_{REF} that gives the lowest mean-square error (0.77%) for percentage of power losses from 0 to 100%. R_{REF} is nominally 50 Ω, but this method of finding the actual value provides a better evaluation of the MFJ-259B.

Measurement Resolution

A measuring instrument is limited by its resolution. Even if the accuracy is perfect, the ability to display the result is controlled by its resolution. The display on the LCD for each parameter measured limits its resolution.

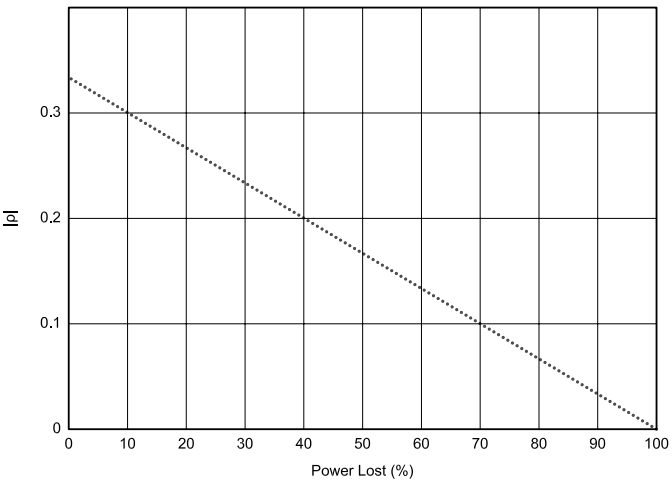

Fig 4—Values of reflection-coefficient magnitude that can be displayed by the MFJ-259B. This results in a resolution capability for percentage of power lost of 0.75%. Notice the linear relationship between percentage of power lost and |ρ|.

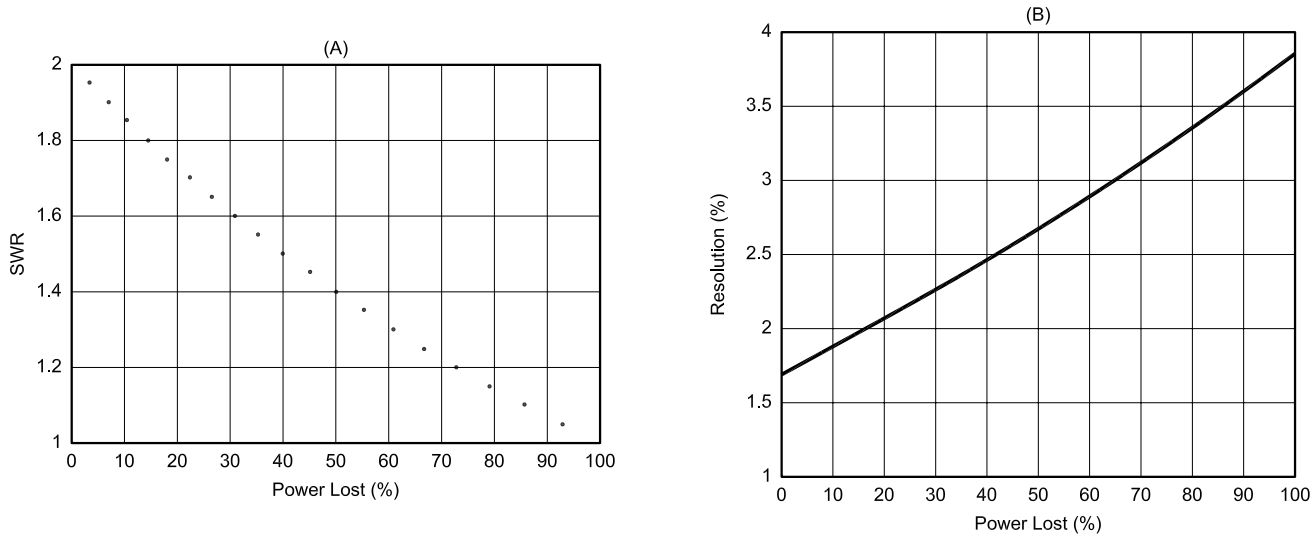

Fig 5—Resolution of the MFJ-259B for *SWR*. In A: The values of *SWR* that may be displayed. In B: The resolution over the 0 to 100% percentage of power lost range.

For the MFJ-259B, *SWR*, $|\rho|$, and *return loss* results are two-digit displays, so only a limited number of data values may be displayed over the range of percentage of power lost from 0 to 100%.

For the purpose of this analysis, assume $|\rho_1| = |\rho_2| = |\rho|$ (and $S_1 = S_2 = SWR$ and $RL_1 = RL_2 = RL$). Reflection coefficient magnitude, $|\rho|$, values range from 0 to 0.33. For example, two adjacent values of $|\rho|$ are 0.11 and 0.12, which correspond to percentage of power losses of 67% and 64%, respectively, from Eq 6. If the displayed $|\rho|$ value bounces between these two values, $|\rho|$ is interpreted as the average of these values, or *0.115* and the percentage of power lost as *65.5%*. All interpolated values are italicized. Thus the resolution in this region of the range of $|\rho|$ is 0.75% [(67 – *65.5*)/2 or (*65.5* – 64)/2)]. In fact, since there is a linear relationship between percentage of power lost and $|\rho|$, the resolution is a constant 0.75% over the entire 0 to 100% percentage of power lost range. Fig 4 shows all the $|\rho|$ data points that can be displayed by the MFJ-259B over the range of interest.

What about *SWR* and *return loss*? Figs 5 and 6 show the resolution capability for those parameters. The *SWR* resolution (Fig 5B) of the MFJ-259B varies from 1.7 to 3.8%. The *return loss* resolution (Fig 6B) has a jagged shape because displayed *return loss* values in decibels are: 9.6, *9.65*, 9.7, . . . *9.95*, 10, *10.5*, 11, *11.5* . . . 30, *30.5*, 31, *31.5*, 32, *33*, 34 . . . *37*, 38, *40*, 42, *45*, 48

The sharp deterioration in resolution occurs at *RL* = 10 dB because only two digits are used to display the *return loss* values. The resolution is as high as 2.6% around *RL* = 10 dB and the percentage of power lost is 10%.

For the MFJ-259B, its resolution (0.75%) makes $|\rho|$ the clear winner for measuring antenna-tuner loss, especially in light of the very good accuracy (3%) shown in Fig 2. However, there are two regions in the measurement range of $|\rho| = 0$ to 0.33 where improved resolution is very desirable. These are the regions at the ends of this range. The antenna tuner is considered tuned when $|\rho| = 0$. The focus of the calibration procedure (described in the next section) is around $|\rho| = 0.33$. A close look at Fig 6B reveals that *return loss* resolution is best for percentage of power lost regions near 0% and near 100%. We will make use of this fact in calibrating the MFJ-259B and in tuning the antenna tuner during the evaluation process.

We can take advantage of the higher internal resolution in the region around $|\rho| = 0$ by just maximizing *return loss* when we are striving to achieve the best tuner settings. In order to take advantage of the better resolution around $|\rho| = 1/3$, we can use Table 1, which shows the relationship between the displayed, interpolated and actual values of *return loss* and reflection coefficient magnitude. This way, we can pick up almost another decimal digit of resolution of $|\rho|$ when the unit is calibrated. The actual values of $|\rho|$ were obtained by evenly distributing values between the displayed values.

Notice that the displayed *return loss* reading that comes closest to $|\rho| = 1/3$ is 9.4 dB, not the actual value of 9.54 dB. Also shown in Table 1 is the value of *return loss* corresponding to the actual value of $|\rho|$, which points up the inaccuracy of the return-loss algorithm

Table 1—Relationship between Return Loss (*RL*) and Reflection-Coefficient Magnitude, $|\rho|$

Interpolated values are in italics

Displayed Values		***Actual Values***	
RL (dB)	*$\|\rho\|$*	*$\|\rho\|$*	*RL (dB)*
9.05	*0.345*	0.345	9.24
9.1	0.34	0.3433	9.29
9.15	0.34	0.3417	9.33
9.2	0.34	0.340	9.37
9.25	0.34	0.3383	9.41
9.3	0.34	0.3367	9.46
9.35	*0.335*	0.335	9.50
9.4	**0.33**	**0.3325**	**9.56**
9.45	0.33	0.330	9.63
9.5	0.33	0.3275	9.70
9.55	*0.325*	0.325	9.76
9.6	0.32	0.3233	9.81
9.65	0.32	0.3217	9.85
9.7	0.32	0.320	9.90
9.75	0.32	0.3183	9.94

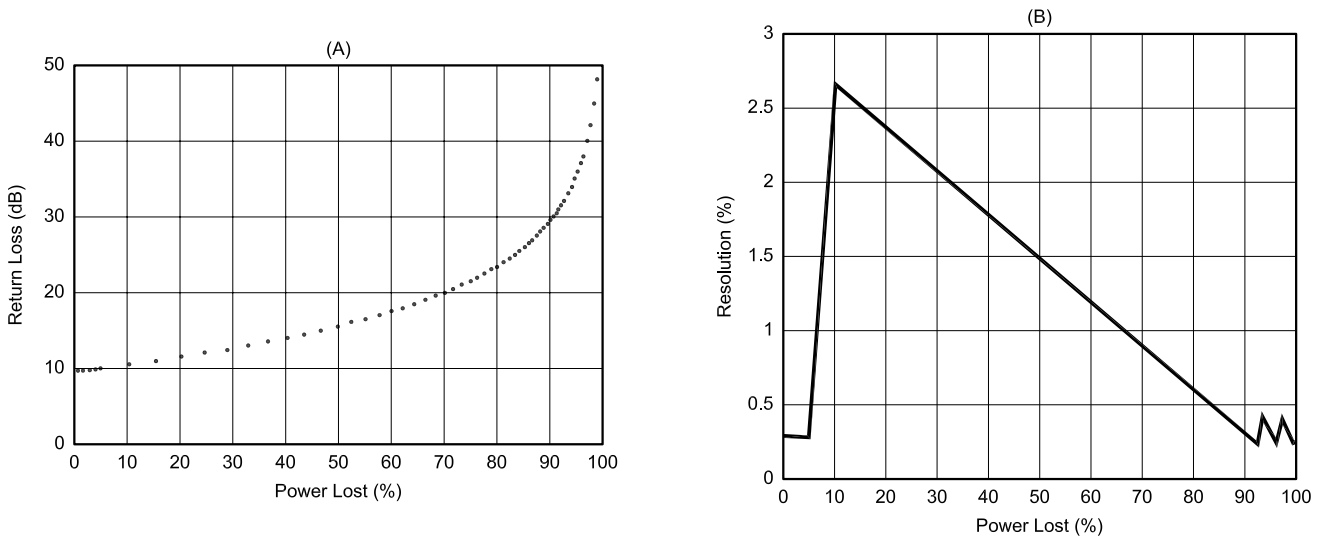

Fig 6—Resolution of the MFJ-259B for *return loss*. In A: The values of *return loss* that may be displayed. In B: The resolution over the 0 to 100% percentage of power lost range.

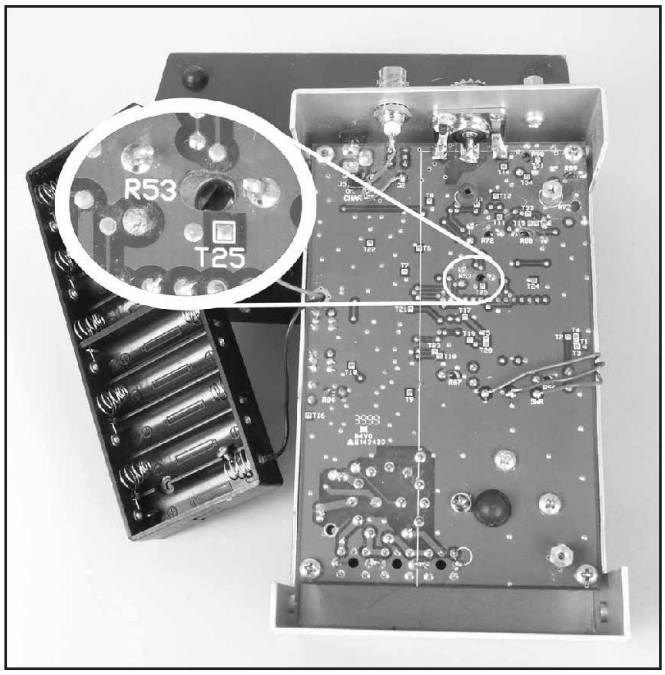

Fig 7—Photograph of MFJ-259B. Notice the location of R53, which is used to calibrate the unit.

in the MFJ-259B software.

Care must be taken in the use of Table 1 for other vintages of MFJ-259B software, if they exist, since the values may be different. This is easy to check by confirming several readings of *return loss* and $|\rho|$ in the region around $|\rho| = 0.33$.

MFJ-259 Calibration Procedure

I do not recommend you try this calibration process unless you have a good reason to do so and unless you are confident that you can do it. If the unit is in warranty, you may void the warranty. There are risks. You could inadvertently turn the wrong adjustment screw and really mess up the instrument. Wires or circuit-board pads could be brought into contact and damage to the unit could result.

I have found that MFJ-259B impedance analyzers as delivered (a sample of two) have adequate accuracy for getting a good idea of how well a particular antenna tuner performs. However, if you want to squeeze the most out of your analyzer, calibration is possible and can be helpful for evaluating an antenna tuner. The effectiveness of the calibration process is seen in Fig 2B, where the percentage-of-power-lost error is less than 1% for power losses up to 30%. As will be seen, the calibration is made in this region.

The basic idea is to connect known load resistances to the unit and then adjust the proper potentiometer (and there are several, so take care) so that the appropriate reading is correct. For our purposes, we want the LCD reading of *SWR*, $|\rho|$ and *return loss* to be correct. Since $|\rho|$ is the fundamental measurement from which SWR and return loss are calculated, calibration involves getting the $|\rho|$ reading (which is displayed only on the LCD and not on an analog meter) to be as close to the correct value as possible. Adjustments to calibrate other quantities such as LCD impedance, analog-meter SWR and analog-meter impedance are also exposed when the $|\rho|$ calibration control is made available for adjustment. These other adjustments need not be touched to calibrate the instrument for antenna tuner and balun evaluation.

You will need two resistive loads, 25 Ω and 100 Ω, for the calibration. These should be 1%-tolerance resistors with minimal parasitic inductance and capacitance, hence very short leads. Ideally, they should be mounted *inside* a PL-259 connector, but this is not essential. Quarter-watt, metal-film resistors are ideal because they fit inside the center conductor tube of the connector. If you have an AI1H geometric resistance box, the 25-Ω and 100-Ω settings provide adequate test loads, since the test frequency is low, 1.8 MHz. These values of resistance, 25 Ω and 100 Ω, should give a $|\rho| \approx 1/3 = 0.\overline{333}$. From Table 1, the closest we can come to this condition is for the *return loss* reading to equal 9.4 dB. Notice the row shown in bold type.

I recommend that you power the MFJ-259B from ac if you want the calibration to hold. This eliminates possible changes in calibration as the batteries age. Perform the following pretest before removing the back cover of the unit.

1. Turn on the MFJ-259B, enter the "Advanced" mode by simultaneously pushing the **GATE** and **MODE** buttons, and set the unit to display "Return Loss & Reflection Coefficient" by depressing only the **MODE** button once. This provides a simultaneous display of frequency, *SWR*, $|\rho|$ and *return loss*.
2. Set the measurement frequency to 1.8 MHz.
3. Connect the 25-Ω load. Wait one hour. This assures thermal stabilization of the unit.
4. Switch between the 25-Ω and 100-Ω loads and observe the values of $|\rho|$. If they equal 0.33, 0.335 or 0.34 for both loads, adjustment is not necessary. If not, follow the procedure below to achieve this condition.

The calibration procedure is as follows:

1. Remove the back cover by removing eight screws on the sides of the unit. Remove the batteries. Loosen the battery holder by removing two screws. Fig 7 shows an MFJ-259B with the back cover and battery holder removed.
2. Place the battery holder to the side without disconnecting it. Be careful to not let any of the exposed contacts touch the case or any metal parts of the MFJ-259B. You may want to wrap it in a paper towel to help avoid problems.
3. Referring to Fig 7, adjust R53 so that for both the

25- and 100-Ω loads the return loss = 9.4 dB. This may require several iterations. I recommend using a plastic alignment screwdriver, however, this is optional. If you cannot achieve *RL* = 9.4 dB with both loads, adjust R53 so that both readings are as close to 9.4 dB as possible.[9]

Other Analyzers

The major effort in improving the accuracy of measurements for antenna-tuner and balun evaluation was focused on the MFJ-259B. This emphasis was based on the potential shown by that unit in a comparison of MFJ, AEA and Autek Research analyzers. To be fair, no effort was made to tweak the AEA and Autek Research units to optimize their performance for this application. Some general observations follow.

The measuring instrument used for the measurements back in 1995, when the indirect measurement technique was discovered, was the Autek Research Model RF1 RF Analyst. This instrument displays SWR with two-digit resolution. The unit evaluated (no serial number or firmware version) was "as purchased" and not calibrated for this application. It was powered by a fresh 9 V battery. The accuracy in measuring percentage of power lost was better than 2% for $R_L > 50\ \Omega$; however, for $R_L < 50\ \Omega$ this error was as high as 15%. The two-digit LCD SWR display prevents precise tuning of the antenna tuner, which leads to a tuning error that will be discussed later.

The Model VF1 RX Analyst is a more recent offering by Autek Research. The unit evaluated (no serial number or firmware version) was tested "as purchased." No calibration was performed. A fresh 9 V battery was installed. For this application, this instrument displays only SWR on a three-digit LCD display. The accuracy in measuring percentage of power lost was better than 5%.

The AEA Model CIA-HF Complex Impedance Analyzer is another candidate for making loss measurements on antenna tuners and baluns. One unit (serial #0136, Firmware Revision 1.4) was evaluated. The unit was evaluated "as delivered" and was not calibrated. It was powered by an external power supply. The analyzer displays *SWR* and *return loss*, but not reflection coefficient magnitude. All results are displayed on an LCD. For most values of *SWR* and *return loss*, three significant figures are shown. For loads > 50 Ω, the error in percentage power loss was 4% or better for both *SWR* and *return loss*; however, for loads < 50 Ω, the error was as much as 10%, again for both *SWR* and *return loss*. It is possible that calibration would improve this performance. The resolution was good (three digits), but the instability of the readings made it impossible to capitalize on this feature.

It is clear from the above tests that the MFJ-259B performed better than the Autek Research and AEA products for this application. I calibrated only the MFJ-259B for these tests. It should not be inferred that the MFJ-259B is to be preferred over the other units for general analyzer applications. More recent units might perform better. These devices will improve with time because radio amateurs are becoming more discriminating and aware of their capabilities. Further, the imaginative ham spirit leads us to applications that are more demanding of these analyzers. Fortunately, such improved capabilities continue to be made available at a reasonable cost.

Other instruments of laboratory grade could be used for this application. The "Cadillac" would be an HP (now Agilent Technologies) Network Analyzer. Also the HP 415-series Standing Wave Indicator with an amplitude-modulated signal generator, a return-loss bridge and a square-law detector would do a good job. The HP 415-series is a selective voltmeter (tuned to 1 kHz) calibrated in SWR units, which assumes that the detector has a square-law behavior. I suspect that each of these will beat the MFJ-259B in precision and resolution, although this has not been confirmed.

Other Sources of Error

Limits of Accuracy of the Indirect Method

Every method for measuring losses in antenna tuners is subject to multiple sources of error. An analysis of error sources for the indirect method is described below. Similar analyses should be performed for competing methods.

Eqs 5 and 6 for calculating the loss in decibels and percentage of power lost are approximations. As explained in Note 1 (*QST*, Apr 1995, p 33): "Through computer simulation of many antenna tuners using a wide range of loads, I have found that this method of estimating loss is accurate to within a few tenths of a decibel, assuming that the SWR tester is perfect." In spite of this, there was lingering healthy skepticism about the accuracy of the indirect method, largely because its validity is not obvious.

I have since been sent independent mathematical analyses from Chris Kirk, NV1E, and Kevin Schmidt, W9CF.[10] They both calculated the error inherent in the use of the indirect method by using the scattering matrix formulation. They determined bounds on the error, that is, the worst-case error. For a given situation, the worst-case error may not occur; but the error caused by the use of the indirect method will never be worse than that value. We will call this source of error the "method error."

The antenna tuner will in general be matched at one port: the input port. At the input port, the tuner is adjusted so that $Z_{in} = R_{REF}$, which is nominally 50 Ω. The output impedance, Z_{OUT}, will be the complex conjugate of Z_L, the load impedance, only if the tuner is loss-less, but we are not measuring loss-less tuners. The source of the error in the indirect method is this mismatch at the output port. How large is this error?

Assuming that the antenna tuner is perfectly tuned, the loads are precise and the *SWR*, $|\rho|$ or *return loss* measurements are perfect, the worst-case method error bounds in decibels and in percentage of power lost are calculated in Eq 7 and 8 below.

Fig 8 shows the worst-case error expressed in decibels as well as percentage plotted against the actual percentage of power lost. Notice that the error in decibels is

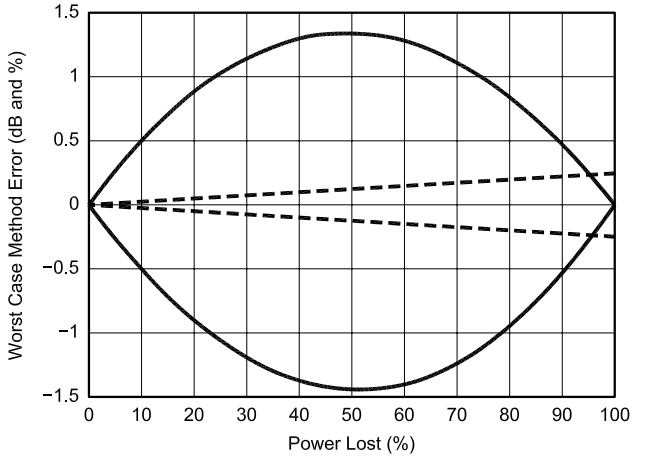

Fig 8—Worst-case method errors for the indirect method. The dashed curves show the bounds for error expressed in decibels. The more useful solid curves define the error bounds in percentage of power lost units.

between –0.26 dB and +0.23 dB when the antenna tuner is absorbing most of the transmitter power. In percentage of power lost, the highest error is between –1.45% and +1.33%, and this occurs when the tuner is absorbing about half of the transmitted power. This means that if perfect instrumentation and measurement skill were applied using the indirect method on a tuner with 50% actual power loss, the loss measurement would be between 48.5% and 51.3%. The worst-case percentage-of-power-lost error goes to zero as the tuner loss goes to either 0 or 100%. *The conclusion is that for all practical purposes, the method error caused by using the indirect method is negligible.*

Why is the method error so low? The error is low because of the use of the geometric averaging of $|\rho_1|$ (halving R_L) and $|\rho_2|$ (doubling R_L). See Eq 6. The process leads to a cancellation of the large first-order error terms, and only a much smaller second-order error term remains. If the loss were calculated by only halving R_L, the calculated value would always be too high and could be off by as much as 10.8%. Doubling R_L yields too little loss, and the value could be off by up to 16%.

One can think of the antenna tuner as an impedance-transforming device. When the loss is low, the impedance ratio at the output will be seen virtually unchanged at the input of the tuner. Hence the error is near zero for low-loss tuners. When the tuner loss is very high, the 50-Ω input impedance of the tuned tuner is mostly made up of lossy elements *within* the tuner. Hence, changes in the load impedance do not much influence the input impedance, and the error is necessarily very low.

Incidentally, Kirk's and Schmidt's analyses showed that with one additional measurement, the error may be found, and hence subtracted. Of course, with such a low worst-case method error, such a correction is unnecessary. Other sources of error will be discussed below.

Initial Setting of Antenna Tuner

When testing an antenna tuner using the indirect method, Step 2 says "Adjust the antenna tuner so that *SWR* = 1:1, $|\rho|$ = 0 or *RL* is maximized." It is not necessary that R_{REF} = 50 Ω exactly, since the tuner behavior will be essentially the same if it is tuned so its input impedance is within a few ohms of that figure. It is important, however, that the input impedance of the tuner be adjusted as close to the analyzer's reference resistance, R_{REF}, (usually near 50 Ω) as possible to get the most accurate results.

We will call the error introduced by imperfect tuning the *mistuning* error. From Kevin Schmidt's S-parameter analysis, the mistuning error bounds in decibels and in percentage of power lost are estimated in Eq 9 below.

The error in percentage of power lost introduced by imperfect tuning is shown in Fig 9. Notice that the effect of mistuning worsens as tuner loss increases.

With the MFJ-259B, what displayed value should be used, *SWR*, $|\rho|$ or *return loss*? All three parameters were examined in the vicinity of the desired tuned condition. *Return loss* is the most sensitive indicator of the "tuned" condition. The *return loss* reading has to drop from 48 dB to 38 dB before $|\rho|$ changes (from 0 to 0.01) and all the way to 25 dB before the SWR changes (from 1.0 to 1.1). This is a direct result of the two-decimal-digit display limitation for *SWR*, $|\rho|$ and *return loss*. The *return loss* display has more resolution for this measurement and may be used. It turns out, however, that $|\rho|$ has enough resolution to be used as well. For the MFJ-259B, SWR should not be used for this appli-

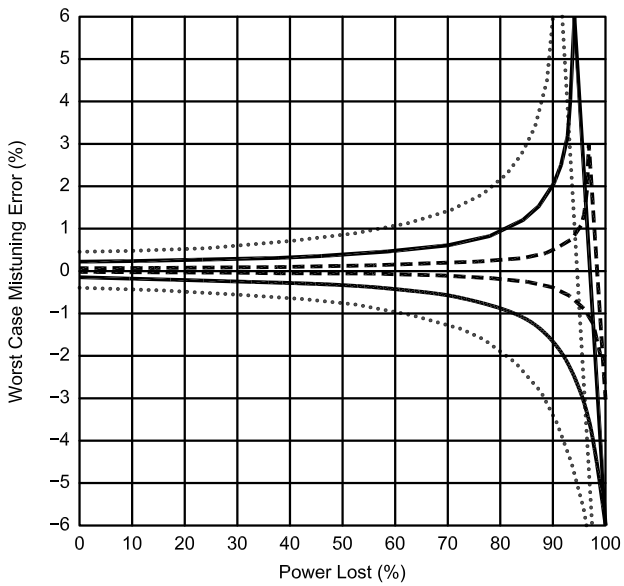

Fig 9—Worst-case error in percentage of power lost introduced by imperfect tuning. The dashed, solid and dotted lines show the error bounds for $|\rho_{in}|$ = 0.01, 0.02 and 0.03, respectively.

$$5\log\left(\frac{8+10^{\frac{-L_{ACTUAL}}{10}}}{9}\right) \le MethErrdB \le 5\log\left(\frac{10-10^{\frac{-L_{ACTUAL}}{10}}}{9}\right) \quad \text{(Eq 7)}$$

$$\left(100-P_{LOST}\right)\left[1-\left(1-\frac{P_{LOST}}{900}\right)^{-\frac{1}{2}}\right] \le MethErr\% \le \left(100-P_{LOST}\right)\left[1-\left(1+\frac{P_{LOST}}{900}\right)^{-\frac{1}{2}}\right] \quad \text{(Eq 8)}$$

where
L_{ACTUAL} = the actual antenna tuner loss in decibels,
P_{LOST} = percentage of power lost, and
MethErrdB and *MethErr%* = the method error in decibels and percentage, respectively.

cation because of the poor SWR resolution.

The best technique is to adjust the antenna tuner to achieve an SWR_{in} near 1:1 on the analog meter. Then look at the LCD indication of RL_{in} and $|\rho_{in}|$ and continue tuning for maximum *return loss*. *If* $|\rho_{in}| \leq 0.02$, *then the error due to mistuning for low-loss tuners is less than 0.2%. The error grows to about 1.2% as the percentage of power lost increases to 85%.* For higher percentage-of-power-lost values, the error gets larger but never higher than 6%. For all practical purposes, this degree of accuracy is sufficient.

In some cases, the $|\rho_{in}| \leq 0.02$ condition cannot be achieved. One reason is that the antenna tuner is difficult

$$\left(100 - P_{LOST}\right)\left[1 - \left|1 + \frac{90000\left|\rho_{in}\right|^2}{\left(100 - P_{LOST}\right)^2}\right|^{\frac{1}{2}}\right] \leq MTErr\% \leq \left(100 - P_{LOST}\right)\left[1 - \left|1 - \frac{90000\left|\rho_{in}\right|^2}{\left(100 - P_{LOST}\right)^2}\right|^{\frac{1}{2}}\right] \quad \text{(Eq 9)}$$

where
$MTErr\%$ = the mistuning error in percentage,
ρ_{in} = the input reflection coefficient due to imperfect tuning, and
P_{LOST} = percentage of power lost.

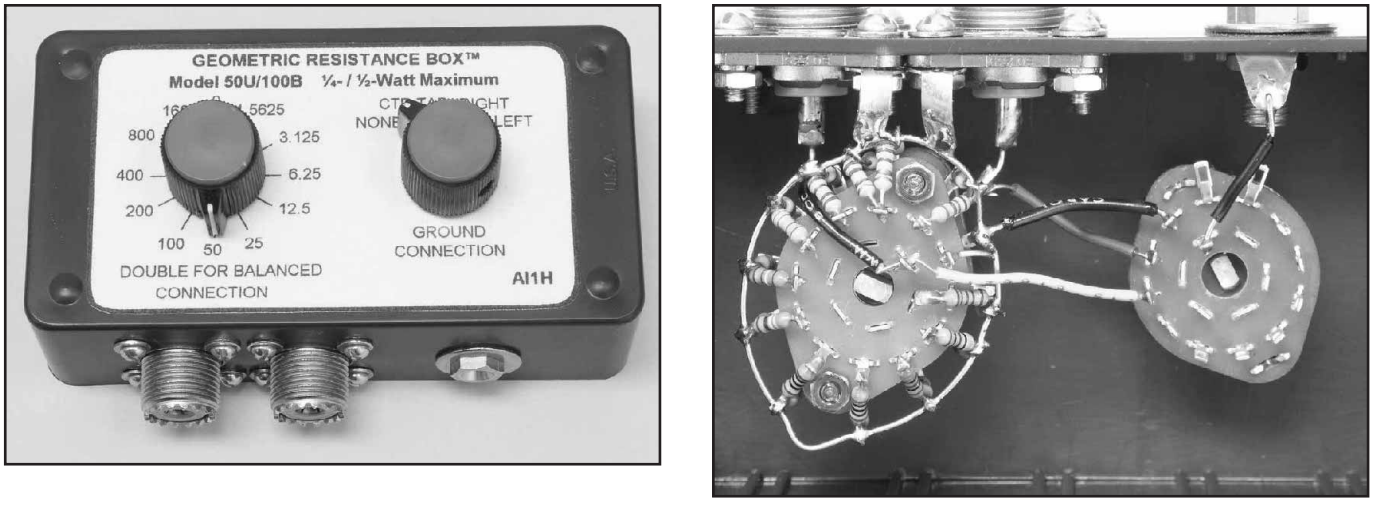

Fig 10—The AI1H geometric resistance box. It is designed to provide both unbalanced and balanced resistive loads.

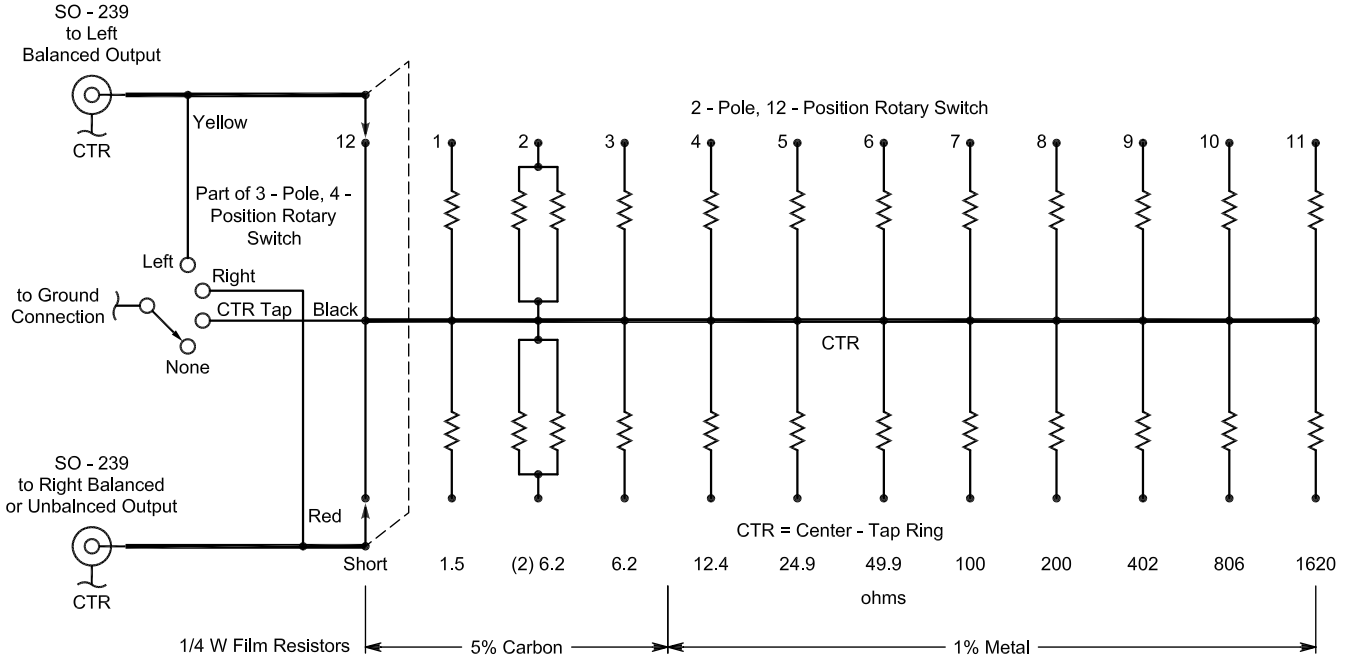

Fig 11—Schematic diagram of the AI1H geometric resistance box.

or impossible to tune for the particular load being used. Another is that the antenna tuner is made up of switched and variable components, and precise tuning ($Z_{in} = R_{REF}$) is not possible. This problem can be overcome by first tuning the unit as close as possible to the $|\rho_{in}| \leq 0.02$ condition. Then insert a low-loss tuner with continuous-tuning capabilities between the tuner under test and the analyzer. The low-loss tuner is then tuned to achieve the $|\rho_{in}| \leq 0.02$ condition. The loss calculation is then the sum of the loss of the two tuners. Most antenna tuners will perform well as the second tuner since they are simply transforming impedances near R_{REF} to R_{REF}.

Another potential problem is that the harmonic content of the analyzer signal source is excessive. When the analyzer is connected to a frequency-independent load impedance equal to R_{REF}, the *SWR*, $|\rho|$ and *return loss* are the same at the fundamental and at harmonics of the source, so the $|\rho_{in}| \leq 0.02$ condition is easily achieved. However, when the analyzer is connected to the input of a tuned antenna tuner, the load impedance equals R_{REF} only at the fundamental frequency. At harmonics of the fundamental frequency, the mismatch is huge, so harmonic signal energy will disturb the reading.

The MFJ-259B contains a sufficiently clean generator so that the $|\rho_{in}| \leq 0.02$ condition is achieved. *The conclusion is that when the signal generator has little harmonic content, mistuning error is a minor error contributor.*

Accuracy of Load Resistance

An advantage of the indirect method for evaluating antenna tuners and baluns is the simple way in which the resistive loads are obtained. A geometric resistance box provides the load resistors and a rotary switch. The physical layout is such that *the parasitic inductance and capacitance of the short connecting leads do not change when the load resistance is changed.* The parasitic inductance and capacitance become a part of the tuner being tested, and have a negligible effect on the test result.

The geometric resistance box was described in the article of Note 1. There were two boxes, one for unbalanced measurements and one for balanced measurements. I have combined these two into a single box, which is pictured in Fig 10. The schematic diagram is shown in Fig 11. Notice that most of the resistors are 1/4 W, 1% metal-film units. For the lesser values, only 5% carbon-film resistors are available, so the desired tolerance is achieved by selection. In addition to the switched resistors, a switch is included for balance quality evaluation.[11]

The absolute value of the load resistance, R_L, does not contribute to the error. The change in tuner loss for a ±5% variation in R_L is negligible. What is important, however, is the error due to imperfect ratios of adjacent loads, since Eqs 5 and 6 are based on an assumed ratio of two. Eq 6 can be generalized to include ratios other than two:

$$P_{LOST} = 100\left(1 - \frac{r+1}{r-1}\sqrt{|\rho_1||\rho_2|}\right) = 100\left(1 - \frac{\sqrt{|\rho_1||\rho_2|}}{|\rho_L|}\right) \qquad \text{(Eq 10)}$$

where

r = the geometric ratio, or the ratio of the resistances of adjacent load resistors, and

$|\rho_L|$ = the load-box reflection-coefficient magnitude.

What is the error introduced when $r \neq 2$ because of the tolerance of the load resistors? An analysis reveals that the worst-case error due to load resistance tolerance in percentage of power lost is given by:

$$\frac{4t}{300}\left(P_{LOST} - 100\right) \leq TolErr\% \leq \frac{4t}{300}\left(100 - P_{LOST}\right) \qquad \text{(Eq 11)}$$

where

t = the tolerance of the load resistors in percentage, and

$TolErr\%$ = error due to load resistance tolerance in percentage.

A subtle factor-of-two error reduction occurs by using the $2R_L$ and $R_L/2$ settings in the measurement process. In effect, the tolerance of R_L, the center setting causes an error in the $2\times R_L$ setting, which is offset by an error of the opposite sign when switching to $R_L/2$**.** *Thus for ±1% resistors, the worst-case error is only 1.33%, and this occurs for the loss-less tuner. The error from this source goes linearly to zero as the percentage of power lost increases to 100%.* See Fig 12.

If the application required it, this error could be reduced by resistor selection. The resistors cost only a few cents each. Another alternative that can essentially remove the resistor tolerance error completely is to calibrate the geometric resistance box at dc with the aid of a precision digital multimeter. The various load resistors are measured and the value of $|\rho_L|$ for each R_L is calculated from:

$$|\rho_L| = \sqrt{\frac{R_{ABOVE} - R_L}{R_{ABOVE} + R_L} \cdot \frac{R_L - R_{BELOW}}{R_L + R_{BELOW}}} \qquad \text{(Eq 12)}$$

where

R_{ABOVE} = the resistance value above R_L, which is very close to $2\times R_L$, and

R_{BELOW} = the resistance value below R_L, which is very close to $R_L/2$.

The value of $|\rho_L|$ is substituted into Eq 10 to find P_{LOST}. The same calibration procedure should be applied for unbalanced and balanced loads.

Human Error

As with any measurement process, the skill of the person performing the measurement is important. Fortunately, the indirect method is simple to apply. Lots of data can be obtained in a relatively short period of time, so the data should be processed in an orderly way. I like to use special forms that are designed for the application. The calculations are simple and can be made with a scientific calculator like the one included with Microsoft *Windows*.

Most antenna tuners have redundant tuning adjustments. For example, the popular CLC T topology has three

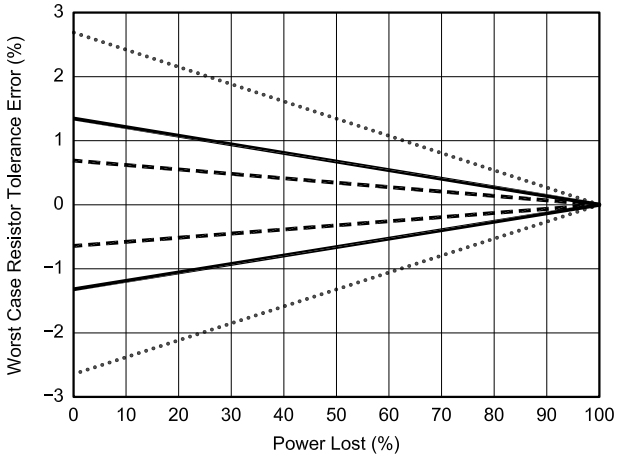

Fig 12—Worst-case error in percentage of power lost introduced by the tolerance of the load resistors. The dashed, solid and dotted lines show the error bounds for resistors with tolerance values of 0.5%, 1% and 2%, respectively.

adjustments, but one can be set and the other two adjusted for the $Z_{in} = R_{REF}$ condition. This means that there are an infinite number of settings that will achieve this condition. If we make a loss measurement with a particular load at a particular frequency, then make some measurements with other loads and frequencies, and then try to repeat the original measurement, chances are good that the result will be different. One reason is that the tuner adjustments have some play, and an earlier setting is difficult to duplicate. Unless great care is taken, there is a high likelihood that the error from this effect will be greater than the other errors discussed thus far, especially when the SWR bandwidth is small or the loss is high.

Human error is common to all methods for evaluating antenna tuners and baluns.

Total Worst-Case Error

Fig 13 shows the bounds on error for percentage power lost between 0 and 90% exclusive of measurement instrument error and human error. It includes method error, mistuning error and load resistance tolerance effects. It assumes that $|\rho_{in}| \le 0.02$ and the tolerance of the resistors is 1%. *The maximum worst-case error from these causes is only about 2.5%. This is entirely acceptable for evaluating tuners and baluns.*

Incidentally, these are worst-case errors. The worst-case errors from several causes were added up to get the total worst-case error. The actual error will usually be much less than the worst-case error.

Balanced Output Evaluation

In the original article describing the evaluation of antenna tuners (Note 1), a method was presented for evaluating the balance quality of antenna tuners. An improved interpretation of the balance measurement was presented in the balun evaluation paper[12] and will be summarized here. This method is applicable to the evaluation of antenna tuners with a balanced output port.

Ideally, a balanced antenna tuner with a balanced load whose center tap is grounded should force equal currents (equal in magnitude and phase, but opposite in direction) to flow in each leg of the load. Let's define these currents as I_1 and I_2. If we have the ideal situation, $I_1 = I_2$. In general, the current flowing from the center tap to ground is $I_1 - I_2$ which ideally should be zero. Hence an excellent measure of the balance quality is "imbalance" or IMB, which is defined as:

$$IMB = \frac{Current\ flowing\ from\ center\ tap}{Average\ current\ in\ the\ balanced\ load} \qquad \text{(Eq 13)}$$

$$IMB = 2 \times \left| \frac{I_1 - I_2}{I_1 + I_2} \right| \qquad \text{(Eq14)}$$

Thus, if *IMB* is zero, the balun in the antenna tuner is doing its job.

IMB has physical significance in an antenna system. For example, if the balanced tuner's load is a balanced antenna fed with a balanced feed line, the common mode radiation from the feed line can be derived from *IMB*.

A good estimate of the imbalance for tuners with current baluns can be found by connecting a balanced geometric resistance box to the balanced output terminals of the tuner. The switchable center tap lead is connected to the tuner ground terminal. The imbalance test is performed as follows:

1. Adjust the antenna tuner for *SWR* = 1 or $|\rho|$ = 0 or maximized return loss when the center tap is floating.

2. Ground the center tap and observe the value of SWR, $|\rho|$, or return loss which we will call S_B, $|\rho_B|$ or RL_B, respectively.

3. For antenna tuners with 1:1 baluns, calculate an estimate of the imbalance, *IMB*, from:

$$IMB = 2(S_B - 1) = 4\frac{|\rho_B|}{1 - |\rho_B|} = \frac{4}{10^{RL_B/20} - 1} \qquad \text{(Eq15)}$$

4. For antenna tuners with 4:1 baluns, calculate an estimate of *IMB* from:

$$IMB = 4(S_B - 1) = 8\frac{|\rho_B|}{1 - |\rho_B|} = \frac{8}{10^{RL_B/20} - 1} \qquad \text{(Eq16)}$$

The measurement of imbalance requires no setup beyond that required for measuring the tuner loss. It simply requires noting the value of *SWR*, $|\rho|$ or *return loss* when the center tap of the load is grounded. Although Eqs 15 and 16 are most accurate for current baluns, they may be used for voltage baluns as well.

Comparison of the Direct and Indirect Methods

The direct method for determining antenna tuner loss is, in concept, very straightforward, but can be done in a variety of ways. The best accuracy can be achieved with a laboratory-grade network analyzer. This test equipment has a built in signal source, a calibrated "standard" attenuator, which operates at a fixed frequency, and a detector. The device under test, in our case the antenna tuner, is inserted between the two ports of the analyzer. The analyzer measures return loss and insertion loss, so both tuning and loss measurement can be performed. Most network analyzers are designed to operate in a 50-Ω unbalanced impedance environment.

For an unbalanced tuner terminated in a 50-Ω load, the measurement is a piece of cake. The problem arises when the load is not 50 Ω or the load is not balanced. Of course, we want to evaluate our antenna tuners for non-50-Ω loads. A simple way to overcome this problem is to construct a set of minimum-loss resistive pads that match the desired load resistances to 50 Ω. These must be calibrated, of course, and this can be done with the network analyzer. The pad is connected to the output of the tuner so that the desired

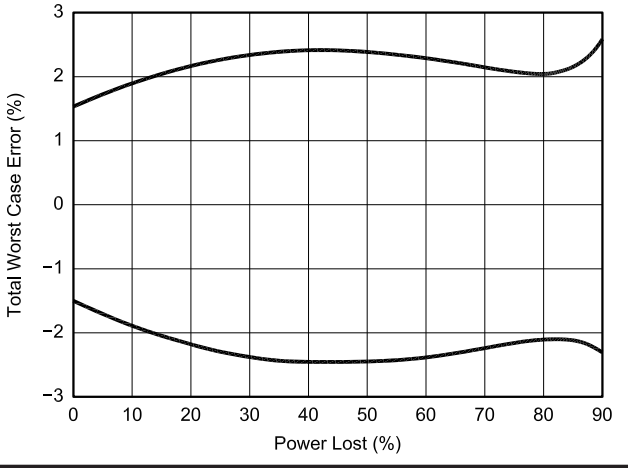

Fig 13—Total error bounds for all causes except for measurement instrument inaccuracy and human error. This includes method, mistuning and load-resistance tolerance effects. It assumes that $|\rho_{in}| \le 0.02$ and the tolerance of the load resistors is 1%.

R_L is achieved, and the combination tuner/pad is tuned and measured. The tuner loss is the measured loss minus the loss of the resistive pad.

The loss of antenna tuners with balanced outputs can be measured directly in a similar way, but the resistive pad design would be more complicated. The pad would be a balanced pad matching the load resistance to 100 Ω. Half of the 100-Ω resistance is a 50-Ω resistor and the other half is the 50-Ω input impedance of the analyzer, so the center tap of the load is grounded. Some indication of balance quality can be obtained by swapping the connection leads at the output of the antenna tuner. If the loss is unchanged, the balance quality is very good.

Theoretically, a simple implementation of the direct method would be to use a power source and two reflected-power meters, one at the input of the tuner and the other at the output of the tuner. At the input to the tuner, the reference resistance of the meter would need to be 50 Ω so that the tuner can be tuned (displayed reflected power equals zero). At the output of the tuner, a reflected-power meter with any reference resistance could be used between the tuner and the load impedance. The input power is the forward power displayed on the input power meter. The output power for the loss calculation is found by subtracting the displayed reflected power value from the displayed forward power value on the output power meter.

For balanced loads, the center tap of the load is grounded. Two output power readings are taken: one for each half load. A measure of the balance quality is how closely the two readings match. Unfortunately, the accuracy of the reflected-power meters available on the Amateur Radio market makes this method unattractive at this time.

A variety of other implementations of the direct method are possible. The direct method with a network analyzer and calibrated pads will yield very accurate loss measurements if done properly and could be considered the "gold standard" when making comparisons with other approaches, both direct and indirect. Extreme care must be exercised to be sure the antenna tuner settings are not disturbed when the different measurement schemes are applied. I have seen the settings change if the table on which the tuner is resting is bumped.

When other methods are compared with the indirect method, the same kind of detailed analysis of the error sources as summarized here for the indirect method should be performed. One variation of the direct method was employed in the evaluation of five antenna tuners. (See Note 5.) It involved the use of a laboratory-grade wattmeter, a switchable power attenuator and a number of non- inductive 50-Ω power resistors mounted in suitable fixtures so that they could be connected in series or in parallel. The source was a 100-W transmitter. The 50-Ω resistors had a tolerance rating of 5%. This approach provides a suitable load for the antenna tuner. However, a part of the composite load was made up of the input impedance of the power attenuator, so a loss contributor resulted from this division of power. The wattmeter and attenuator accuracy and the stability of the output power of the source are all potential error sources. All of these loss error contributors must be included in the worst-case error analysis.

All of the above direct methods involve swapping equipment and/or load resistors. Hence, the measurements are tedious and take more time than those required with the indirect method.

Summary

In terms of cost, speed and convenience, the indirect method is hard to beat. A very wide range of loads is provided. Evaluation with complex impedance loads is possible. Evaluations of antenna tuners with balanced outputs are as easy as those made on tuners with unbalanced outputs. In addition, balance quality is easy to find with the indirect method.

Improvements in the MFJ antenna analyzer have made the indirect method for evaluating antenna tuners and baluns very competitive with other methods for doing the same job. A careful characterization of the MFJ-259B has shown that the LCD readout of reflection coefficient magnitude (rather than SWR or return loss) provides adequate accuracy for this application.

I am grateful to Chris Kirk, NV1E, and Kevin Schmidt, W9CF, who each independently performed the mathematical analyses using the scattering matrix to determine the accuracy potential of the indirect method. I am indebted to Chris Kirk who offered valuable corrections and suggestions. Kevin Schmidt offered favorable comments as well.

Notes

[1]F. Witt, AI1H, "How to Evaluate Your Antenna Tuner," *QST*, Apr 1995, pp 30-34 (*Part 1*) and May 1995, pp 33-37 (*Part 2*).

[2]F. Witt, AI1H, "Baluns in the Real (and Complex) World," *The ARRL Antenna Compendium*, Vol 5, (Newington: ARRL 1996), pp 171-181.

[3]"*QST* Compares*:* Four High-Power Antenna Tuners," *QST*, Mar 1997, pp 73-77.

[4]*TLW* is bundled with the 19th edition of *The ARRL Antenna Book.*

[5]"*QST* Reviews Five High-Power Antenna Tuners," *QST*, Feb 2003, pp 69-75. The Ameritron Model ATR-30 is an example of an antenna tuner design that benefits from more enlightened design concepts.

[6]F. Witt, AI1H, "SWR Bandwidth," *The ARRL Antenna Compendium*, Vol 7, (Newington: ARRL 2002), pp 65-69.

[7]Dan Maguire, AC6LA, "**T**-Time for the Analyzers." *The ARRL Antenna Compendium*, Vol 7, (Newington: ARRL 2002), pp 40-49.

[8]The mathematical analysis, data processing and graphs for this article were done with the aid of *Mathcad*. See: W. Sabin, W0IYH, "*Mathcad* 6.0: A Tool for the Amateur Experimenter," *QST*, Apr 1996, pp 44-47.

[9]A refinement of this process takes advantage of the excellent resolution of the return-loss display in this region. The 25-Ω and 100-Ω resistors are measured with a precision digital multimeter. The target reflection-coefficient magnitudes are calculated by assuming R_{REF} of the MFJ-259B is 50 Ω. Then Table 1 is used to convert these into target *return-loss* values. This mapping between $|\rho|$ and *return loss* may be different for other software versions, so Table 1 should be checked if the version is not 2.02.

[10]Private communication.

[11]Model 50U/100B Geometric Resistance Boxes (as pictured in Fig 10) are available from the author. The units are completely assembled and tested and come with the necessary test leads, adapters and forms for recording the data.

[12]F. Witt, AI1H, "Baluns in the Real (and Complex) World," *The ARRL Antenna Compendium*, Vol 5, (Newington: ARRL 1996), p 179.

Frank was first licensed in 1948 and has held the calls W3NMU, K2TOP, W1DTV and EI3VUT. He holds BS and MS degrees in Electrical Engineering from Johns Hopkins University and is a Life Member of the IEEE. He is retired from AT&T Bell Telephone Laboratories where he worked for 37 years. He is one of five hams in his family: Barbara, N1DIS; Mike, N1BMI; Chris, N1BDT; and Jerry, N1BEB.

Frank's novel Amateur Radio contributions include the top-loaded delta loop, the coaxial-resonator match, the transmission-line resonator match and the geometric resistance box. He is a recipient of the ARRL Technical Excellence Award and serves as ARRL Technical Advisor. His other interests include golf and tennis. □□

CAD Analysis of the Grounded-Grid Amplifier Shows a Better Method for Stabilization

Tame a vacuum-tube amplifier by moving the parasitic suppressor to the grid circuit.

By Ralph Crumrine, NØKC

The risk of damage because of parasitic oscillations is one of the biggest drawbacks to implementation of expensive, high-power tubes in linear amplifiers. Computer-aided design (CAD), an analysis method particularly useful for studying amplifier stability, has been applied to a detailed model of the triode tube as it is used in a grounded-grid HF linear power amplifier. Circuit modeling includes the many parasitic elements within the tube envelope. This work has lead to a new and more effective means of stabilization and protection against parasitic oscillations. Results are given that compare this new method and the classical method of a plate connected parallel resistance and inductance parasitic suppressor.

1621 E. Sunvale Dr
Olathe, KS 66062-2108
n0kc@arrl.net

Selection of the Circuit for Analysis

The usual grounded-grid amplifier takes the form of an input matching network between the driver and the cathode of the amplifier tube and an output matching network connecting the anode (plate) to the load. The output network most often takes the form of a π network, often with embellishments such as the π-L circuit topology. Fig 1 shows a typical block diagram without any parasitic suppression.

On the input side of the amplifier there is usually little impedance transforming to be done. The input can be a π network, a coupled band-pass pole pair or something as simple as a shunt resonator. Any of these networks at the input should satisfy design requirements concerning maintaining a reasonable circuit *Q* in the cathode circuit for best performance of the tube.[1]

There is a common thread to the input and output networks that allows a general solution to the stability problem. These networks are generally of low-pass or band-pass topology, useful in suppressing harmonic energy, and hence will have shunt capacitive elements in their makeup; shunt capacitive elements that face the cathode at the input and the plate at the output. This is important in the consideration of stabilizing the amplifier stage because the usual parasitic oscillations take place in the

[1]Notes appear on page 21.

VHF and higher frequencies. The shunt capacitive leg of the input or output network defines a bypass point such that the elements of the networks ahead of the shunt capacitance at the cathode and after the shunt capacitance of the plate have little effect on the circuit that supports the parasitic oscillation.

Tube Equivalent Circuit

Fig 2 shows a schematic of a triode with its many possible internal parasitic elements. A variation of this schematic, not shown, would be the case of a directly heated cathode with simplified connections for the common filament and cathode connections. The triode selected for this study was the 8877/3CX1500A7. The equivalent circuit for the tube shows the elements and values in Table 1.

These elements are fixed in the mechanical design of the tube and, it is fair to say, vary somewhat for different tube types. For example, the 8877 is in a family of tubes known as external-anode designs. The plate-to-pin-out inductance, *L*p, is essentially zero. The capacitances are normally given in the data sheets.

Usually, nothing is given concerning the inductances. An exact stability analysis cannot be made without these data. They can be computed to a good approximation from mechanical dimensions. Internal pieces of the 8877 tube (see Fig 3) used in this study were supplied to the author by the manufacturer for an assessment of the parasitic inductances.

The theory developed here is common to all grid tubes including triode-connected multi-electrode types pressed into grounded-grid service. The 8877/3CX1500A7 triode was chosen for this analysis because of previous construction experience with it. Its high amplification factor assures adequate gain, particularly in amateur service where 50 to 100 W output is common to transceivers being used as the driver sources. This tube can be driven to the full legal limit of 1500 W with somewhat less than 100 W.

Amplifier Equivalent Circuit

Fig 4 shows the ac equivalent circuit that was used in this analysis and subsequently tested by me in an experimental amplifier using the 8877 tube. Input and output circuit details are shown. The tube is modeled as a voltage-controlled voltage source (VCVS) gain block with the tube's parasitic elements included. The VCVS model accounts for gain, time

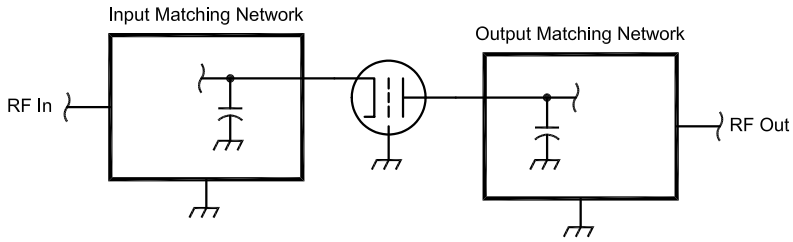

Fig 1—Block diagram of a grounded-grid linear amplifier.

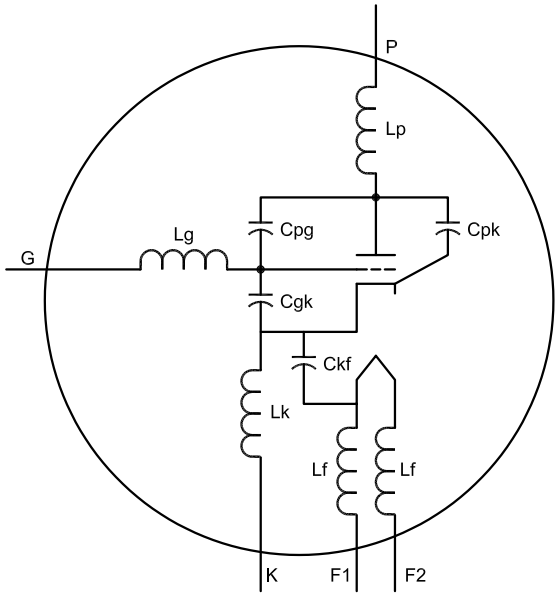

Fig 2—Vacuum-tube diagram showing interelectrode capacitances and inductance elements.

Fig 3—8877/3CX1500A7 internal structure.

Table 1—8877/3CX1500A7 Model Elements

Element	*Description*	*Value*
Cgk	Grid structure to cathode structure capacitance	38.5 pF
Cgp	Grid structure to anode structure capacitance	10.0 pF
Cpk	Feedthrough capacitance, plate to cathode	0.1 pF
Ckf	Cathode to filament capacitance	9.7 pF
Lg	Grid to pin out series inductance	2-3 nH
Lk	Cathode to pin out series inductance	5-7 nH
Lf	Filament to pin out series inductance	15-25 nH
Lp	Plate to pin out series inductance	Nil

delay, input and output impedances and frequency cutoff of the tube. Stray capacitances at the cathode and plate are included, as are the stray inductances necessary to get the cathode and plate connections wired to the input and output circuits. The new method of parasitic suppression, determined from this study, a parallel combination of resistance and inductance, labeled R1 and L1 inserted between the grid and ground is also shown in place. Also included in the equivalent circuit are the external stray capacitances to chassis associated with the cathode and the plate. The breaks in the circuit to apply Boyles' Method—more will be said about this method shortly—are shown as P1K, P2K, P1A and P2A. The physical connection points to the tube are labeled G, K and P: grid, cathode and plate, respectively.

New Means of Parasitic Suppression

With the speed and flexibility of computer analysis comes the ability to try a myriad of solutions to a problem. After several circuit topologies were tried without success, it was theorized that a parallel network of a resistor and an inductor at the grid of the tube, rather than at the plate, might have some usefulness from a consideration of stability. A search of the literature showed no evidence of this being implemented as prior art.

The capacitance from anode to grid, the Miller capacitance, is not grounded, as it should be, because of the internal parasitic series inductance in the grid lead. This leads to possible instability. This novel network has the ability to provide a dc ground return to the grid circuit, provide a low impedance to the grid circuit over the desired HF

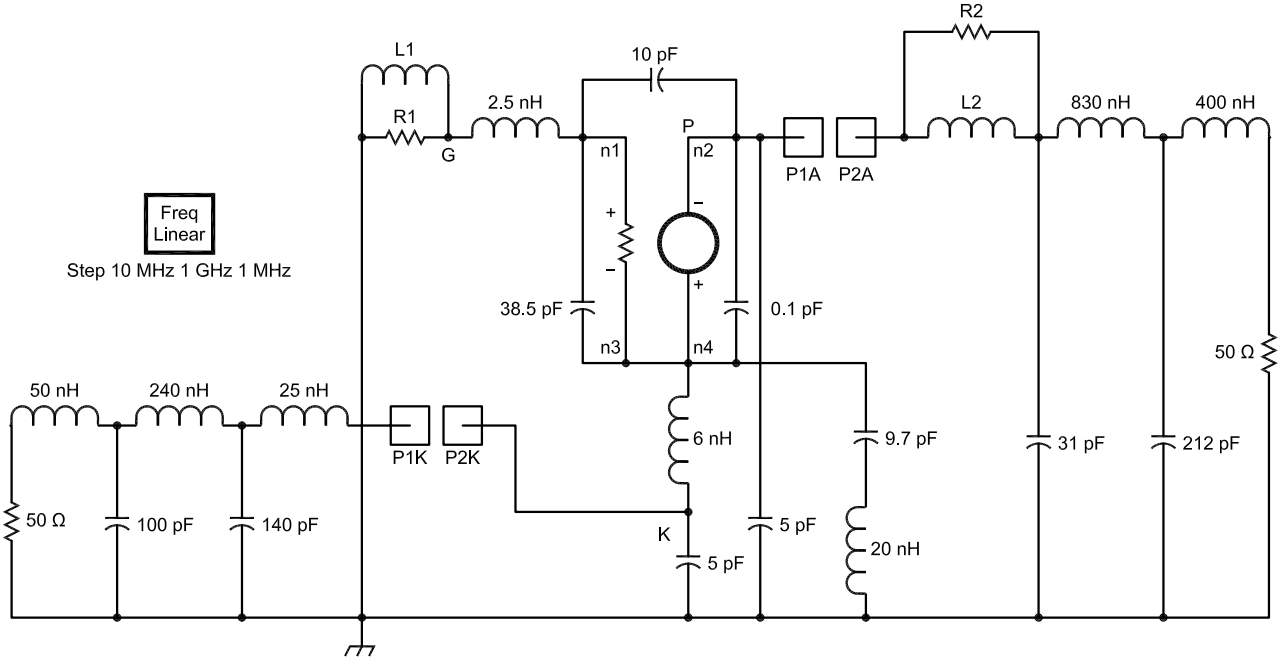

Fig 4—AC equivalent circuit of a grounded-grid amplifier.

Configuration	*L1*	*R1*	*L2*	*R2*
No Stabilization	**0**	**0**	**25 nH**	**∞**
Grid Stabilization	**20 nH**	**20 Ω**	**25 nH**	**∞**
Plate Stabilization	**0**	**0**	**90 nH**	**50 Ω**

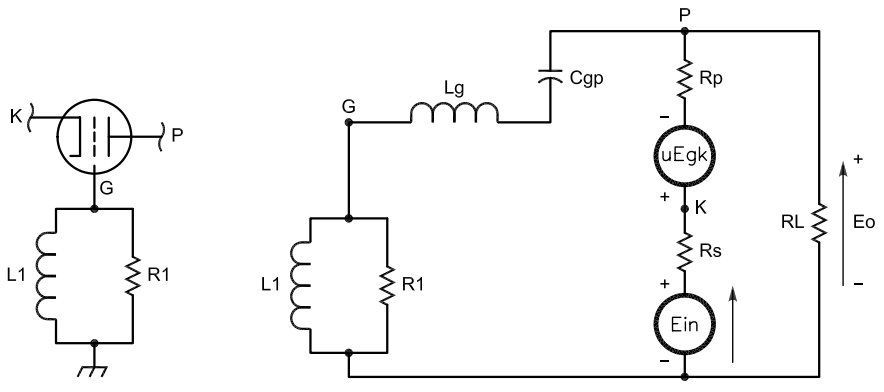

Fig 5—AC model circuit with parasitic suppression installed.

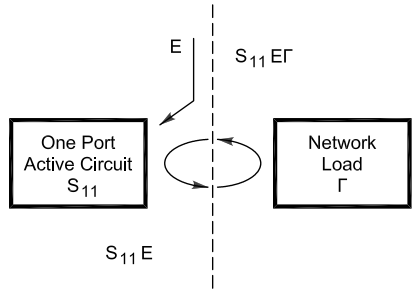

Fig 6—Amplifier separated into component parts.

operation range and then turn resistive, becoming substantial negative feedback and gain reduction in the region of VHF and UHF instability.

Analysis

The effect of the parallel L1 and R1 network between the grid and ground may be evaluated in two ways. First, looking at the ac model circuit of Fig 5, we have a triode with the parasitic suppression installed between the grid and ground. The equivalent circuit includes *Lg* and *Cgp*. The effect of *Cgp*—*Cgp* is known as the Miller capacitance—on the grounded-grid circuit would be insignificant if it weren't for the fact that the grid inductance, *Lg*, has some finite value. Current through *Cgp* drives through *Lg* and causes a voltage rise internal to the tube structure and leads to instability.

The expression for gain of the circuit in Fig 5 can be shown to be:

$$A = \frac{[(u+1)\times R1]}{[Rp + R1 + (u+1)Rs] + \left[\frac{u \times R1 \times Z2}{(Z2 + Z2)}\right]} \quad \text{(Eq 1)}$$

where
u = triode amplification factor (u = 200 in the case of the 8877)

$$Z1 = \frac{1}{s \times Cpg} \quad \text{(Eq 2)}$$

$$Z2 = s \times Lg + \frac{s \times L1 \times R1}{s \times L1 + R1} \quad \text{(Eq 3)}$$

At low frequencies, the impedance of *Z2* approaches zero and the gain, *A*, simplifies to the familiar result given by Millman:[2]

$$A = \frac{(u+1)\times R1}{Rp + R1 + (u+1)\times Rs} \quad \text{(Eq 4)}$$

The maximum, or full, dc gain is shown in Eq 4. With a judicious selection of *Z2*, the denominator of Eq 1 is greatly increased in magnitude at VHF frequencies and beyond, hence reducing the gain in the frequency range where parasitic oscillations are likely to take place. All this is done while having little effect on the gain at the lower operating frequencies.

A second and more powerful means of understanding the operation of the amplifier and its possible instability comes from the application of what is known as "Boyles' Method." This method of analysis gets its name from the author of a paper[3] titled: "The Oscillator as a Reflection Amplifier: An Intuitive Approach to Oscillator Design." Actually conceived of as a better and more comprehensive tool for designing oscillators than currently existing methods—and used by me on past projects in oscillator design—this method has the ability to show the tendency of a circuit to be either stable or oscillatory.

With this method, the analysis proceeds by breaking into the complete circuit, forming two one-port networks. This creates a passive resonator as one of the one-port

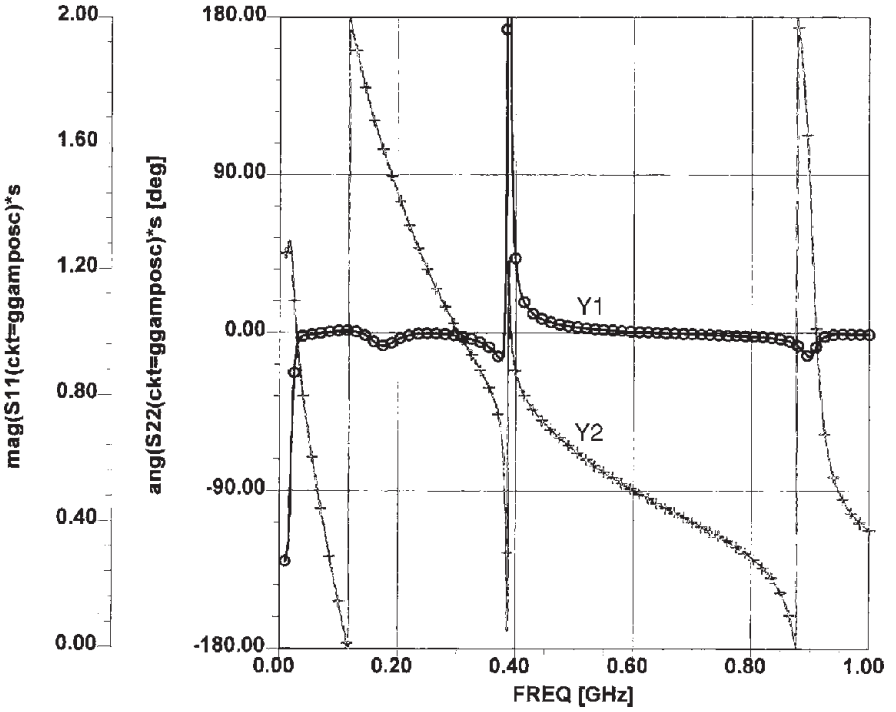

Fig 7—Stability plot, no stabilization, plate test point.

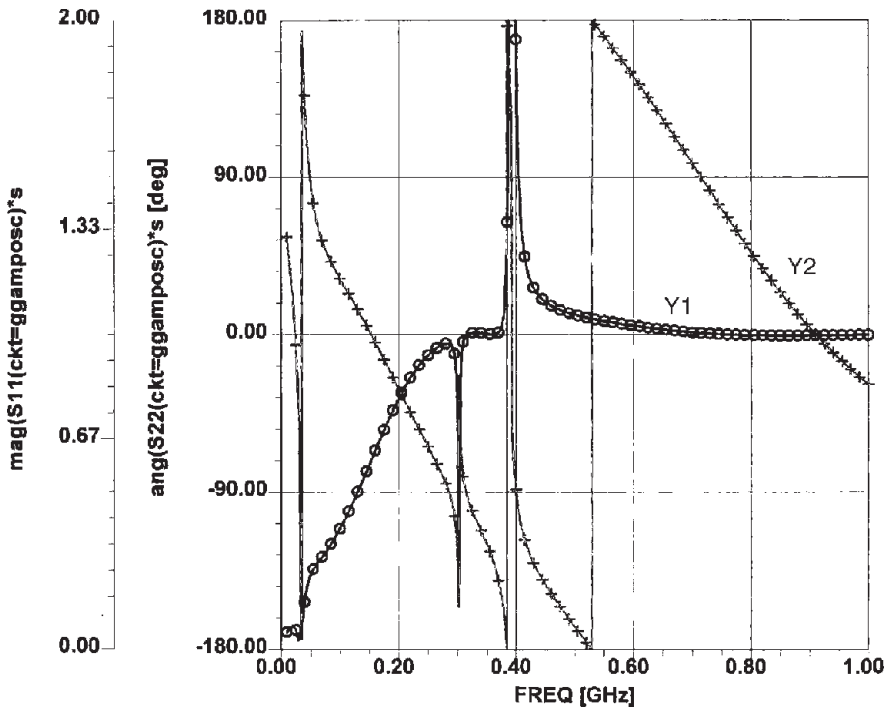

Fig 8—Stability plot, no stabilization, cathode test point.

networks and the active circuit portion as a second one-port network. Fig 6 illustrates the dissection of a circuit to be analyzed with Boyles' Method. This figure can be further understood by perusing Boyles' paper.

Using S-parameter analysis, the reflection coefficient, Γ, of the passive resonator half of the circuit and *S11* of the active portion of the circuit are processed by the CAD program as a product over the frequency domain of interest, looking at the magnitude and angle of the result. The conditions for oscillation are:

MAG(1/*S11*)<MAG(Γ)

and

ANG(1/*S11*)=ANG(Γ)

An RF design program such as Ansoft *Serenade Harmonica* has the ability to carry out the complex network mathematics required here. If, in the plot of the frequency domain, the magnitude of the result is greater than unity at the point where the phase of the result is zero, then at that point in the frequency-domain oscillation will likely be established.

If, in the frequency range of the analysis, the magnitude is less than unity at the points of the zero phase crossings, the circuit will not oscillate. This is the desired result required to indicate a stable amplifier.

A single application of this method to a circuit may not be exhaustive in determining its stability. In this study both the input and output circuit interfaces were used as points to break in and apply this method. Both tests must show stable operation to ensure a stable result.

To begin the study, the amplifier network of Fig 4 was considered without any stabilization network. That is, the circuit as shown with *L1* and *R1* set to zero, *L2* set to the typical interconnecting value of 25 nH and *R2* set to infinity, was analyzed at both the plate and cathode interfaces. Results of these analyses are shown in Figs 7 and 8.

On these plots, curves marked *X*, are phase plots and curves marked with O are magnitude plots. Both plots show instability with oscillation likely at approximately 380 MHz. Fig 8, looking in at the plate, shows four phase-zero crossings: one at 380 MHz occurring with a corresponding magnitude greater than unity. Fig 7, looking in at the cathode, also shows four zero-crossings for phase, again with the crossing at 380 MHz being accompanied with a magnitude greater than unity.

Note: Take care when interpreting the plots in Figs 7 through 12. In many instances, vertical lines connect or nearly connect the upper and lower boundaries of the phase plots. These lines are not part of the phase plots. They are retrace lines. They are not zero-phase crossings and not part of the phase variation over frequency.

It should be pointed out here that this analysis has the desirable quality of being done with linear equivalent circuits and loss-less components. It produces a worst-case result. If there were an opportunity for instability, the study would find it because of these qualities. This amplifier may seem to work fine but at an opportunity brought on by a transient or some

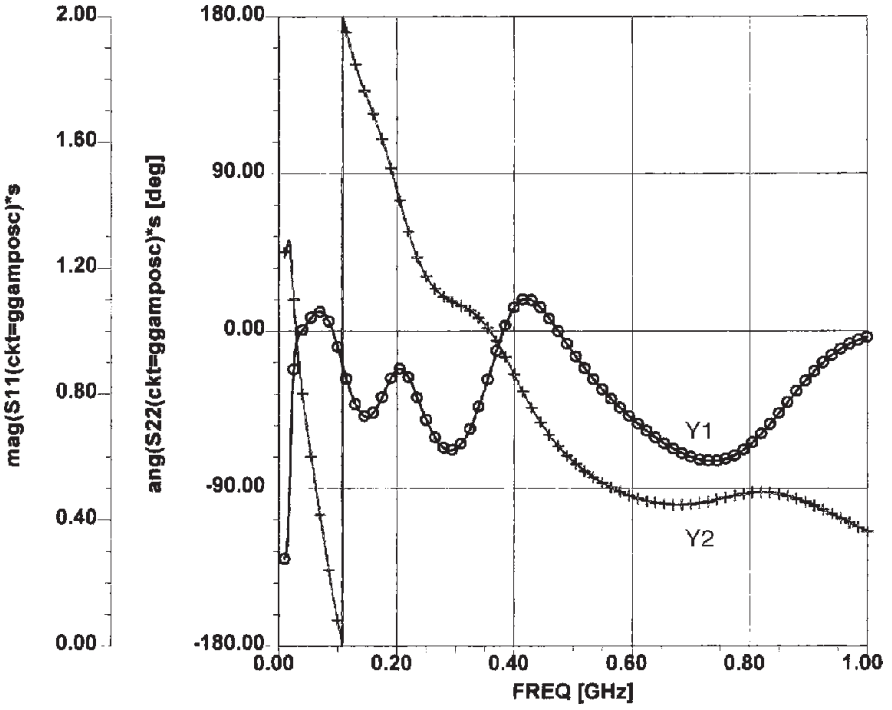

Fig 9—Stability plot, grid stabilization, plate test point.

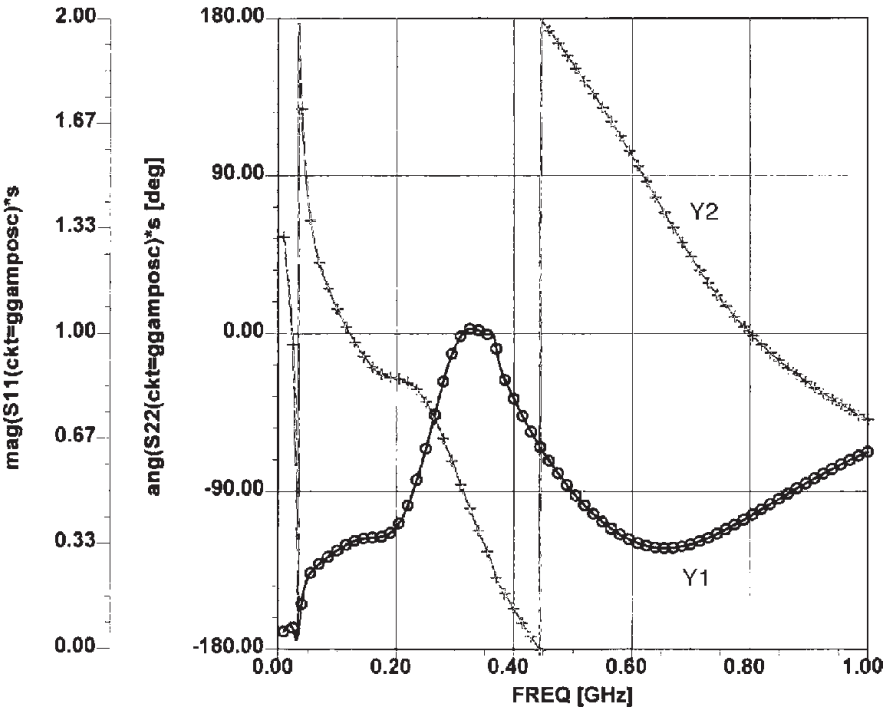

Fig 10— Stability plot, grid stabilization, cathode test point.

other means of excitation, the parasitic oscillation could get started.

The circuit of Fig 4 was again analyzed using the new grid stabilization, L1/R1, first; then analyzed again with plate stabilization, L2 and R2 in parallel and then in series with the plate lead. Figs 9, 10, 11 and 12 show the results of the analysis of these configurations. The values for the plate suppressor circuit, L2/R2 are taken from the *The Radio Amateur's Handbook,* ARRL, 1985 and 1986, from an article in Chapter 13 describing the construction of an 8877/3CX1500A7 grounded-grid linear amplifier.

Fig 9 shows that for the new grid stabilization, testing at the anode, there are two zero-phase crossings, neither of which is accompanied by a magnitude greater than unity. Fig 10 shows that for grid stabilization, testing at the cathode, there are three zero-phase crossings, none of which occurs at a magnitude greater than unity. Stability is indicated. We will come back to the discussions of these curves and the phase crossings later on.

The results for the new grid stabilization may be compared with results for the classic plate suppression circuit shown in Figs 11 and 12. Stability is indicated for the plate-suppression circuit, but the results are tenuous. A close look at these plots shows that there is still a possible problem at the same point in frequency where instability is shown in Figs 7 and 8 for the unstabilized amplifier. The magnitude plots show suppressed values, but there is little change in the phase plots.

Studying this detailed amplifier circuit, including the parasitic circuit elements in and around the tube, has revealed which of the parasitic elements contribute to instability and how sensitive that stability is to the variation of the parasitic element.

When the phase changes as radically as it does in the plots for the plate parasitic suppressors, one can show that variation of parasitic reactive elements in the tube can cause radical changes in the magnitude curve at the point associated with the radical phase change. That is a result that is difficult to control and predict—a result that can produce a magnitude of greater than unity at the zero-phase crossing with ensuing instability.

The desirable feature of the new grid-stabilization circuit is the better behaved phase characteristics observed at both the cathode and plate interfaces; fewer zero-phase crossings and no abrupt phase reversals, as are revealed in the plots for plate parasitic suppression.

Implementation

A look at Fig 13 shows that the implementation of grid stabilization works out rather handily for the 8877/3CX1500A7 triode tube. It can be integrated into the grounded-grid socket, taking up no extra space whatever. The conversion involves removing a pair of grid-ring contacts and modifying the remaining two to be insulating standoffs, with a coil wrapped around the insulating standoff and a chip resistor being connected across the coil. The spring contacts are

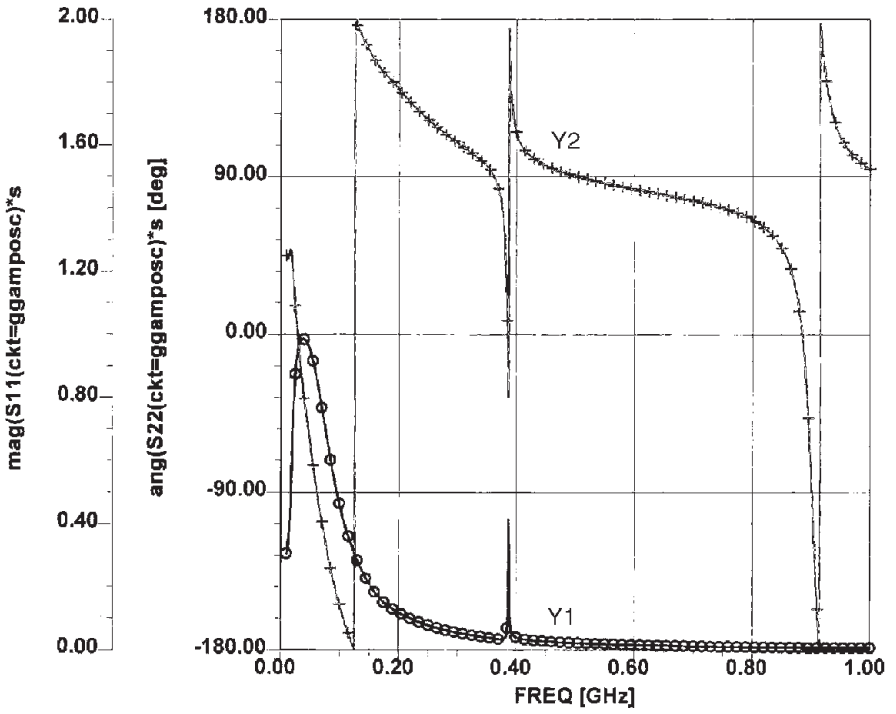

Fig 11—Stability plot, plate stabilization, plate test point.

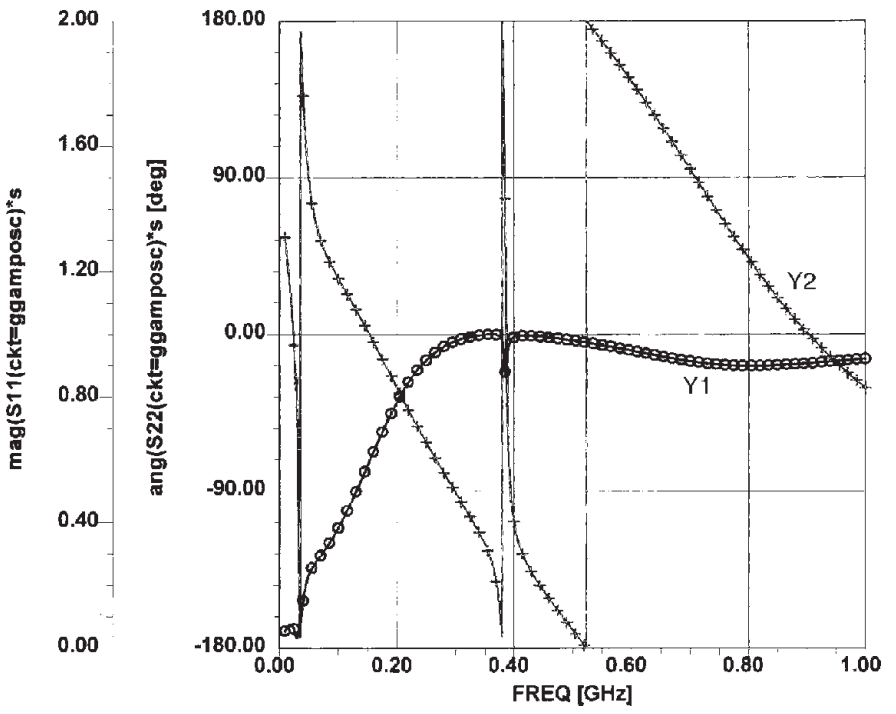

Fig 12—Stability plot, plate stabilization, cathode test point.

reshaped and turned upside down to give a ground connection to the grid through the coil and resistor combinations.

With little extra cost, all four grid contacts could be modified for a high level of redundancy. The values given for the single resistor and inductor in Fig 4 would be multiplied by the number of paralleled grid connections to get the values actually installed at each point.

Conclusion

These results concur with years of experience gained without the benefit of exact computer analysis. The plate suppressor works with some degree of promise of improved stability. The analyses show why it works. Parasitic suppression at the grid terminal appears, however, to be a more powerful and sure means of stabilization—in part because of the calculated gain reduction, and in part, because of the better behaved phase characteristic.

The experimental amplifier (see Fig 14), with grid stabilization incorporated, was tested, mistreated and abused in every conceivable way. It was keyed with open- and short-circuited inputs and outputs, incorrect band-switch settings, grossly misadjusted tune and load capacitors, chattered keying, and so on, without a hint of parasitic oscillation or instability.

Noise problems have been reported in linear amplifiers. Noise is usually generated in amplifiers that are marginally stable: showing what we in the trade call regeneration—on the verge of oscillation. While this was not specifically investigated, noise has not been a problem in this amplifier and my experience and intuition leads me to believe that grid stabilization is very effective against the noise problem.

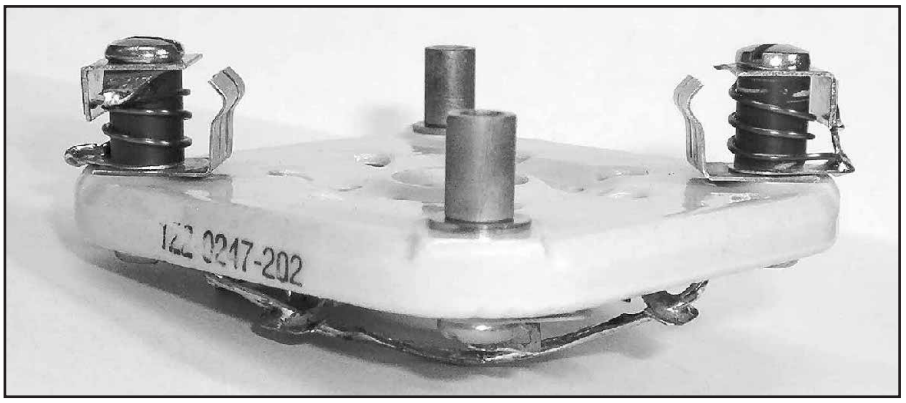

Fig 13—8877/3CX1500A7 socket modified with grid stabilization.

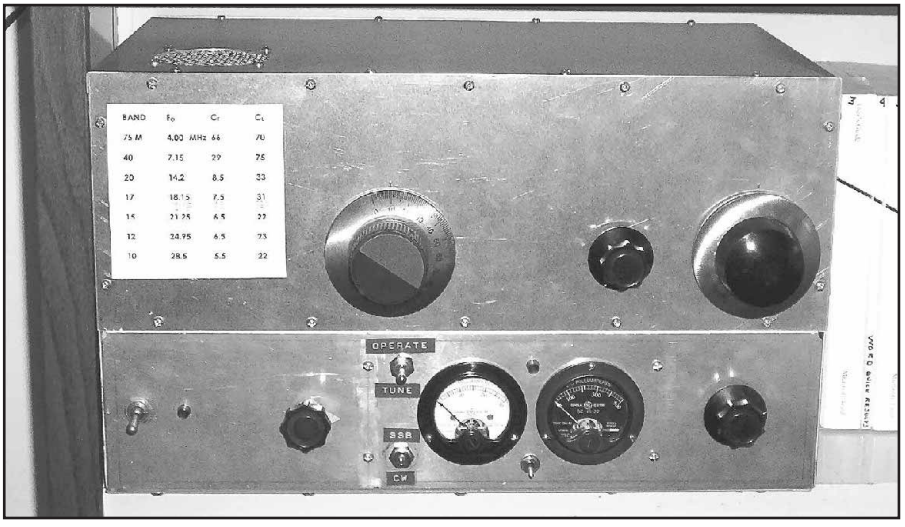

Fig 14—Experimental 8877/3CX1500A7 linear amplifier.

Acknowledgement

I wish to thank Greg Triplett, WA8KAM, for his time taken to review this work. Thanks are extended to Ansoft Corp for the use of their *Serenade Harmonica* CAD software tool and the technical support to get me up and running in it quickly. Thanks are also extended to Reid Brandon of CPI-Eimac for supplying me with the internal pieces of the 8877 used in my analysis of stray inductances.

Notes

[1]"Technical Data, 8877/3CX1500A7 High-Mu Power Triode," Eimac/Varian, p 5, June 1991.

[2]J. Millman, *Vacuum Tube and Semiconductor Electronics*, (New York: McGraw-Hill, 1958) pp 192-193.

[3]J. W. Boyles, "The Oscillator as a Reflection Amplifier: an Intuitive Approach To Oscillator Design," *Microwave Journal*, June 1986, pp 83-98.

Ralph Crumrine, NØKC, was first licensed as WN3WFZ in 1953. Shortly thereafter, he upgraded to W3WFZ (General class). He served in the USAF as an avionics technician, being honorably discharged in 1957. He graduated with honors from Pennsylvania State University in 1961 with a BSEE. Graduate studies followed at PSU and NYU. Ralph upgraded to the Amateur Extra class license in 1977. After 30 years in aviation electronics product design and design management, he is retired and now active once again in Amateur Radio. □□

D-STAR, Part 2: Design Considerations

Come learn what JARL put into their proposed new VHF communication standard.

By John Gibbs, KC7YXD

In the first segment of this series, we considered the attributes we would like to see in any new VHF/UHF Amateur Radio system. In this second segment, we discuss the technical issues involved with selecting the parameters of an Amateur Radio digital system to meet those attributes.

Perhaps the easiest way to organize the design considerations for a digital radio system is to use the OSI Model. The OSI Model is officially known as The Basic Reference Model for Open Systems Interconnection. We start the description with the bottom level of the OSI model, the physical layer. Then we will work our way up to the top levels, which are open to amateur experimentation and application development.

Physical Layer

Transceiver Frequency

We hams have a large spectrum allocation at 1.2 GHz (60 MHz wide in the US) that is little used today. In fact, we should use this spectrum or risk losing it to commercial interests. Also, if we want to develop a system to send high-speed data, we will need a wide-bandwidth signal and there is little available spectrum at 70 cm. If it is desired to use the D-STAR protocol at lower frequencies, the high-speed data mode could be dropped. In fact, a prototype portable 2-m HT using only the digital voice mode has been developed and was shown this spring at IWCE.

Like the previous FM system, the system design logically calls for half-duplex operation for digital voice and simplex for high-speed data.

Repeater Link Frequency

Since it is desired to have multiple contacts and high-speed data packets on the repeater link, a wide bandwidth is required. Therefore the repeater backbone must be at microwave frequencies and the amateur band at 10 GHz is a logical choice. Today's equipment generates usable 10 GHz power, is affordable and the 10 MHz of bandwidth is practical. The bi-directional, asynchronous nature of multiple contacts demands a full-duplex repeater link.

Given the high-speed data requirements of the system and the desire to use digital voice to reduce transceiver spectrum requirements, the repeater link should be digital. With the asynchronous nature of the system, packet mode is a natural choice. However, because a packet system does not guarantee real-time communication, voice should be given priority over data to minimize the possibility of voice disruptions.

Modulation

An ideal modulation system should generate a signal that has a narrow spectrum, with low side lobes so that it does not interfere with other nearby users. On our crowded ham bands, this is becoming more of an issue daily.

There are several commonly used modulations for digital data. The digital modulation scheme chosen will significantly affect the performance of a communication system. Generally we want to maximize the data rate within

18225 69th Pl W
Lynnwood, WA 98037
kc7yxd@arrl.net

the constraints of acceptable level of latency, available bandwidth, acceptable error rate, product costs and operating environment (that is mobile, portable, fixed-link). In particular, mobile and portable operation causes variable multipath fading and fast phase shifts that can wreak havoc with digital radios.

Less spectrally efficient modulations generally have better operation characteristics in poorer SNR conditions. Also, they are more forgiving of frequency-offset errors between the transmitter and receiver and frequency and phase response error on the channel—an important consideration if costs are to be kept down in a UHF system.

4 FSK—FSK, MSK and GMSK are very attractive because they are constant amplitude modulation. This means that the power amplifier can be class C, which offers low cost and excellent power efficiency.

FSK has of course been used in amateur systems for years, dating back at least to the introduction of RTTY. Newer variations on FSK use more frequencies than just mark and space. For instance, the new weak signal mode, JT44 uses very slow FSK (about 5 Hz data rate) with 44 different frequencies each corresponding to a character.[1] But at the higher data rates needed for a VHF/UHF digital voice system, four FSK frequencies offers an attractive option for improved FSK performance.

GMSK—Among FSK, MSK and GMSK, GMSK offers the best spectral efficiency with only a slight degradation in the BER compared to FSK and MSK. These advantages have made GMSK one of the most popular digital modulations worldwide. Other more complex modulations like QPSK require a more expensive linear power amplifier that also typically requires more current, which is critical in portable operation.

GMSK low-pass-filters the data stream with a filter that approximates a Gaussian time and frequency response. A Gaussian filter is used because of its desirable properties in both the time and frequency domains. This filtering reduces the high-frequency content of the modulation and therefore narrows the frequency spectrum of the modulated signal while widening the data response minimally. However, as you continue to narrow the filter, the spectrum continues to narrow and the time response of the filter lengthens. This causes the peak amplitude to decrease and the adjacent data tails of the time response to interfere with the decoding of the desired symbol, a phenomenon called inter-symbol interference (ISI).

A typical compromise between ISI and bandwidth used by many systems is for the bandwidth/data rate ratio to be equal to 0.5. This yields almost no degradation due to ISI compared to MSK and yet dramatically reduces the spectral occupancy of GMSK compared to MSK.

QPSK—In theory, quadrature phase-shift modulation could have a constant amplitude format. However, the rapid switching of the input data causes a QPSK signal to have large sidebands that destroy its spectral efficiency. Therefore in practice, raised cosine filters are used on input data to reduce these sidebands. To preserve the wave shape induced by these filters requires the use of a more expensive and less power-efficient linear amplifier. If a class-C amplifier were used with QPSK, the sidebands that were removed by the cosine filter would be regenerated.

In the presence of additive white Gaussian noise (AWGN), QPSK requires about 3 dB less signal-to-noise than does FSK. However, in real channels, with multipath and poorly synchronized receivers, the 3-dB advantage quickly disappears.

Data Link Layer

Time Division Multiple Access (TDMA)

TDMA is one of the two commonly used multiplexing standards for cellular phones. The cell tower site acts as the master clock and assigns a time slot to each of several cell phones that are assigned the same frequency. For proper operation, it is critical that each phone transmit and receive exactly in its assigned time slot. This is not attractive for amateur simplex operations because operations are as two or more equals, and there is no master to determine the clock and assign time slots.

Any Amateur Radio system has to work without a centralized frequency reference and master clock. In addition, the radios must be able to acquire signals that are somewhat off frequency and acquire timing without the need for a separately transmitted clock signal. These requirements may make an amateur system less spectrally efficient than a centrally-controlled system like the cell phone, but they are more in keeping with the spirit of Amateur Radio, particularly the capability to operate when the infrastructure is destroyed.

Code Division Multiple Access (CDMA)

CDMA (also known as spread spectrum) is also used for multiplexing cellular phones. In CDMA, several cell phones share the same frequency and transmit simultaneously. Each phone on a frequency is modulated with a code sequence that spreads the spectrum in a unique way. If the receiver is synchronized and has the same code sequence, then the signal is restored. Otherwise, the signals from other phones become part of the background noise.

An important limitation on the system is that undesired signals are not completely rejected. Depending on the length of the codes used and the attendant difficulty in synchronizing, perhaps 20-30 dB of so-called processing gain can be attained. Therefore, a strong nearby CDMA signal can overpower a more distant signal. This classic problem with spread-spectrum communications is called "the near-far problem."

In a cell-phone system, this problem is addressed by power control. Since all the nearby phones are communicating with the same nearby cell site, the cell site remotely controls the power level of each phone to minimize the possibility of interference. However, in Amateur Radio, particularly with multiple simplex contacts, this is not a solution.

Frequency Domain Multiplexing (FDM)

TDMA, CDMA and other modern multiplexing schemes require coordination between the units that is incompatible with the basic goals of the Amateur Radio Service. One of the major justifications for our service in the US is emergency service. TDMA and CDMA require an infrastructure to provide the coordination. This infrastructure would quite possibly be destroyed in an emergency. So, the best solution for Amateur Radio is what we have traditionally used, FDM.

Network Layer

In the network layer, the binary data stream is divided into discrete packets of finite length. In addition, error checking is performed by cyclic redundancy check (CRC) at this level. If an error is detected, it is corrected by the retransmission of packets.

Transport Layer

In the transport layer, we multiplex and split all the data streams we need to send and receive. In an Amateur Radio system, we would typically need to include repeater control data; source, destination and routing information (that is, call signs of both operators and repeaters used); and what is called the payload, which is the voice or data to be sent.

[1]Notes appear on page 28.

Presentation Layer

Codec

As mentioned in the first segment of this series, simple PCM encoding of voice results in a 64,000 bits/s data stream. Codecs have been developed to compress voice with good quality down to 2400 bits/s and lower. These codecs develop their extreme data compression by modeling short segments of the human voice and only transmitting the reduced information needed to describe the voice model.

One of the major difficulties in designing a digital voice radio is in testing the voice quality. High-compression codecs are designed to work with a human voice; traditional tests like frequency response and harmonic distortion with sinusoidal tones do not generate meaningful results. Consequently, a subjective method of testing called *mean opinion score* (MOS) has been developed. MOS is estimated by a test with a group of normal listeners who are asked their opinion on a five-point scale (1 = bad, 5 = excellent) and the results are averaged together.[2]

A very important factor in conducting MOS tests is the acoustical environment. Since the codec is designed to highly compress the information in a human voice, it is easy to imagine that the presence of other signals and noise can severely affect the performance of the system. An excellent test for Amateur Radio is performance in an automotive environment including engine noise and wind noise from an open window.

A final issue in codec selection is the MOS performance in the presence of the channel impairments we commonly find in VHF/UHF communication paths. As Digital Voice Systems point out on their Web site, "Vocoders…designed for extremely low bit-error rates, such as those encountered in land-line communications, often experience serious degradation when applied to the much higher bit-error rates found in wireless communications. Consequently, it is important to consider robustness to channel degradations during the vocoder-algorithm design process."

Scrambling

Bit synchronization and accurate level slicing in the receiver require frequent transitions in the data (no long

Table 1—D-STAR Transmission Characteristics

Mode	*Transmission Speed*	*Bandwidth*
Backbone	10 Mbps or less	10.5 MHz
Data	128 kbps or less	130 kHz
Digital Voice		
ITU	8 kbps	9 kHz
AMBE	2.4 kbps	5 kHz

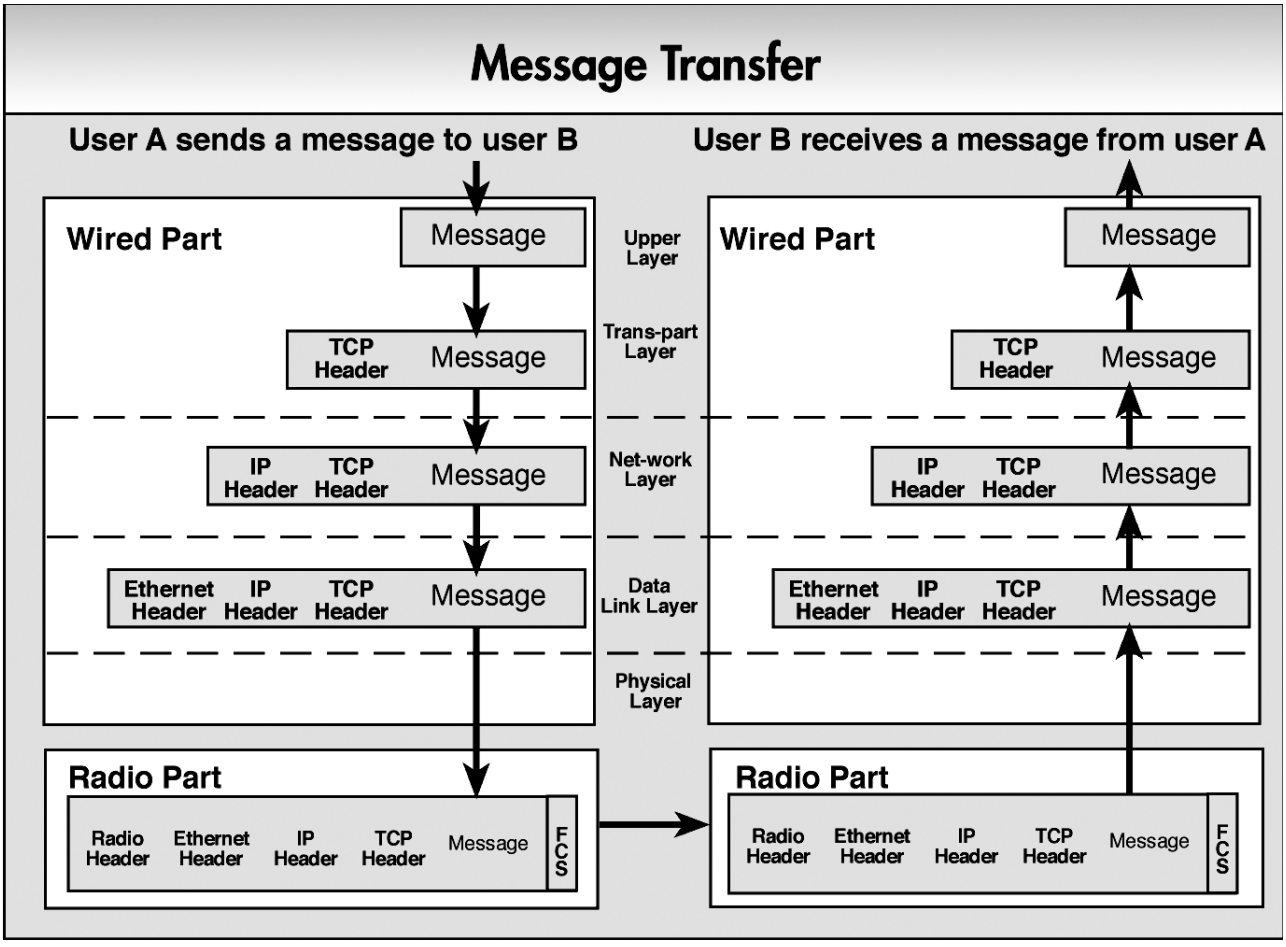

Fig 1—Header additions with TCP/IP protocol.

strings of ones or zeros). To ensure that condition, most digital radio systems use a device called a scrambler to randomize the input data stream.

"Scrambler" is an unfortunate term for people who are familiar with analog radios; it is common to interpret this as encryption. The FCC of course forbids encryption for amateurs. Scrambling is not an attempt to hide the message content, however; it is a fixed and published method known by all potential receivers for converting the input data stream into a data stream with short strings of ones or zeros.

Scrambling is typically done with a shift register and exclusive **OR** gates. CCITT recommendation V.26 recommends this procedure.

Application Layer

This is the layer where hams can begin to customize the system and add their own applications. In addition, this is the level where the system design allows for user control entry and data entry, both data from the IEEE 10BaseT Ethernet and analog audio from the microphone.

D-STAR Proposed Standards

As stated in the first part of this article, D-STAR is not a finalized standard at the time of this writing. However, the field trials are finished and standard publication begins here. Table 1 shows the system as it stands at this writing.

To describe the proposed D-STAR standard, we will start at the input side of the transceiver and work our way out to the antenna, working our way down the OSI model. We will then see how the standard defines the repeater operation and the links between repeaters. First we will consider the high-speed data mode and then the digital voice.

High-Speed Data

The standard interface for high-speed data into and from the D-Star system is IEEE802.3 (10BaseT Ethernet.) In Fig 1 you can see how the D-STAR transmitter adds a radio header extension to the Ethernet message just as the Ethernet protocol added a header to the Internet Protocol, TCP/IP. Since this radio header is stripped off in the receiver, the radio link appears to be a "wireless Ethernet cable." Therefore, it is possible using existing software (such as browsers) to communicate the same images, text and voice as is handled by Ethernet, including links to the Internet, without modification.

Data Multiplexing

Fig 2 shows the details of a communication packet from the radio part in Fig 1. Each packet consists of a radio header and the Ethernet packet described above followed by an error-checking frame. The radio header is worthwhile to study in some depth as it shows many of the D-STAR system capabilities.

Each frame of the radio header is identical in both the high-speed data mode and in the digital voice mode. If the standard is approved as proposed, it will contain the following information:

The first two fields are common to most digital radios, the bit sync and the frame sync. These preambles are designed to allow the receive modem to establish timing and level lock as quickly as possible.

The flag field describes the content of the data field.

Bit 7 Data or voice communication flag.
Bit 6 Repeater or simplex flag.
Bit 5 Communication-interruption flag.
Bit 4 Control signal, data or voice signal flag.
Bit 3 Emergency/normal signal flag.
Bits 2-0 Transmission-control bits (see below).

The ID field can hold four call signs:

1. The local repeater you are accessing (optional).
2. The linked distant repeater the called party is using (optional).
3. The station you are calling (can be CQ).
4. Your own call sign.

The PFCS field is a check word for the header. Some of these bits require a little more explanation if we are to understand the operation of the system. Notice that when bit 3 of the flag field is set, you are asking for an emergency break-in. (On many FM repeaters you would say "break" today.) For

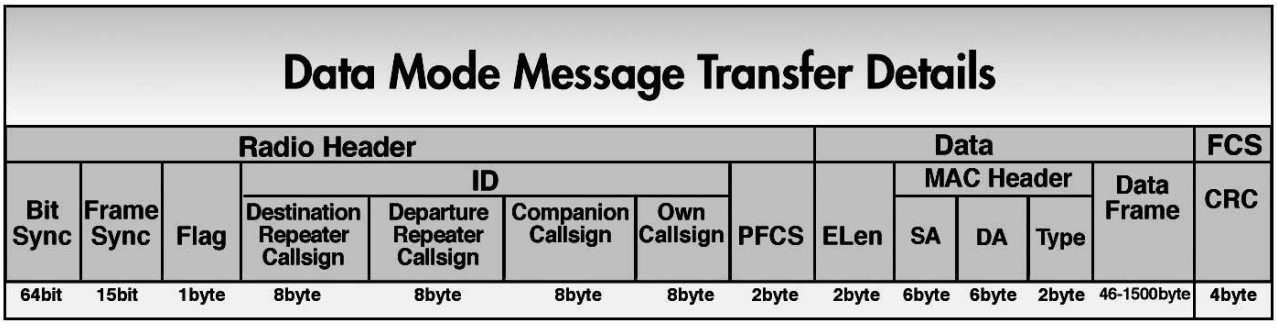

Fig 2—Proposed bit pattern in high-speed digital mode.

Table 2—Call-Sign Combinations and the System Function

(Uses Evergreen Intertie Call sign examples[3])

Called Station	*Departure Repeater*	*Destination Repeater*	*Own Station*	*Function*
CQCQCQ	KB7WUK	K7NWS	KC7YXD	CQ Portland
N7ABC	KB7WUK	K7NWS	KC7YXD	Call N7ABC in Portland
N7ABC	K7NWS	K7NWS	KC7YXD	Call N7ABC on local repeater
N7ABC	DIRECT	DIRECT	KC7YXD	Simplex

instance if you want to report an accident, pushing the emergency key on the radio will set bit 3 and all D-STAR radios within range will open squelch and their volume to be set high.

The flag field bits 0, 1 and 2 are used for transmission control. They implement functions like ACK, ARQ and repeater control.

One of these repeater control functions is repeater lockout. Repeater lockout is used mainly to block illegal stations. A D-STAR repeater can hold a black list of call signs that have consistently violated repeater and/or FCC rules. If a blacklisted station calls the repeater, the repeater does not repeat the message but instead calls the offending station back with the lockout bit set. The offending station's radio will then display a message indicating that it is blocked from the repeater. So now, it is not necessary to shut down the repeater for everyone when one individual is misusing the repeater.

Another important field for understanding the capabilities of the system is the ID field. Understanding the ID field is important because it shows the great flexibility available in the system calling capabilities. The first thing to notice is that the D-STAR protocol automatically IDs at every transmission. This easily meets the FCC ID requirements for ID at start, end and every 10 minutes of transmission.

Next, to understand how the four ID fields work, Table 2 illustrates the contents of each field if KC7YXD were to transmit on a fictional D-STAR Evergreen Inter-tie system. It is not necessary to always fill in all the ID fields. If you respond to a CQ or a call directed at you, your D-STAR transceiver will automatically fill in the fields for you.

Digital Voice

Codec—Those of you who had a chance to see the D-STAR presentation at last year's Dayton Hamvention or at the DCC in Denver last fall may recall that the Digital Voice mode occupied 8 kHz of bandwidth using the ITU G.723.1 Codec standard. At that time, the two codecs were undergoing field trials; today the JARL has selected AMBE as the standard. The two standards under consideration were the ITU standard G723.1 and a Digital Voice Systems proprietary codec that uses the AMBE algorithm.

ITU G.723.1 uses an ACELP (algebraic code-excited linear prediction) algorithm that generates a 5.3-kbps data stream. With an algorithm delay of 37 ms, the total wireless-communication-throughput delay is a little over 100 ms, quite reasonable for half-duplex communications.

AMBE stands for advanced multiband excitation. AMBE can use different levels of compression to trade off voice quality and bit rate. Tests show that at the 2.4-kbps data rate, the voice quality was at least as good as the higher-data-rate ITU G.723.1 over real radio links. The algorithmic delay is only slightly longer than G723.1 (44 ms), so the factor-of-two improvement in data rate (and spectral efficiency) comes with no noticeable latency increase.

The data-rate reduction from the AMBE codec is particularly significant because of worldwide pressure from regulatory agencies to reduce the occupied bandwidth of voice communications sufficiently to allow 6.25-kHz signal spacing. When using a modulation scheme sufficiently robust to give reliable communication in mobile and portable applications, only the AMBE data rate meets this signal-spacing requirement.

The decision between codecs is complicated by the fact that G.723.1 is an open public standard codec whereas AMBE is the patented intellectual property of Digital Voice Systems. Unlike many companies, however, the present owner of this technology supports the Amateur Radio community and is willing to sell these parts in small quantities.

Table 3—AMBE Vocoder-Based Systems

Inmarsat
Thuraya
Iridium
APCO Project 25 (IMBE)
G4GUO & G4JNT HF Digital Voice System

The JARL is not alone in deciding on AMBE for its high voice quality and very low bit rate. Table 3 shows several digital systems that have standardized on this codec technology. For instance, the Telecommunications Industry Association (TIA) selected DSVI's codec technology over CELP and other codecs for the APCO Project 25 North American land-mobile radio-communication system. This is particularly significant because at least two Amateur Radio groups are evaluating Project 25 radios as an alternative digital radio standard for amateur usage.

Fig 3 illustrates the bit pattern used in the digital voice mode when the AMBE codec is used. As mentioned before, the radio header is identical to the high-speed digital mode radio header and so will not be discussed here.

The most interesting part of Fig 3 is that the digital-voice data frames are interleaved with data frames. These frames are currently reserved by the D-STAR standard with no dedicated usage by the system overhead. This means that the system is capable of supporting a 2400-bits/s data stream from a user application while the user is talking on the system! Notice that the D-STAR system itself provides no error detection for this data, so it would be up to the user's application to provide error detection and error correction. This and other overhead would decrease the end-to-end data rate slightly; but if radios are built to exploit this capability, hams could potentially add many interesting features to the D-STAR system.

What is not shown in Fig 3 is that the frame and sync fields are repeated often so that the errors between the transmitter and receiver clocks can be

Voice Mode Message Transfer Details

Radio Header								Data						
			ID											
Bit Sync	Frame Sync	Flag	Destination Repeater Callsign	Departure Repeater Callsign	Companion Callsign	Own Callsign	PFCS	Voice Frame	Data Frame	Voice Frame	Data Frame	- - -	Voice Frame	Last Frame
64bit	15bit	1byte	8byte	8byte	8byte	8byte	2byte	48bit	48bit	48bit	48bbit		48bit	48bit

Fig 3—Bit pattern in digital-voice mode.

corrected without requiring a master clock signal. It also means that another amateur can tune into the middle of a contact and listen to the conversation without waiting for the sync frames of the radio header at the next over.

Modulation

Several modulation methods were investigated during the development of the D-STAR standard. Modulations tested included GMSK, FSK, 4-FSK, MSK and QPSK. GMSK has been selected for the backbone line between repeaters. The standard for the portable and mobile transceivers may include more than one modulation format.

Gaussian minimum-shift keying (GMSK) and quadrature phase-shift keying (QPSK) are the two finalists. A third, 4-FSK, has been recently proposed as an alternate standard and is now under investigation. The reason for the delay is that selecting the best modulation for D-STAR real world applications is not a trivial exercise. In real mobile communications systems, the link between a moving node and a base station will be subject to multipath, which results in Rayleigh fading. This will have a significant effect on the resultant BER performance, possibly increasing the required C/N for a specific BER by as much as 10 dB.

QPSK is commonly used in fixed-link communication systems. Under ideal conditions, QPSK would give better performance than GMSK or 4-FSK and its higher spectral efficiency is obviously attractive. However, QPSK's higher spectral efficiency also leads to higher susceptibility to transmission impairments such as multipath and phase hits. Yet, the biggest disadvantage of QPSK is the need for extremely linear power amplifiers to avoid spectral growth—what we Amateurs call splatter.

The front-runner at the time this article is written is GMSK. In its favor, GMSK is a well-proven technology, and probably the most commonly used digital modulation in the world for portable applications (see Table 4). GMSK has two basic advantages. First, it is more robust than QPSK to common transmission impairments. Second, GMSK, as a form of FSK, has constant amplitude and can therefore use very efficient class-C power amplifiers. Third, GMSK is not as sensitive to frequency errors between the transmitter and receiver. Because no master frequency reference is available in the D-STAR system, tuning errors on a 1.2-GHz signal can be substantial, particularly with the extremes of temperature found in portable operation. The alternatives are to suffer the expense of a precision frequency reference in all the radios or adopt a modulation method like GMSK that is more tolerant of frequency errors.

Table 4—GMSK is used in Systems Worldwide

GSM cell phone
DECT
Cellular Digital Packet Data (CDPD)
Mobiltex

However, GMSK is not so spectrally efficient as QPSK. For instance, at 128 kbps, GMSK with a BT product of ½ occupies a bandwidth of 135 kHz. For the same data rate, QPSK requires only 83 kHz.

The best solution is probably to use a codec with the AMBE algorithm described earlier that reduces the data rate as far as possible and then use GMSK for more robust communications, but the tests still continue.

Fig 4 is a somewhat busy graph that dramatically shows the difference in occupied bandwidth. The existing FM system bandwidth can be determined by Carson's Rule to be about 16 kHz. While not all combinations of modulation and codec algorithms are shown, you can clearly see that you can fit many more digital voice contacts into the same spectrum.

Repeater

The digital voice mode is half-duplex with a 20-MHz offset between transmit and receive frequencies. High-speed data is simplex.

As shown in Fig 5, much of the repeater site function is to provide a

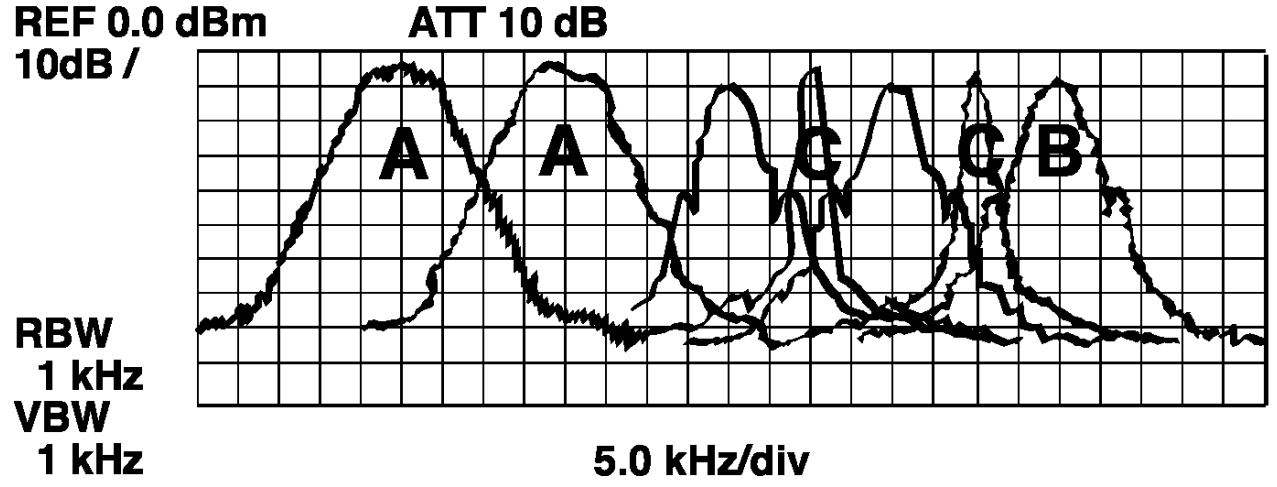

A: Conventional FM
B: GMSK and ITU G.723.1
C: GMSK and 2.4 kpbs AMBE
Unmarked: QPSK and ITU G.723.1

Fig 4—Occupied bandwidth of digital radio.

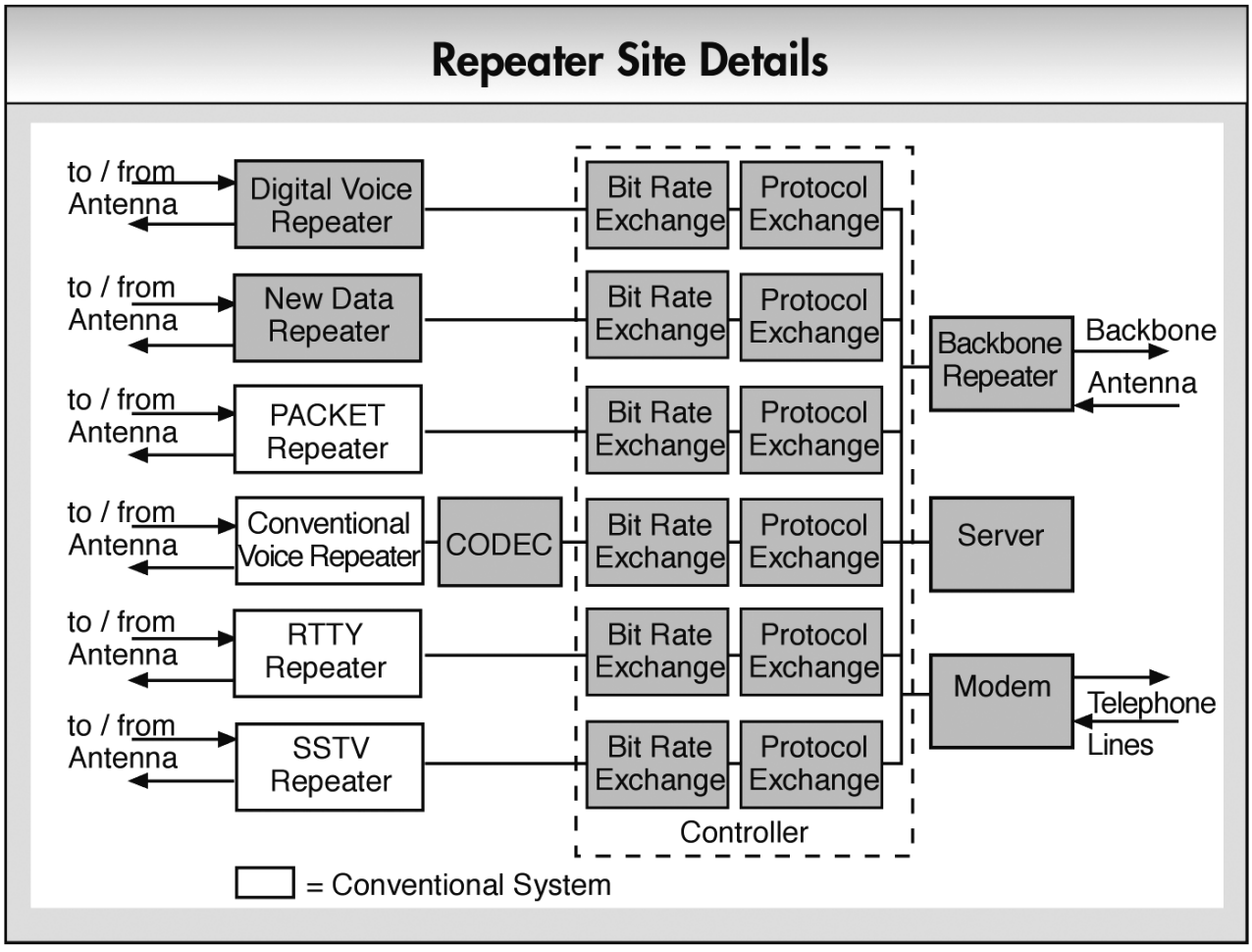

Fig 5—Integrated site with analog and digital radio repeaters, high-speed backbone and Internet connection.

gateway to other repeaters, both at other sites and to repeaters on different modes. The repeater also provides an interface to the repeater backbone link to the Internet if desired. The system is designed to support remote control of the repeater over radio and/or landline links.

Repeaters could be linked via the Internet instead of the backbone, but because of bandwidth limitations, much of the high-speed multiple contact capability would be lost.

Repeater Call Sign Protection

To protect repeaters from co-channel interference, CTCSS tones are used to prevent interfering signals from triggering the repeater. In the D-STAR system, the digital header contains the call sign of the repeater to be accessed. If the repeater does not see its call sign in the message, the repeater is not opened.

The Backbone Repeater Link

One of the major advantages of the D-STAR system is the full-duplex 10-MHz-bandwidth backbone link between repeaters. This wide bandwidth allows multiple voice and data contacts to occur simultaneously on the link. An analysis of the frequency of use of data and voice communications demonstrated that a 10-Mbit/s full-duplex link would support the needs of up to 12 linked repeaters.

The high-speed data and digital-voice data streams from multiple repeaters are multiplexed into a single data stream according to the asynchronous transfer mode (ATM) standard. This 10-Mbit/s data stream is GMSK modulated onto a 10-GHz carrier, resulting in an approximately 10-MHz wide signal.

The ATM cell is made up of a short 53-byte packet that consists of a 5-byte header and a 48-byte payload. The ATM cell is sent to the required destination according to the preset list that is set by the ATM switch set at each repeater site. Because the priority level can be designated in the header, voice signals arrive in real time. This avoids the delays that happen with VoIP on the existing Internet Protocol.

Backbone field tests have been carried out with a 36-dB-gain parabolic antenna and a 1-W transmitter. Heavy rains in southern Japan of more than 12 inches per hour limit the practical distance that the repeaters can be separated. It was found that taking into consideration these extreme weather conditions, the maximum range for uninterrupted communications is about 12 miles. Obviously, the fog and rainfall at the location and the acceptable probability of communication interruption dramatically affect this number.

Notes

[1]"JT44: New Digital Mode for Weak Signals," (World Above 50 MHz) *QST*, June 2002, pp 81-82.

[2]D. Smith, KF6DX, "Digital Voice: The Next New Mode?" *QST*, January 2002. For a discussion of MOS, see the sidebar, "How Do I Sound?" on pp 29.

[3]K7NWS is a Seattle, Washington, repeater and KB7WUK is a Portland, Oregon, repeater on the Evergreen Intertie. These examples assume an identical system to the Evergreen Intertie but based on D-STAR. □□

Linrad: *New Possibilities for the Communications Experimenter, Part 4*

Examples of simple Linrad *use with an amateur transceiver (IC-706) yield improved noise blanking and filtering*

By Leif Åsbrink, SM5BSZ

Linrad is designed to fit any hardware that can supply a digital data stream to a PC computer. Of course, station performance improves with two channels having a large bandwidth, but running *Linrad* with only one channel at a bandwidth of a few kilohertz can produce dramatic performance improvements for a conventional amateur receiver. *Linrad* is still at an early stage of development and the only processing mode currently available is "weak-signal CW." This mode has no AGC and it is fine for 144-MHz EME. It can be used for ordinary CW and SSB just by setting suitable bandwidths, but dedicated modes with AGC and AFC optimized for these activities will be incorporated in the future.

Dynamic Range with and without Noise Blanker

Dynamic range, the ability of a receiver to receive a weak signal without degradation in the presence of one or more strong signals, is one of the most important characteristics of a receiver. It is well known that intermodulation-distortion measurements are often inaccurate. See, for example, Ulrich Rohde's article in *QEX*, Jan/Feb 2003. Also the dynamic range achievable when there is only one strong undesired signal is often seriously incorrect due to inadequate measurement procedures.

Before going into how *Linrad* can be used to improve the dynamic range of a receiver, I think it is appropriate to define things carefully. Firstly, definitions may differ in a way that makes numbers very different while the actual measurement behind the numbers is the same. Such measurements can be converted from one definition to another. Secondly, completely different dynamic-range properties of a receiver may be characterized by similar names. If such measurements are compared with each other, the result is meaningless.

All dynamic-range measurements relate something to the weakest signal that can be received. Let us call it MDS (for minimum discernible signal) without going into details at this point.

Dynamic-range measurements can be classified into four types:

1. One-signal dynamic range: The power of the strongest signal that can be received without distortion divided by the power of the MDS.

2. Two-signal dynamic range: The power of the strongest signal that can be present at the same time as a signal at the MDS power level is received, divided by the MDS power level.

3. Three-signal dynamic range: The power of the strongest signal pair that can be present at the same time as a signal at the MDS power level is received, divided by the MDS power level. Both interfering signals have the same power level and the power to divide by the MDS power is the power of one of them.

Type 1 is not often interesting in Amateur Radio. Very good values can be achieved by use of AGC in RF and IF sections. The ARRL lab has their own definition of blocking dynamic range which is denoted BDR* in this article. BDR* measurements of the FT-1000D show that this receiver can tolerate a 0.1 W signal into the front end without blocking.

Type 2 is typically limited by reciprocal mixing due to phase noise in the local oscillator(s). This dynamic range can be greatly improved by *Linrad*

Jaders Prastgard 3265
63505 Eskilstuna, Sweden
leif.asbrink@mbox300.swipnet.se

under certain circumstances, as will be shown below. State-of-the-art variable-frequency local oscillators set a limit somewhere around 140 dBc/Hz with 20-kHz frequency separation, which corresponds to 116 dB in 250 Hz. BDR* values are often much higher and should not be confused with type-2 measurements.

Type 3 has been discussed extensively in amateur literature. Details are beyond the scope of this article, but the setup described below is easily extended to a very accurate and reproducible method for measuring intermodulation-free dynamic range.

To make the above definitions exact, one must define the MDS and a precise level of degradation as negligible. MDS can be defined in many ways and it may depend on the mode CW, SSB or FM. For the purpose of comparing amateur receivers—where the interesting dynamic range limitations, type 2 and type 3, originate in circuits ahead of the bandwidth limiting filter—it is enough to measure MDS in one mode. It is natural then to use one of the linear modes CW or SSB.

The ultimate limit for receiver sensitivity is the noise floor. The MDS is directly proportional to the noise floor, and I propose using the power level of the noise floor in 1 Hz bandwidth to define the MDS power. For the definitions, I assume the receiver is connected to a signal source that is impedance-matched to the nominal impedance of the receiver, typically 50 Ω. A completely noise-free receiver then has the MDS power equal to kT, where k is Boltzmann's constant (1.38066×10^{-23}) and T is the absolute temperature of the resistor. With T = 293 K (room temperature), one finds $P = 4.045 \times 10^{-21}$ W = –173.93 dBm. For simplicity, we define room temperature as the temperature where a resistor delivers –174 dBm for each hertz of bandwidth.

Rather than specifying the MDS power in dBm, or more precisely in dBm/Hz (it is a power density in W/Hz), one can specify the MDS power density in decibels above the room temperature resistor at –174 dBm/Hz. This number is the noise figure of the receiver and it is a generally accepted figure of merit for receiver sensitivity.

To make measurements easy and compatible to transmitter measurements, it is a good idea to define acceptable degradation as 3 dB. If the sideband noise of a transmitter with a poor local oscillator is measured to a certain power density in –dBc/Hz, an otherwise perfect receiver with the same local oscillator will have exactly the same type-2 dynamic range. This could also be specified as an effective noise floor in dBc/Hz where the "c" stands for the power of the carrier of the undesired signal.

The two-signal dynamic-range noise floor in dBc/Hz is equal to $NF–P–174$, where P is the power level (dBm) of a signal that degrades the S/N of a weak signal by 3 dB, and NF is the noise figure in decibels. This is a very precise definition and it is easy to set up a measurement that will give reproducible results with a known accuracy. If we want the dynamic range itself, not its associated noise floor, we must divide the other way around: $DR = (174 + P – NF)$ dBc × Hz.

It is obvious what this definition means if the receiver dynamic range is limited by reciprocal mixing—and this is usually the case in modern receivers. If the dynamic range were limited by blocking, it would be less clear. There is a chance that both signal and noise are reduced simultaneously when a strong, off channel signal is applied. This kind of blocking, to the extent that it does not change S/N, can be compensated by a fast AGC and is less serious than a loss of S/N, which cannot be compensated. Blocking can be measured separately and the corresponding figure of merit is BDR*, the blocking dynamic range. It's good practice to specify BDR* in those rare cases where it's less than the two-signal dynamic range defined above.

To show how *Linrad* can be used to improve the dynamic range of an IC-706MKIIG, the setup of Fig 1 was used.

The HP-8657A generator was set to –106 dBm. The star connector contains 25-Ω resistors so the power level reaching the spectrum analyzer and the IC-706 is –130 dBm. The spectrum analyzer is connected to monitor the frequency and amplitude of the free-running vacuum-tube signal generator, which has very low phase noise but lacks calibration in both frequency and amplitude. The 10-dB attenuators are identical to within 0.1 dB, so the input signals to the IC-706 are identical to those to the HP-8591A to within 0.2 dB. Each signal level is probably accurate to within 1 dB.

When only the HP-8657 was running, the signal level as measured by the *Linrad* S-meter was 48 dB, while the noise floor was 31 dB in a 100-Hz bandwidth. A –130-dBm input signal thus produces 37 dBc/Hz, so the noise floor is at –167 dBm/Hz. That means the noise figure of the IC-706MKIIG is 7 dB.

In the measurement setup, the strong signal is passed through a filter with a deep notch at 10.683 MHz, as can seen in Fig 1. The frequency response of this filter is shown in Fig 2 and the schematic diagram is in Fig 3.

A notch filter like this is reasonably easy to design. To make it useful for intermodulation measurements, the input and output transformers are wound on rather large iron-powder cores, T80-6 from Amidon. With a high transformation ratio, the notch becomes deeper and wider. The filter I have used is rather narrow with a transformation ratio of only 4:1. The notch is then only about 5 kHz wide at the 1-dB points while the attenuation is about 60 dB at the notch center. The filter is flat from 9 to 12 MHz.

The desired signal is placed at the frequency of the notch and the sideband noise of the strong signal is improved by 40 dB by the notch filter. This way, the measurement setup has much greater dynamic range than the IC-706 or any other receiver. The amplitude of the strong signal is adjusted until the S/N for the desired signal is degraded

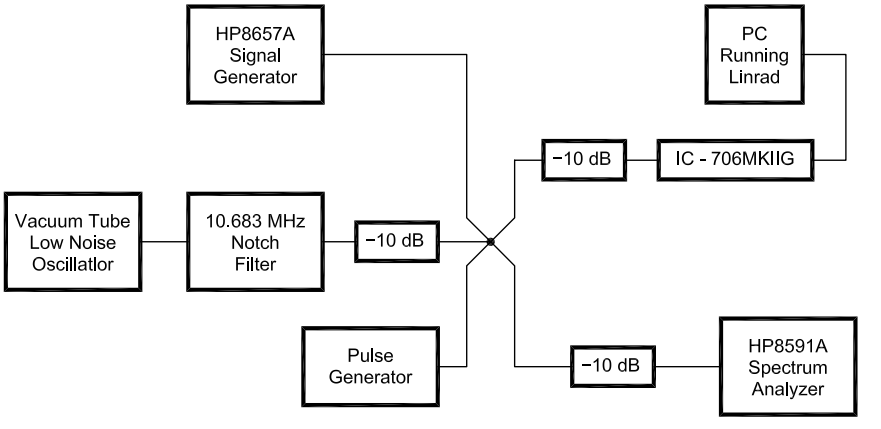

Fig 1—Setup for dynamic range measurement. One strong and one weak signal are summed and a pulse generator can be switched on to measure how the noise blanker is disturbed by strong signals.

by 3 dB, and the corresponding power level is recorded for each frequency.

The measurement procedure mimics the real situation for which the two-signal dynamic range is the relevant figure of merit. It is up to the tester to find a combination of gain control, AGC, blanker and other settings that maximize the dynamic range.

Two series of measurements were made on the IC-706: one with the weak and the strong signal only, another with the pulse generator added. For the measurement, the pulse generator was set to emit pulses repeating at 250 Hz. Without a noise blanker, the pulses lifted the noise floor of the IC-706 by 35 dB. When the IC-706 noise blanker is switched on, the noise from the pulse generator is reduced by 28 dB for a remaining degradation of 7 dB. Table 1 shows what signal level is required to degrade S/N by 3 dB in the two cases. Since the noise floor is at –167 dBm/Hz, the dynamic range is 127 dBc Hz at a frequency separation of 20 kHz.

Now, what has all this to do with *Linrad*? The interesting thing is that if the IC-706 noise blanker is switched off and the *Linrad* noise blanker is switched on, the big losses of dynamic range caused by the noise blanker disappear completely. This is a qualitative difference, not just a small improvement. The reason is obvious: The narrow filter of the IC-706 prevents the strong signal from reaching *Linrad* at all. Actually, it is even better than that because the dynamic range of the IC-706 is limited by reciprocal mixing. The strong signal can be made another 6 dB stronger before reciprocal mixing causes degradation of the elevated noise floor. With the IC-706 blanker switched off and the *Linrad* blanker switched on, the pulse generator lifts the noise floor by 6 dB, which adds one more decibel in favor of the *Linrad* blanker.

If the pulse generator were run at 500 Hz, the IC-706 blanker would not work well any more. The S/N of the desired signal is degraded by 17 dB. If the IC-706 blanker was switched off and *Linrad* allowed to take care of the problem, the 500-Hz pulse repetition frequency would cause a S/N loss of 8 dB only.

If the pulse amplitude were reduced by 6 dB for a S/N degradation of 29 dB without any noise blanker, the IC-706 blanker would reduce the degradation to 6 dB; while the *Linrad* blanker would reduce the S/N loss to below 0.5 dB at a pulse repetition frequency of 250 Hz. As soon as the pulses are small enough to stay within the linear range of the IC-706's IF, product detector and audio sections, the blanker works with mathematical precision and removes interference pulses almost completely.

In case the pulse amplitude were reduced by 20 dB, the degradation due to 500-Hz pulses would be 17 dB if no blanker were used. The IC-706 blanker does not work at all in this situation, but the *Linrad* blanker is very successful: The S/N loss is less than 3 dB. Pulses that are too weak to trigger the IC-706 blanker are nearly eliminated by the *Linrad* blanker. The 3 dB S/N loss is due to loss of signal. If the level of the desired signal were reduced to a typical 144-MHz EME level corresponding to –150 dBm into the IC-706, the signal loss caused by the blanker would affect the noise to the same degree as it affected the desired signal. The S/N loss would be a few tenths of a decibel only. The pulses have to be made much stronger even at 500-Hz repetition rate to give any noticeable S/N degradation.

I do not know how the IC-706MKIIG compares to other receivers, but I believe the results for the IC-706 are typical. What may differ is the linearity and noise floor of the IF, product detector and audio section. A traditional noise blanker is always a compromise. More bandwidth for the blanker improves pulse suppression and allows somewhat stronger undesired signals in the blanker passband. On the other hand, the number of strong signals and the risk for getting a very strong signal into the passband increases with blanker bandwidth. A variable blanker threshold is valuable; if there are no strong signals to worry about one can set the threshold low and eliminate weaker pulses.

How the *Linrad* Noise Blanker Works

Unlike conventional blankers, the *Linrad* noise blanker does not gate out the entire signal for the duration of a noise spike. *Linrad* has a calibration procedure during which a pulse generator is used to send pulses into the antenna connector of the radio hardware. The calibration pulses are typically 20 ns and they have a flat spectrum from dc to 30 MHz. *Linrad* assumes the radio hardware is perfectly linear and can calculate the exact properties of the entire filter chain that is between the antenna and the digital world inside the PC. Knowing exactly what total filter response the signal has been subjected to, *Linrad* can add one more filter in the signal path that gives the total filter chain any desired characteristics that are compatible with modest gain in the digital filter. It is of course impossible to recover frequencies that have been strongly attenuated without serious loss of dynamic range.

Thanks to the calibration, *Linrad* has an optimum pulse response for the available bandwidth. This makes it easier to locate pulses. *Linrad* also knows the exact shape of an interference pulse, so it will subtract the known shape from the data stream. The data stream on which the blanker operates does not contain any strong signals. The first FFT is used to split the incoming signal in two groups. One group contains all strong signals, the other contains all weak signals and the noise floor.

Since most of the spectrum belongs to the weak group, most of the pulse energy is there and the pulses are not much distorted. To compensate for the distortion, one just divides the peak amplitude by the square root of the fraction that the weak signals constitute out of the entire spectrum. This way, the correct pulse is subtracted. Pulses are correctly subtracted from the entire signal—the strong signals too, despite the fact that they were excluded from the blanker input data. At present, the need of using MMX instructions destroys the blanker operation on strong signals. There are several other complications arising from the fact that *Linrad* is designed to work with two channels at 96 kHz bandwidth on a 600 MHz Pentium III. By the time computers are fast enough, it will probably be more interesting to increase the bandwidth than to avoid the CPU-load-related complications that are already in the code; but someday, they can be removed, which will make setup somewhat easier.

Table 1—Level of Interference Required to Degrade Sensitivity by 3 dB at Different Frequency Separations

Offset (kHz)	*Pulses Off (dBm)*	*Pulses On (dBm)*	*Loss due to Pulses (dB)*
5	–55	–97	42
10	–47	–91	44
15	–43	–71	28
20	–40	–60	20
25	–39	–54	15

Linrad uses several averaged power spectra to decide whether a frequency bin should be routed to the group of strong signals or whether it should be routed to the blanker input. The two averaging numbers for fft1 as well as the fft2 average number therefore affect the blanker operation. There are two level controls for the blanker: One selects what S/N should be considered a strong signal. The other sets the blanker threshold that controls what signal-level peak is considered to be a noise pulse. *Linrad* also has a conventional blanker, but it is of lesser use when the input bandwidth is only 3 kHz. For more information about the *Linrad* noise blanker, look at **antennspecialisten.se/~sm5bsz/linuxdsp/blanker/leonids.htm**.

The *Linrad* Blanker on 7 MHz With the IC-706

Fig 4 shows a sequence recorded from 7 MHz. About a dozen CW stations are visible during the 35 seconds of the recording. The numbers at the left side of the waterfall show minutes and seconds of the recording. The recording was made with a pulse generator connected in parallel with the antenna. The pulse repetition frequency was set to 100 Hz and the noise floor was lifted by 30 dB when no blanker was running. The IC-706 blanker reduced the degradation caused by the pulse generator to 10 dB while the *Linrad* blanker reduced

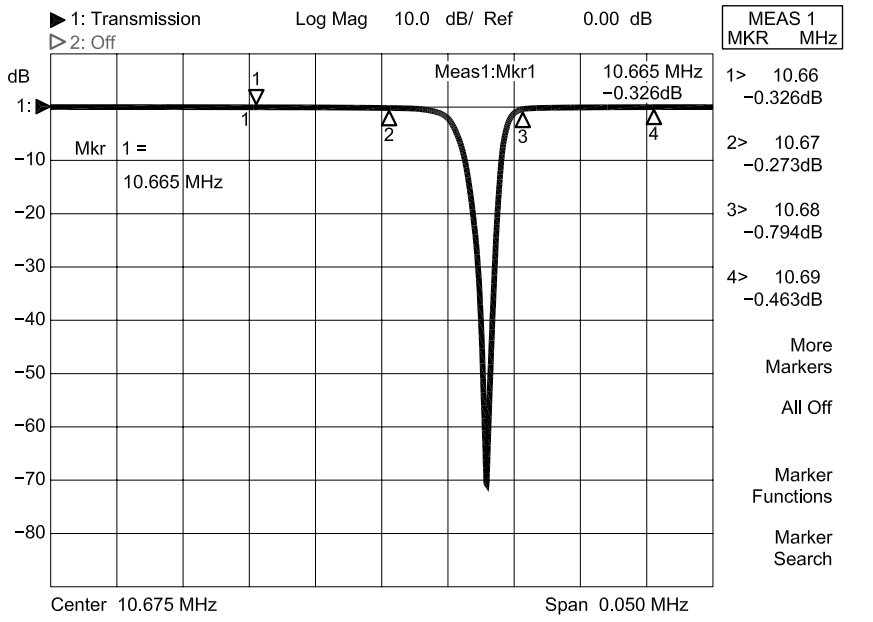

Fig 2—Frequency response of the notch filter.

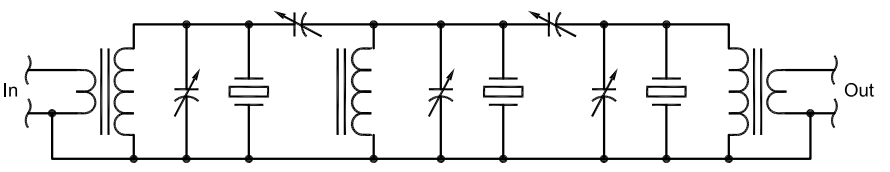

Fig 3—Schematic diagram of the notch filter.

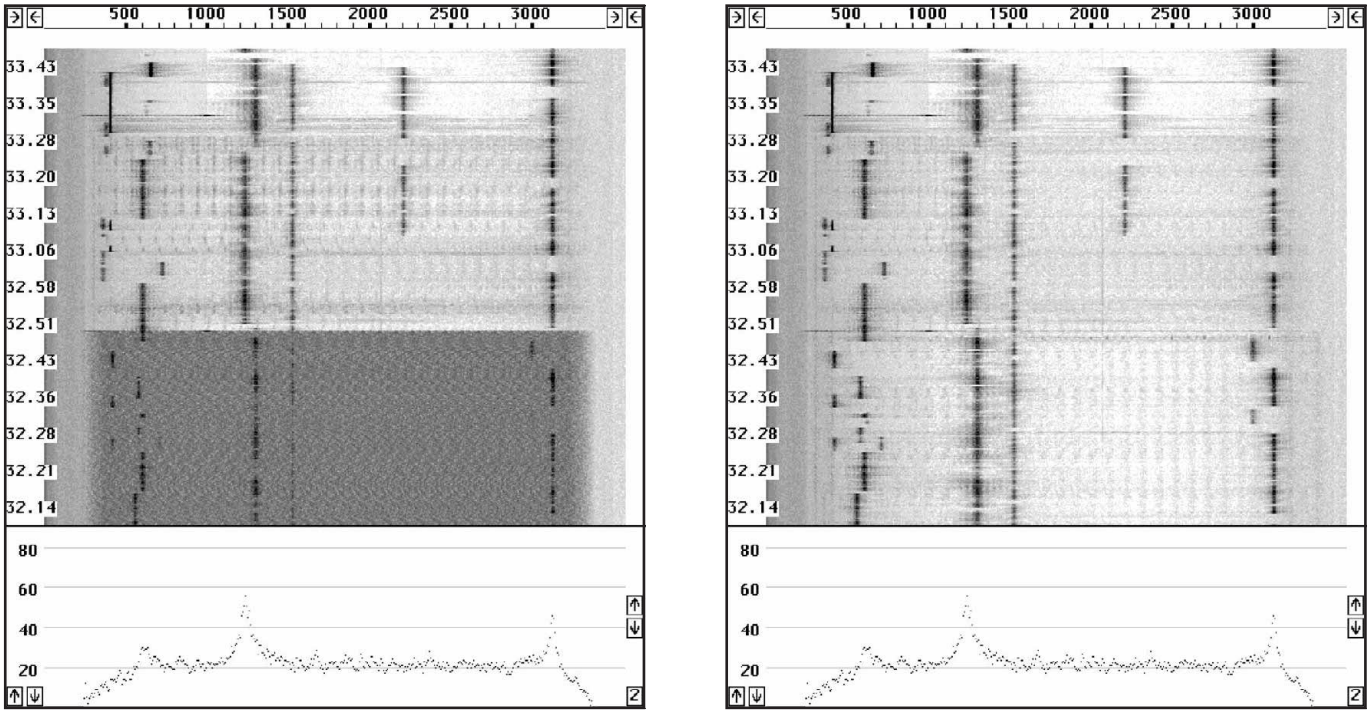

Fig 4—A digital sequence recorded with the IC-706 operating on 7 MHz processed with *Linrad*. A is with the *Linrad* noise blanker off, while the B is the same data with the *Linrad* blanker on. The pulse generator is added to the antenna signal from 32.10 to 33.30 and the IC-706 blanker is running from 32.50 to 33.32. From white to black is 40 dB. Note that the lowest noise floor is with the IC-706 blanker disabled.

it to 5 dB. The IC-706 RF gain was reduced until the AGC no longer reacted on the strongest signals and the AF volume was set just below the level where audio overtones were produced. The passband ranges from 300 to 3300 Hz and the *Linrad* mode-dependent parameters are set as described below.

Fig 4 shows the minimum improvement by use of *Linrad* instead of the built-in blanker of the IC-706 under circumstances when there is no signal within the 3 kHz passband that drives the product detector or audio section non-linear.

If the amplitude of the pulses were reduced, the difference between the built-in blanker and *Linrad* would become bigger; and if a strong signal occurred outside the 3 kHz passband, the difference would be enormous.

Setting up *Linrad* for Use With an IC-706 or Similar Receiver

A suitable sampling speed is 8 kHz. Place the 3 kHz passband of the IC-706 from 0.5 to 3.5 kHz or so. Set these parameters on the first mode parameter screen:

- First FFT bandwidth [10]
- First FFT window (power of sin) [3]
- First forward FFT version [2]
- First FFT storage time (s) [0]
- First FFT amplitude [30]
- Enable second FFT [1]

With a desired bandwidth of 10 Hz and a sine^3 window, *Linrad* selects a transform size of 1024 at a sampling speed of 8 kHz, which leads to a delay of 0.26 seconds because the input is in real format, so 2048 points are needed to compute one transform. Since the second fft is enabled, there is no reason to store old fft1 transforms. (This may change in the future.) Setting the first FFT amplitude to 30 is a good idea only if the radio hardware has much less dynamic range in the audio section than the sound card. It is easier than attenuating the signal from the IC-706 with resistors and serves the same purpose.

Then set these parameters on the second mode parameter screen:

- First backward FFT version [0]
- Sellim maxlevel [6000]
- First backward FFT *att. N* [4]
- Second FFT bandwidth factor in powers of [0]
- Second FFT window (power of sin) [2]
- Second forward FFT version [0]
- Second forward FFT *att. N* [7]
- Second FFT storage time [15]

If your computer is modern enough to support MMX instructions, there is no need to use them when processing a single channel that is sampled at 8-kHz only; so it is safe to set fft versions to 0. If your computer is better than a Pentium I, you may as well set the highest number. The *att. N* parameters control how the bits are shifted to prevent overflow or quantization noise. This is one of the complications coming from use of 16-bit arithmetic to save CPU time. It is completely useless in this case, but the code is optimized for other more demanding tasks. This link gives information about the *att. N* parameters and how they influence the processing: **antennspecialisten.se/~sm5bsz/linuxdsp/install/dlevel.htm**. Enable AFC/SPUR/DECODE on the next screen, and select the default parameters on the screen that follows.

Then set the final mode parameter screen like this:

- First mixer bandwidth reduction in powers of 2 [1]
- First mixer no of channels [1]
- Baseband storage time (s) [30]
- Output delay margin (0.1 s) [3]
- Output sampling speed (Hz) [8000]
- Default output mode [1]
- Audio expander exponent [3]

The baseband will be represented as *I* and *Q* with a sampling rate of 2 kHz. Make the bandwidth reduction larger if you want to save memory or CPU time when playing with really narrow filters. Notice that 1 kHz is the largest bandwidth you can have in the

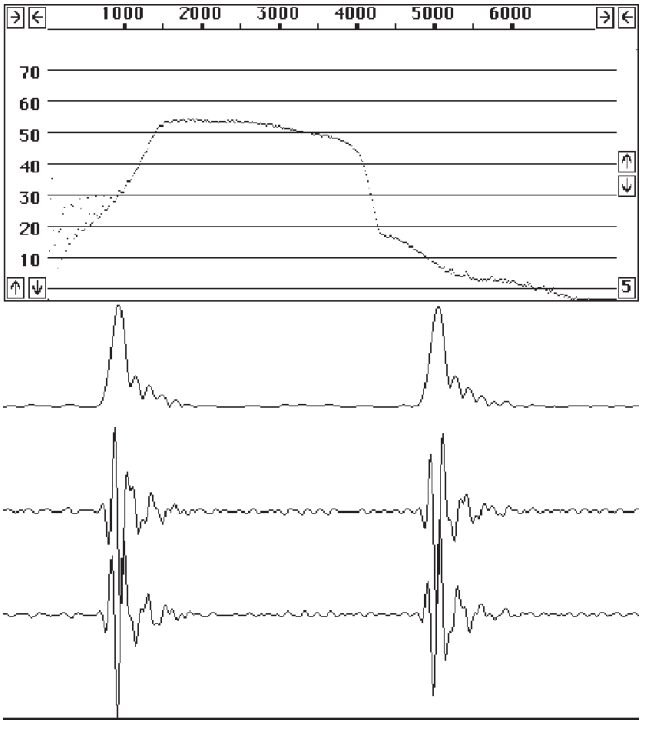

Fig 5—Frequency response and pulse response of the IC-706 as measured with *Linrad* in the uncalibrated state.

Fig 6—With one more filter in the signal path *Linrad* converts the frequency response to the curve selected by the operator during the calibration process. The pulse response is made symmetric and as short as possible with the skirt steepness selected.

output with the above settings, which maximize the output bandwidth. *Linrad* never gives more output bandwidth than 25% of the input bandwidth. If you want to process SSB signals, you must oversample the input at, for example, 24 kHz.

When set up as suggested here, *Linrad* should run with a CPU usage of about 22% on a 200-MHz Pentium MMX and 75% on a Pentium at 60 MHz. With the above parameters, 16 MB of memory is sufficient.

The *Linrad* Calibration Procedure

Besides the various spectra that display the signal in the frequency domain, *Linrad* has oscilloscope functions that display signals in the time domain. Fig 4 shows the result of feeding pulses into the IC-706 in both the frequency domain and in the time domain. In the frequency domain, we just see the frequency response of the signal reaching the loudspeaker. The filter bandwidth is 2.7 kHz at the –6 dB points if the slope of nearly 10 dB across the passband is accounted for. The lower amplitude towards the upper edge of the passband does not affect receiver performance, and it does not matter whether it originates in the IF filter or comes from the audio section. It is a matter of taste how the operator wants bass or treble set in the audio section and presumably ICOM has adjusted it to fit the built-in loudspeakers in a way that is generally acceptable.

There is only one problem with a sloping frequency response like that of the IC-706. If one measures the minimum discernible signal, MDS, in the way adopted by ARRL Lab, one must measure the frequency response and evaluate the correct noise bandwidth, which is a bit less than the filter bandwidth. The noise floor (in dBm/Hz) is constant across the passband regardless of the audio response.

The pulse response in the time domain is the Fourier transform of the frequency response. There is a lot to say about Fourier transforms in general; it can be found in mathematical textbooks. The transform of a soft function will be sharp and vice versa, for example. The steep edges of the filter at about 1 kHz and at about 4 kHz causes oscillations at 1 and 4 kHz in the time domain, while the wide flat region in the frequency domain corresponds to a short pulse in the time domain.

The oscilloscope traces of Fig 5 show the time-domain signal after it has been converted to a complex signal pair (I and Q) at half the original sampling speed. In the time function, the two lower tracks are I and Q, respectively, and the upper track amplitude is $(I^2 + Q^2)^{1/2}$. Most of the pulse energy is an oscillation at 2.5 kHz that lasts about one-and-a-half cycles. This is the energy from the essentially flat region of the passband. After the main structure, there are oscillations at about 1 kHz and about 4 kHz. These oscillations decay about five times more slowly than the main oscillation because the skirt steepness corresponds to a filter with five times higher Q than that associated with the filter bandwidth. The oscillation at 4 kHz is about 10 dB weaker than the oscillation at 1 kHz because of the 10 dB slope.

To show more clearly what happens, Fig 5 is produced with a sampling speed of 48 kHz, which results in a time function with eight times more resolution. This has no other good effects than making the oscilloscope traces easier to see. The CPU load increases and the calibration procedure becomes difficult because there is no pulse energy over most of the sampled frequency range.

Fig 6 shows the time-domain and the frequency-domain responses after *Linrad* has been calibrated. The input signal is identical to the signal used for Fig 5. The pulse is still an oscillation at about 2.5 kHz that lasts for one and a half cycles, but the wider oscillations associated with the filter skirts are now symmetrical around the main peak, and the peak amplitude of the oscillations is about 6 dB lower. Notice that the frequency response is absolutely flat from 1.8 to 3.4 kHz. This is the frequency response associated with the time function shown in the oscilloscope tracings. Since the curvature of the filter is precisely known, it can be accounted for: The waterfall diagram is perfectly flat from 1.0 to 4.3 kHz.

It is up to the operator to select the frequency response. It is not very critical and something like Fig 6 is fine. The operator can choose because the *Linrad* noise blanker is still based on rather simple routines and 16-bit arithmetic is used to save CPU time. A very soft filter may cause quantization noise toward the spectrum ends, while very steep skirts may cause loss of accuracy due to overlapping pulses.

The first screen of the calibration procedure is shown in Fig 7. This screen is intended for adjustment of signal levels and pulse-repetition frequency. The upper track shows the power in a logarithmic scale, while the lower track shows the input signal in linear scale exactly as it is read from the sound card. The pulse-repetition frequency must be set low enough for the flat noise floor between the pulses in the logarithmic scale to be at least 50% of the total time. RF and audio volume controls as well as the amplitude of the pulse generator should be set to maximize the S/N of the pulses.

When the screen looks good, press [Enter] to start collecting an average of the pulse response. The next screen will show how the accumulated pulses look when translated to a frequency response.

As can be seen from Fig 7, the pulses cannot be averaged directly. They have a random phase and direct averaging will produce zero. Instead, the Fourier

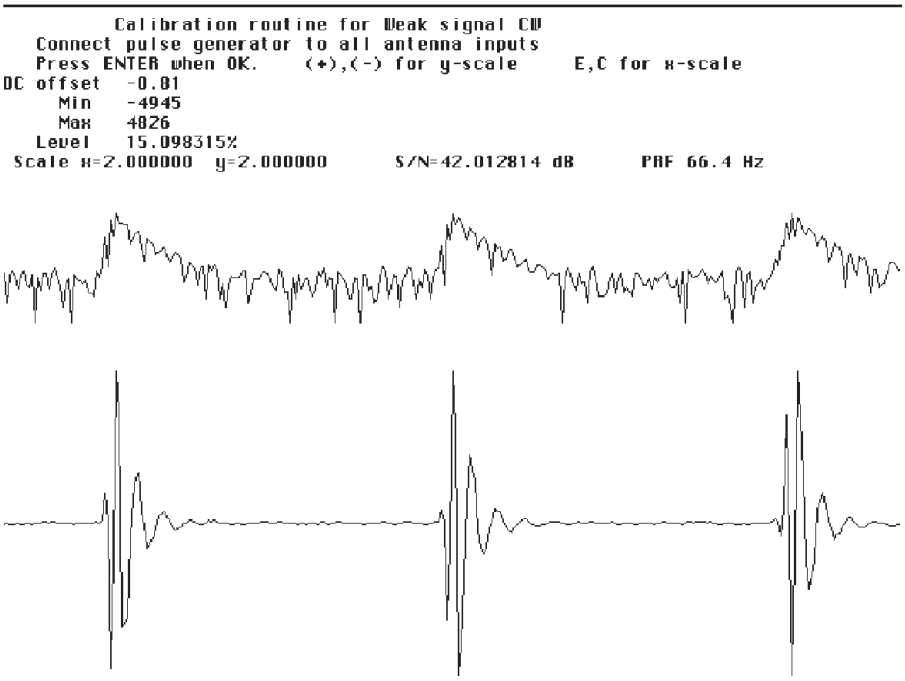

Fig 7—The first screen of the *Linrad* calibration procedure.

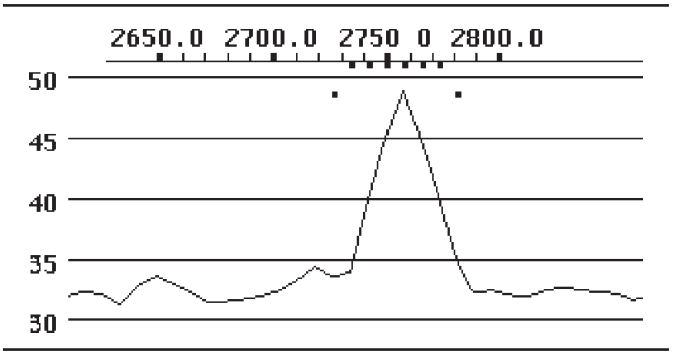

Fig 8—Baseband filter with 40-Hz bandwidth from a 256-point FFT. On screen, the size is indicated in the upper right corner as 8, the corresponding power of two, but that is not visible in this image. Carrier and sidebands of the CW signal are not resolved at this modest resolution.

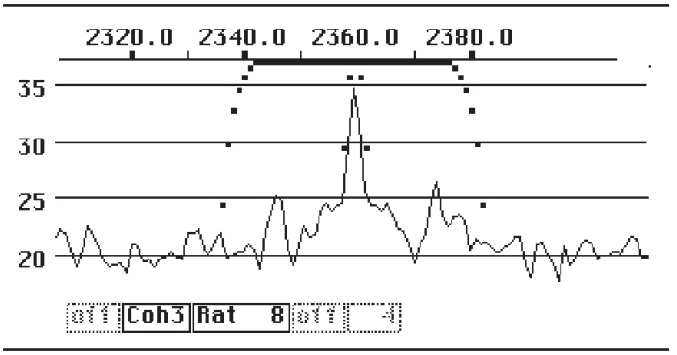

Fig 9—Baseband filter with 40 Hz bandwidth from a 2048 FFT. The signal filter is 40 bins wide, while the carrier filter is two bins wide. With about 1 Hz per fft bin, one can see the CW carrier and the principal keying sidebands.

transform is taken for each pulse. The amplitudes are averaged directly, but the phase is differentiated twice before averaging. The accumulated second derivative is then integrated twice to produce the average phase function. Read more about the details of the *Linrad* calibration procedure here at **antennspecialisten.se/~sm5bsz/linuxdsp/flat/flat.htm**.

Normal Operation of *Linrad*

When everything is set up, watch the waterfall graph. When something looks interesting, click on it and the corresponding signal is routed into the headphones immediately.

With the mode-dependent parameters described above, a typical bandwidth for CW could be 40 Hz. The baseband filter, like all other filters in *Linrad*, is implemented in the frequency domain, so it involves an FFT and an inverse FFT. The time delay through the filter is at least the time it takes to collect all the data points for one transform. With a 2-kHz sampling rate at baseband, the delay for a filter with 256 points is 0.13 seconds. This corresponds to a bin width of 7.8 Hz; so for a 40-Hz bandwidth, one needs six data bins over the flat region of the baseband filter.

Fig 8 shows the baseband graph with such a filter. When *Linrad* is set up like this, the processing delay is 1 s, which is about as much one can tolerate in normal CW traffic. Half of that is a margin that is not required on fast computers. It is set by the "Output delay margin" parameter. The little boxes in the upper-right corner set the size of the baseband FFT. One cannot set a number that is smaller than the size of the window, but the arrows in the upper-right corner can be used to expand the X-axis which will allow a smaller FFT size.

For extremely weak signals, one can switch to coherent processing. To do that, one needs a very narrow filter for the CW carrier so the baseband FFT size has to be larger. Fig 9 shows a typical filter for coherent CW. Here the baseband FFT size is set to 2048, which causes a delay of 1 s for a total processing delay of 2 s. In case where the AFC must run with a delay, the total processing delay will increase correspondingly. Use the F1 (help) key to find out about the different controls in the baseband graph and read more about it at **antennspecialisten.se/~sm5bsz/linuxdsp/run/basebgr.htm**. This link gives some more information about coherent CW: **antennspecialisten.se/~sm5bsz/linuxdsp/demo/coheme.htm**.

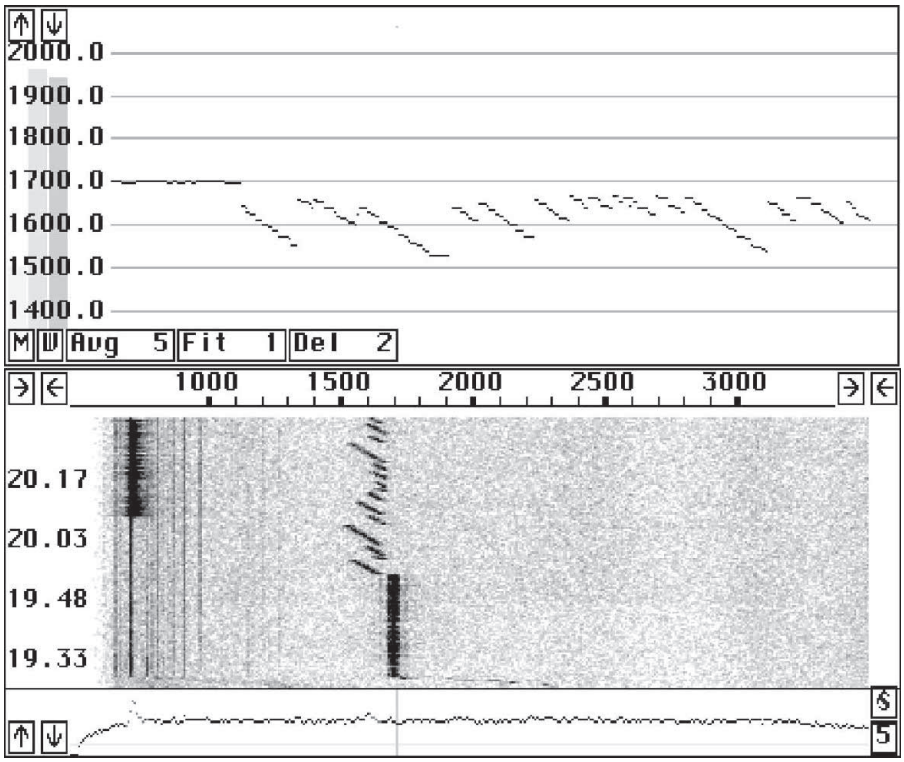

Fig 10—AFC graph (upper) and waterfall graph (lower) showing first a stable station, then a very unstable station drifting at about 1.5 kHz/min.

Using the AFC

It is well known that CW signals can be seen on a waterfall display at levels well below those at which they can be copied by ear. That means of course that the computer can locate CW signals precisely at signal levels below the detection threshold. This is used in *Linrad*. The AFC routine uses the same power spectrum used for the waterfall graph: The second FFT, if enabled, otherwise the first FFT is used.

The AFC is affected by the resolution at which the power spectra are available. The sensitivity increases with reduced bandwidth, but not proportionally, because wider bandwidths allow more averaging. Setting the FFT

resolution narrower than the bandwidth of the signal does not improve sensitivity, but it does degrade time resolution for unstable signals.

The parameters suggested above give a second FFT size of 1024, which yields 4 Hz per bin and a bin bandwidth of about 8 Hz with a sine^2 window. This is adequate to keep signals centered in the desired passband within 1 Hz or so, and a signal that drifts by less than 100 Hz per minute can be located well enough by extrapolation of the frequency from several seconds back in time. That, in turn, means that the frequency is evaluated from typically 25 transforms, giving a S/N improvement of typically 7 dB.

For very unstable signals, the AFC can be run with very little averaging. Fig 10 shows the AFC graph and waterfall graph of a station that drifts by 100 Hz in 30 transforms. The mode parameters are set as described above, so that each transform spans 0.26 s. They overlap by 50% so they arrive at an interval of 0.13 s. The frequency drift is thus 25 Hz/s, which can also be read from the waterfall diagram, since it has both time and frequency scales. For the AFC, an average frequency is computed from five transforms or about 0.8 s. Over this time, the frequency drifts by about 20 Hz, twice the bin width of the FFT. In the waterfall, the averaging is four so it gives a good idea about the input data used to calculate the average frequency for the AFC.

Up to about 19.50, the stable and much stronger QSO partner is transmitting. The S/N is 25 dB in an 8-Hz bandwidth. On screen the AFC graph shows S/N in yellow, not visible in Fig 10. The stable station is at 1700 Hz. For the unstable station, S/N goes from about 17 dB to 13 dB during the transmission. The reason for the sawtooth frequency variation is that short interrupts are made in the transmission now and then. During these interrupts, the S/N falls to about 5 dB, which corresponds to the largest noise component with an averaging of only 2.5 times.

The AFC would normally fit a straight line to the average frequency so as to allow a more precise frequency determination. This will fail for a signal that makes abrupt frequency jumps, therefore the fit parameter is set to 1, which means that the average is used directly. The delay parameter is set to 2, which means that the average frequency is used to process the signal that belongs to the midpoint of the time span from which the frequency is determined. With a S/N of 13 dB in an 8-Hz bandwidth, this signal is not easy to copy at high speed even if the real S/N is a bit higher; the peak is smeared a little by frequency drift. With the AFC keeping the signal at the passband center within a few Hertz or so, the 60-Hz filter that fits the keying speed can be used for reception; at least 200 Hz would be required without AFC.

The example in Fig 10 is not intended to suggest that there is a great advantage in going from 200 Hz to 60 Hz. A trained operator already has a very sophisticated "signal processor" in his brain with a very efficient AFC. The example is intended to show principles only. If the keying speed had been four times slower to fit in a 15-Hz filter, everything would work exactly the same but at a four-times-slower time scale. Then, going from 50 Hz to 15 Hz would be a very significant advantage because the human brain cannot go much below 50 Hz in bandwidth. If the instability is much worse, so the signal moves around by tens of kilohertz, as could be the case on microwaves, the AFC can be set to produce a readable signal at a modest bandwidth if the hardware has bandwidth enough to accommodate the signal.

The UNKN422 challenge at **www.af9y.com** is a really weak 144-MHz EME signal with severe frequency drift. The AFC graph when running this file through *Linrad* is well suited to describe how the AFC can be set up for very weak signals. The ultimate goal is to make the AFC follow the frequency well enough to allow coherent processing of signals far below the level where copying is possible, and then perform averaging on the coherent data. For coherent data, S/N grows in proportion to the number of averages in contrast to non-coherent averaging that improves as the square root of *N* only.

Fig 11 shows how the *Linrad* AFC operates on the UNKN422 challenge. The size of the FFT used to produce Fig 11 was 4096 with a sine^2 window. This means that each transform spans a time of one second and that the bandwidth of each FFT bin is about 2 Hz. The transforms are interleaved by 50%, so two transforms are computed each second. Fig 12 shows a waterfall diagram from the transforms used to produce Fig 11.

The AFC averaging parameter was set to seven, which means that a spectrum was calculated from the average of seven transforms spanning a time of 3.5 seconds. A new average spectrum arrives every 0.5 second, and from each one a frequency and an associated S/N value is calculated. The crosses in Fig 11 show these frequency values and the boxes show the associated S/N values.

Fig 11 has been manually converted to black and white. On the *Linrad* screen the frequencies are green dots while the S/N values are yellow dots. The AFC fit parameter was set to 20, which means that a frequency is obtained by fitting a straight line to 20 of the crosses in Fig 11. This linear least-squares fitting is done with each frequency weighted by its associated S/N value, which should maximize the

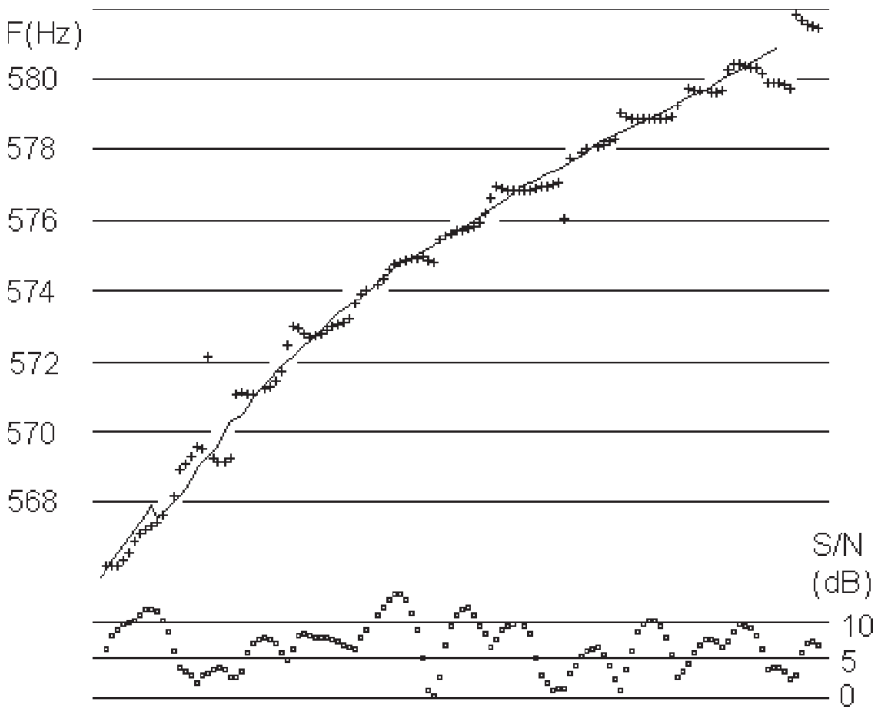

Fig 11—The *Linrad* ACF locked to the UNKN422.WAV file, a very weak EME signal.

probability that the fitted line is correct. This procedure means that the frequency-versus-time function is obtained over a 10 s period, and it does not matter that the signal is below the noise now and then, as can be seen from a comparison of Fig 11 and Fig 12.

The AFC delay parameter was set to 13, which means that the frequency of the straight line 6.5 s back in time is used to process the signal, which is 6.5 s old. This will give the best estimate of the frequency since each frequency value is based on what happened 6.5 s before and 6.5 s after the moment of time where the signal is extracted. The final AFC frequency forms the line in Fig 11 and a corresponding white line on the *Linrad* screen. The latest fitted straight line is shown in red on the *Linrad* screen, but that is not visible in Fig 11.

It is possible to set the delay parameter to zero for somewhat more stable or slightly stronger signals. The fitted straight line would then be an extrapolation and the AFC would not cause any time delay for the processed signal. An extrapolated frequency is of course less accurate, but the operator is free to choose the compromise between time delay and AFC accuracy that he or she finds best.

Spur Removal

Linrad has a procedure that locates very stable signals, spurs, which do not drift by more than a small fraction of the FFT bin width between transforms. This procedure is not yet automated; the user must point to each target signal. The frequency bin with maximum power is located and then a second-order polynomial is fitted to the phase-versus-time function from transform to transform. The phase information is then used to generate a constant-amplitude carrier in anti-phase, which is then added. The result is a very deep and extremely narrow notch filter. Since it is done in the frequency domain, it is very CPU-efficient. *Linrad* can process hundreds of spurs simultaneously and a CW signal that happens to come on top of a spur will be unaffected by the spur removal.

Baseband Processing

The desired signal is converted to frequency zero by means of a fixed frequency or by the frequency calculated by the AFC, if it is enabled. The sampling speed is reduced simultaneously as was described in a previous article *QEX* (May/Jun, 2003, pp 36-43). One of the interesting consequences of using AFC is that the spectrum of an unstable signal becomes narrower. This means that it is meaningful to make a new analysis of the power spectrum and use the improved S/N that can be obtained because of the narrower spectrum. When the AFC is enabled or coherent processing is selected, the baseband filter is not centered on the frequency zero, it is centered at the peak found in the averaged baseband power spectrum. Moving the filter to follow the carrier is a second AFC. It is controlled by the baseband spectrum averaging parameter *fft3 (avgnum)*, and it assures that the filter from which the carrier is extracted truly is centered on the carrier, even if it is only a fraction of a hertz wide. If the primary AFC is used, the time constant of it should be made longer than the time constant of the secondary AFC. The baseband window of the *Linrad* screen shows the frequency selected by the secondary AFC with a green cursor that will automatically place itself on the peak of the carrier. The yellow curves showing the filter in use are not moved around to reflect the filter position, that would be a waste of processing power in the event the process is run at higher data rates for high speed meteor scatter or some digital mode.

The filtered baseband signal can be sent directly to the loudspeaker output after the frequency has been shifted by the amount specified by the BFO setting. It is possible to send the baseband signal to one ear and the carrier to the other. When doing this, one can make the carrier filter wide enough to allow the keying to go through but one can also make it narrower so it will be more like a phase reference for the ear receiving the keying information. Another possibility is to split the baseband signal into two components: I in phase with the carrier and Q 90° out of phase. One can elect to send these two signals I and Q to the two outputs to allow the operator to do the further mental processing. One can also elect to send I to both ears and skip the Q signal entirely.

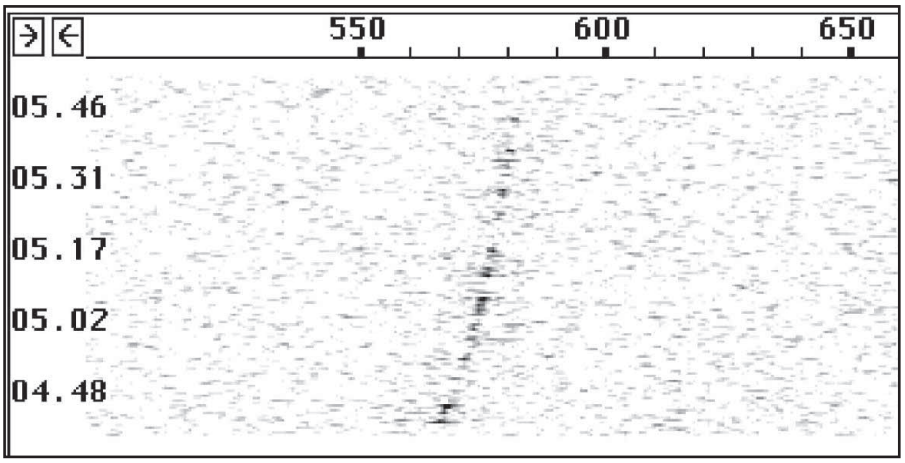

Fig 12—The transforms used to produce Fig 11 presented as a waterfall diagram. There is no averaging, each line is the power spectrum of a single transform.

At the present time, *Linrad* has only a mode for weak-signal CW. Therefore, there is no conventional AGC. The baseband signal is in a complex format, however. When it is limited to make sure it will not saturate the output, the phase angle is retained; the two components of the complex signal are attenuated by the same amount. This corresponds to RF clipping in a SSB transmitter and is equivalent to an AGC with immediate attack and release. A sine wave will not be distorted at all and the weak CW mode is quite useful for normal CW and for SSB despite the lack of a proper AGC function. In the future, I plan to add the conventional operating modes with AGC and noise-reduction algorithms that fit the larger bandwidth. When listening to weak signals, it may help to allow the signal to saturate in the conventional way, in the real-valued format of the output signal. The limiting of the baseband can therefore be disabled so one can get a sensitive measure of signal level by listening to the overtone content of the audio signal. Another possibility is to enable the audio expander, which will magnify amplitude variations of the baseband signal without introducing audio overtones.

Summary

This article has shown how *Linrad* can be used to improve performance of a standard Amateur Radio receiver both by improved noise blanking and by DSP filtering of the audio signal. The next article will focus on the high-end use of *Linrad* with two channels at large bandwidth. □□

Crystal Parameter Measurement and Ladder Crystal-Filter Design

A crystal text fixture, procedures and a spreadsheet smooth this traditionally complicated process.

By Randy Evans, KJ6PO

When designing crystal filters or crystal oscillators, it is essential to accurately measure the parameters of the crystals used if results are to agree with the design calculations. While a number of articles have been written to describe measurement techniques, most require several measurements and numerous calculations to obtain the crystal parameters.[1-5] Since many crystals often need to be measured to select those crystals that have the necessary parameters, the entire process can be very unwieldy and time consuming. The goal of this article is to simplify that task. I present two measurement techniques from which the reader can select one based upon available test equipment. With the measurements done, we can use *Excel* spreadsheets to ease the calculations. Last, a spreadsheet based upon a previous article in *QST* (see Note 3) is presented for taking measured crystal parameters and designing simple ladder crystal filters.

[1]Notes appear on page 42.

2688 Middleborough Cir
San Jose, CA 95132
randallgrayevans@yahoo.com

Tutorial

To understand how the crystal parameters are measured, let's have a short tutorial on crystal models. The typical four-element crystal model is shown in Fig 1 (more complex models have been developed, but they are not needed for most applications). The crystal model consists of a series of lumped elements (inductor L_m, a capacitor C_m, and a series resistance R_s) in parallel with capacitor C_o. L_m and C_m represent the "motional" inductance and capacitance of the crystal and R_s represents the series resistance of the crystal. C_o represents the shunt holder capacitance of the crystal.

The transmission response of a crystal is shown in Fig 2. This is based upon a simple test setup shown in Fig 3. The crystal has a very low resistive impedance equal to R_s at the series-resonant frequency because the inductor and capacitance impedances cancel at this frequency, leaving only the series resistance, R_s . Therefore, the transmission signal output amplitude is maximum at the series-resonance frequency because this is the lowest series impedance possible. The series-resonance frequency is given by:

$$F_s = \frac{1}{2\pi\sqrt{L_m C_m}} \quad \text{(Eq 1)}$$

The parallel resonance frequency is a function of C_o and any stray capaci-

tance (C_s) plus L_m. It presents high transmission impedance, hence the low output amplitude shown in Fig 3 for the parallel-resonance frequency. The parallel-resonant frequency is:

$$F_p = \frac{1}{2\pi\sqrt{\frac{L_m C_m (C_o + C_s)}{C_m + C_o + C_s}}} \quad \text{(Eq 2)}$$

where C_s is the stray capacitance across the crystal's terminal leads. Notice that the parallel-resonance frequency is affected by the presence of stray capacitance.

This test setup will measure the series-resonance frequency correctly, but not the true crystal parallel-resonance frequency because of stray capacitance added by the simple test setup. Therefore, to accurately measure the true crystal parameters, it is necessary to cancel out the effects of the stray capacitance caused by the test fixture. This may be achieved by means of an anti-phase voltage through another capacitor equal to that from the stray capacitance as shown in Fig 4. Notice that both V_{in} voltage sources have the same magnitude but differ in phase by exactly 180°. They go through equal-value capacitors (C_{adj} is set to equal C_{stray}). Therefore the current through C_{stray} is exactly cancelled by the current through C_{adj}, and the net result is that the circuit behaves as if only L_m, C_m, R_s and C_o were present, thus canceling the effects of C_{stray}.

In terms of a practical circuit, the two opposite-phase voltage sources can be implemented with a transmission-line transformer, as shown in Fig 5. The 1:1 transformer is used to generate an anti-phase voltage for the neutralizing capacitor leg by inverting the polarity of the input voltage going into the crystal.

The input and output resistor pads lower the impedance of the source and load (to 19.1 Ω) as seen by the crystal to better match the series resistance of the crystal (typically in the 10-35 Ω range for most crystals in the 1-20 MHz range) for more accurate measurements.

Test Fixture Construction

The crystal measurement test fixture is based upon a Tektronix Application Note (see Note 1). It is relatively easy to build and its layout is not critical, as long as leads are kept short. I constructed my crystal-measuring test fixture in an aluminum case for shielding, using a die-cast enclosure made by LMB (model CAB-123). It is $3^3/_8 \times 1^1/_2 \times 1^1/_{16}$ inches (LWH). I used five-way

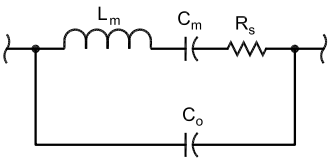

Fig 1—Lumped-element model of a crystal.

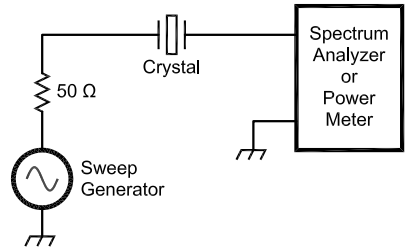

Fig 2—Crystal transmission response.

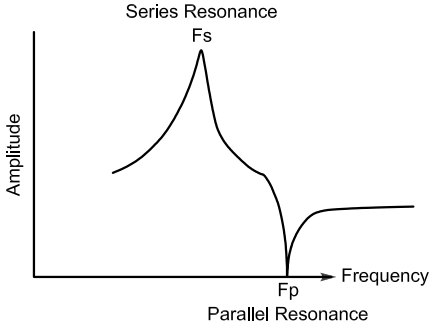

Fig 3—Simple crystal measurement test setup.

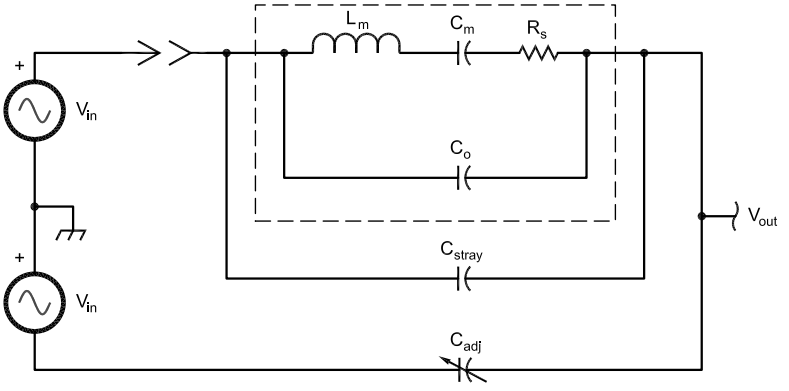

Fig 4—C_{stray} cancellation circuit.

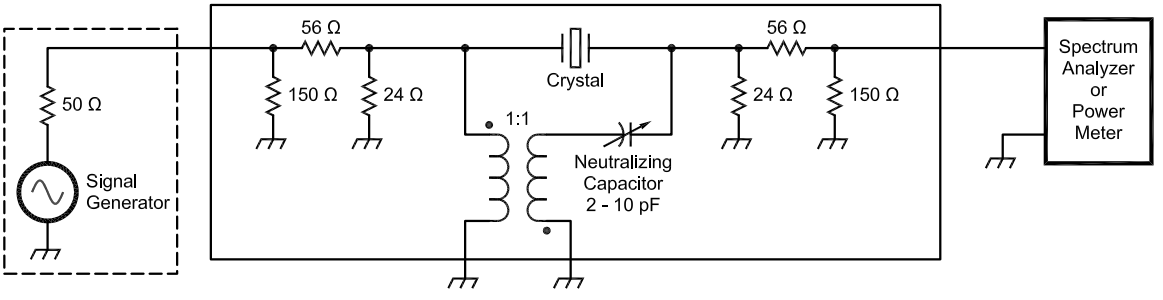

Fig 5—Crystal measurement test fixture.

terminal posts for the crystal connectors and BNC connectors for the signal input and output connectors. The 1:1 transformer was made with an Amidon FT37-43 toroid core, wound with two sets of windings, each consisting of 16 turns of #28 AWG wire, as shown in Fig 6. The neutralizing capacitor is a 2-10 pF piston capacitor, although any type should work. Make sure that it can be insulated from the chassis. A picture of the outside of the test fixture is shown in Fig 7 and a picture of the inside of the test fixture is shown in Fig 8.

Measurement Techniques

This article describes two alternative measurement techniques, with *Excel* spreadsheets to ease the calculation process. The first technique uses either a signal generator and power meter (or spectrum analyzer) or a scalar or vector network analyzer with the test fixture. A second technique uses a vector voltmeter for those individuals that have access to one. It does not require the test fixture. Regardless of the particular technique used, each will give accurate results using the *Excel* spreadsheets. The end result is a relatively painless technique to accurately characterize crystals.

The first approach only requires a signal source (CW signal generator or sweep generator) and a level measuring device (power meter or spectrum analyzer), as shown in Fig 5. The main requirement of the signal generator (or frequency counter) is that it can be set accurately in frequency and that it is stable during the measurement. That is ideally a setting accuracy to 1 Hz or better and drift of less than 1 Hz during the measurement. The power meter or spectrum analyzer needs to resolve levels to 0.1 dB or better. The absolute accuracy is not very important because only power differences (over a typical range of 2-4 dB for most crystals) are measured.

Table 1 gives a detailed measurement procedure using this method. Notice that the value of C_o is extremely sensitive to the measured value of the parallel-resonant frequency, so take care that you measure the frequency of the minimum signal point corresponding to F_p. This is not always easy to do because the signal is often down in the noise where the true null is difficult to identify.

A vector RF impedance meter, such as the HP-4815A, can also be used for determining the parameters of a crystal. The technique is based upon the crystal-impedance characteristics as shown in Fig 9. The key characteristics of the crystal impedance are that

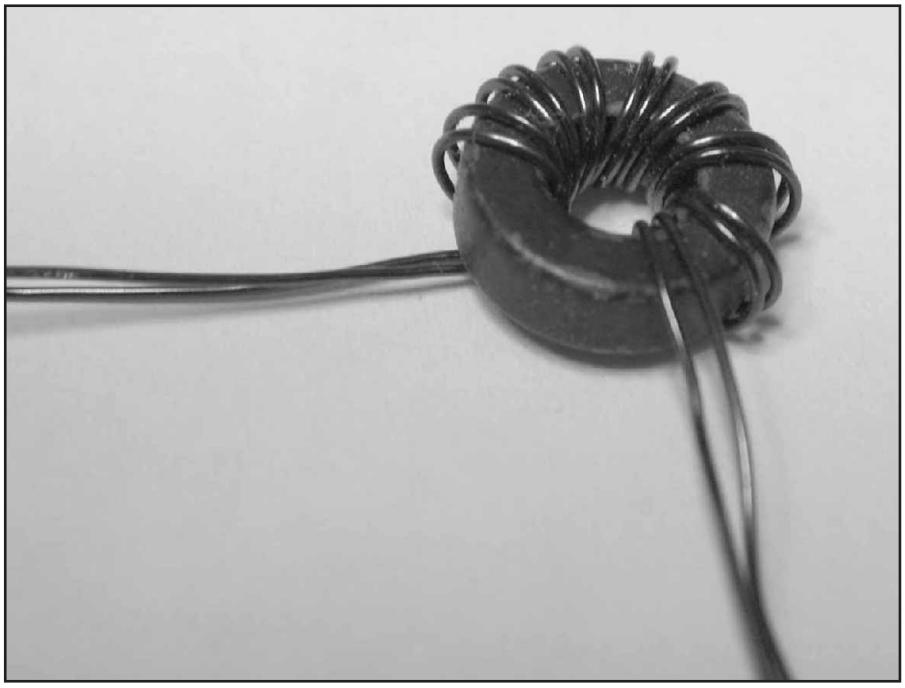

Fig 6—Construction of a 1:1 transformer.

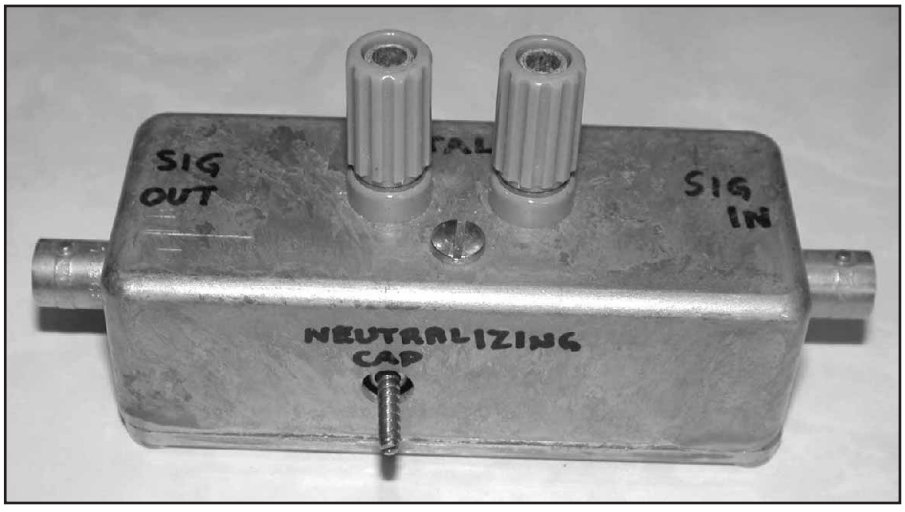

Fig 7—Outside view of crystal measuring test fixture.

Fig 8—Inside view of crystal measuring test fixture.

the phase angle is 0° at the series-resonance frequency. In addition, the bandwidth of the crystal is measured by noting the frequencies at the ±45° phase angles. From these parameters, the unloaded Q and the motional inductance and capacitance, L_m and C_m, respectively, are calculated in the spreadsheet. Lastly, the shunt capacitance is determined by offsetting the frequency well below the series-resonance frequency, typically ≤ 0.99 F_s, where C_o essentially determines the crystal impedance. The spreadsheet for a vector RF impedance meter is shown in Table 2. Notice that the residual capacitance C_r of the test fixture must be measured and subtracted from the reading to obtain an accurate measurement of C_o.

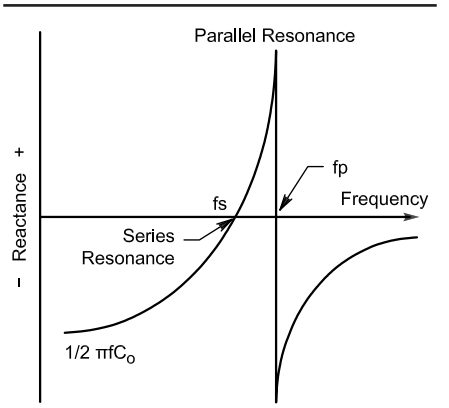

Fig 9—Crystal impedance characteristics.

Ladder Crystal Filter Design

This section describes the design of ladder crystal filters using the techniques described in Hayward's *QST* article (see Note 3). The article requires that the crystal parameters be accurately modeled for F_s, R_s and unloaded crystal bandwidth and Q before the design process can be started. The original article gave design tables for circuits of two to five crystals and provided equations for calculating the filter component values, coupling capacitors and termination resistance. This article presents a spreadsheet that expands the table to cover circuits of two to eight crystals, using data from Zverev's book.[6] The spreadsheet simplifies the design process, reducing the likelihood of errors during the calculation process, as well as allowing larger filter sizes. Notice there was an error in the original article for Butterworth N = 4, k23 (was 0.4512 but should be 0.5412 per Zverev's *Handbook of Filter Synthesis*). This error has been corrected in the spreadsheet. In addition, the equations used in the original article to calculate C_m and L_m give quite different answers than those derived from the Tektronix article (see Note 1), which I believe to be correct. In any event, the values are not needed for the filter design.

The reader should refer to Hayward's original article for greater details, but the pertinent issues are summarized here. The first consideration is that the crystal unloaded Q be at least 10 times the filter Q. The filter Q is defined as:

$$Q_{\text{filter}} = \frac{\textit{Filter Center Frequency}}{\textit{Filter Bandwidth}} \qquad \text{(Eq 3)}$$

Therefore, if you wish to design a ladder crystal filter with a bandwidth of 500 Hz using 6-MHz crystals, then the filter Q is 12,000. This implies that you want to use crystals with an unloaded Q of at least 120,000. As stated in Hayward's article, lower-Q crystals would increase the filter losses, the

Table 1 - Detailed Crystal Measurement Procedure Using a Power Meter or Spectrum Analyzer

Step 1:	Remove crystal and adjust neutralizing capacitor for minimum signal into power meter or spectrum analyzer at the crystal frequency.			
Step 2:	Short out crystal and measure signal level with power meter or spectrum analyzer (P1 dBm).			
Step 3:	Insert crystal and measure signal level with power meter or spectrum analyzer (P2 dBm).			
Step 4:	Determine power difference between P1 and P2.			
	Power Difference	**2.12**	**dB**	P1 - P2
	Rs	**10.6**	ohms	Rs = (38.2*10^([P1-P2]/20)-38.2)
Step 5:	Measure crystal series resonance frequency on the power meter or spectrum analyzer.			
	Fs	**5.998042**	**MHz**	
Step 6:	Measure 3 dB bandwidth on power meter or spectrum analyzer.			
	BW3dB Measured	**249**	**Hz**	Q, hence BW, is lowered by test fixture
	Q (loaded)	**24089**		Qu = Fs*10^6/BW3dB, ref 2.
				Loaded Q, includes effects of test fixture.
	Q(unloaded)	**111227**		Take out effects of test fixture. Q = 2*PI*Fs*Lm/Rs, ref 3.
	BW3db Unloaded	**54**		BWunloaded = Fs/Qunloaded, ref 2.
	Cm	**0.0226**	pF	Cm = BW3dB/((2*PI*(Rs + 38.2)*Fs^2), ref 2.
	Lm	**31.2**	mH	Lm = 1/((2*PI*Fs)^2 * Cm), ref 2.
Step 7:	Measure the parallel resonant frequency Fp on the spectrum analyzer.			
	Fp	**6.0128**	**MHz**	
	Co	**4.6**	pF	Co = ((10^12)*(Cm*10^-12)*Fp*10^6)/(2*(Fp-Fs)*10^6)

filter bandwidth will be narrower and the shape will be rounded.

The next step is to enter the "Input" values into the spreadsheet as shown in Table 2. These are the calculated *unloaded* crystal bandwidth, the desired filter bandwidth, the end-termination resistance to be used, the measured crystal center frequency, the measured crystal series loss resistance and the measured crystal parallel capacitance.

It is important that the unloaded crystal bandwidth be used and not the test fixture measured crystal bandwidth. This is important because the measured test-fixture crystal bandwidth is a function of the test-fixture resistance plus the crystal series loss resistance. The spreadsheet in Table 1 takes the crystal bandwidth measured in the test fixture and compensates the effects of the test-fixture resistance to calculate the true crystal bandwidth.

The "end termination" is the source and termination impedances that will be used for the crystal filter. It must be greater than the R_{end} value calculated in the spreadsheet. If it is not, the values for C_{end} are invalid for those values of N where R_{end} is less than the end-termination value. For example, see the C_{end} column for N = 7 and 8 in Table 3. The solution is to either increase the value for the end termination until it exceeds R_{end} or to design using a smaller value of N where the results are valid. The remaining input values are self-explanatory.

Once the input values are entered, the spreadsheet calculates the crystal coupling capacitors required for the desired filter characteristics. At this point, it remains only to build the crystal filter. I hope these spreadsheets and the crystal-parameter measurement methods presented will make crystal filter design relatively painless.

Notes

[1]M. Engelson, "Crystal Device Measurements Using the Spectrum Analyzer," Tektronix, AX-3525, Feb 1977.

[2]HP Application Note 171-1, "Measurements with Signal Generators, Crystal Testing with the HP 8640A/B and HP 8405A," Apr 1974.

[3]W. Hayward, W7ZOI, "A Unified Approach to the Design of Crystal Ladder Filters," *QST*, May 1982, pp 21-27.

[4]D. DeMaw, W1FB, "A Tester for Crystal *F*, *Q* and *R*," *QST*, Jan 1990, pp 21-23.

[5]Bill Carver, K6OLG, "High Performance Crystal-Filter Design," *Communications Quarterly*, Winter 1993, pp 11-18.

[6]A. Zverev, *Handbook of Filter Synthesis*, (New York: John Wiley & Sons, 1967).

References

1. B. Parzen and A. Ballato, *Design of Crystal and Other Harmonic Oscillators*, (New York: John Wiley & Sons, 1983) pp 424-425.
2. R. Kinsman, *Crystal Filters, Design, Manufacture, and Application*, (New York: John Wiley & Sons, 1987) p 14.

Table 2 - Detailed Crystal Measurement Procedure Using a Vector Voltmeter

Step 1	Freq set for |Z| = min and phase = 0 degrees. The |Z| reading is then Rs and the frequency is Fs.			
	Rs	**12.5**	ohms	
	Fs	**5.998072**	MHz	
Step 2	The frequency is changed slightly until phase = +45 degrees and F45 noted.			
	F45	**5.998102**	MHz	
Step 3	The frequency is then adjusted until phase = -45 degrees and F-45 noted.			
	F-45	**5.998043**	MHz	
	BW unloaded	**59**	Hz	
Step 4	Calculate Q = Fs/(F45 - F-45)			
	Q (unloaded)	**101662**		Qu = Fs*10^6/((F45-F-45)*10^6), ref 2.
	Cm =	**0.0209**	pF	Cm = 1/(2*PI()*Fs*Qu*(Rs)), ref 2.
	Lm =	**33.7**	mH	Lm = 1/(((2*PI*Fs)^2)*Cm), ref 2.
Step 5	Co is obtained by shifting the frequency <= 0.99Fs, reading |Z|, and then computing Co.			
	Z	**4600**	ohms	
	F (<=.99Fs)	**5.9**	MHz	
	Cr (residual cap.)	**1.4**	pF	Residual capacitance of component fixture
	Co =	**4.46**	pF	Co = 1/(2*PI*F*Z) - Cr

Table 3 - Crystal Ladder Filter Design Sheet

Input Values:

ΔF	Unloaded crystal bandwidth	**66**	Hz	Unloaded BW, not BW measured in test fixture
B	Filter bandwidth	**250**	Hz	
Ro	end termination to be used	**1000**	ohms	must be greater than Rend in table
Fs	crystal center frequency	**5.998086**	MHz	series resonance frequency
Rs	crystal series loss resistance	**16**	ohms	
Cp	crystal parallel capacitance	**4.7**	pF	

Calculated Values:

Rend	end resistance	**See Table below**	ohms	Required to terminate the filter without matching capacitors
Qu	crystal unloaded Q	**90880.091**		Q = 2*PI*Fs*Lm/Rs
Cm	crystal motional capacitance	**1.825E-14**	F	0.0182 pF Cm = BW3dB/((2*PI*Rs*Fs^2)
Lm	crystal motional inductance	**0.038583**	H	38.58 mH Lm = 1/(((2*PI*Fs)^2)*Cm)
Cjk	coupling capacitor		pF	
Cend	matching end capacitor		pF	
kjk	normalized coupling coefficient, given inTables 1 and 2.			
q	normalized end-section Q, given in Tables 1 and 2.			
N	number of cystals to be used in the filter			

Values calculated per Wes Hayward's article:
2.433E-15 F Cm = 1.326E-15*(ΔF/Fs^2)
0.28939 H Lm = 19.1/ΔF

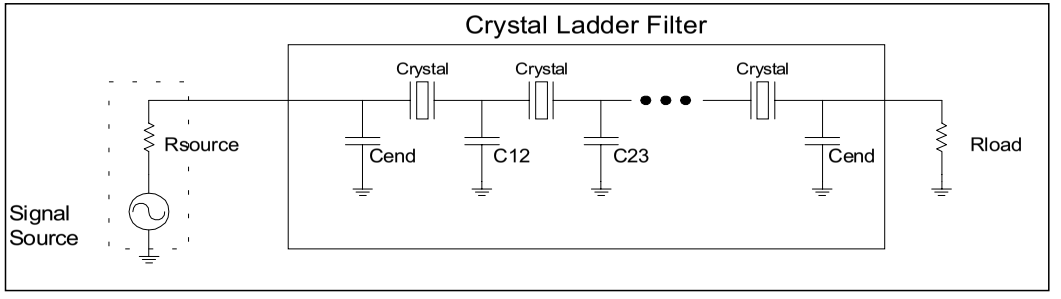

Normalized k and q values for a Butterworth response Without Predistortion **Coupling Capacitors (pF)**

N	q	k12	k23	k34	k45	k56	k67	k78	C12	C23	C34	C45	C56	C67	C78	Rend	Cend
2	1.4140	0.7071							**72.5**							**305.5**	**35.3**
3	1.0000	0.7071	0.7071						**72.5**	**72.5**						**438.5**	**25.3**
4	0.7654	0.8409	0.4512	0.8409					**59.4**	**119.3**	**59.4**					**577.9**	**18.0**
5	0.6180	1.0000	0.5559	0.5559	1.0000				**48.4**	**95.0**	**95.0**	**48.4**				**719.5**	**11.9**
6	0.5176	1.1688	0.6050	0.5176	0.6050	1.1688			**39.9**	**86.5**	**102.8**	**86.5**	**39.9**			**862.2**	**5.9**
7	0.4450	1.3424	0.6671	0.5268	0.5268	0.6671	1.3424		**33.5**	**77.5**	**100.8**	**100.8**	**77.5**	**33.5**		**1005.5**	**#NUM!**
8	0.3902	1.5187	0.7357	0.5537	0.5098	0.5537	0.7357	1.5187	**28.4**	**69.3**	**95.4**	**104.5**	**95.4**	**69.3**	**28.4**	**1148.9**	**#NUM!**

Normalized k and q values for a 0.1 dB ripple Chebyshev Filter Without Predistortion

N	q	k12	k23	k34	k45	k56	k67	k78	C12	C23	C34	C45	C56	C67	C78	Rend	Cend
2	1.6382	0.7106							**72.1**							**261.5**	**39.9**
3	1.4328	0.6618	0.6618						**78.2**	**78.2**						**301.2**	**35.7**
4	1.3451	0.6850	0.5421	0.6850					**75.2**	**97.7**	**75.2**					**321.9**	**33.8**
5	1.3013	0.7028	0.5355	0.5355	0.7028				**73.0**	**99.0**	**99.0**	**73.0**				**333.3**	**32.8**
6	1.2767	0.7145	0.5385	0.5180	0.5385	0.7145			**71.7**	**98.4**	**102.7**	**98.4**	**71.7**			**340.0**	**32.2**
7	1.2615	0.7223	0.5421	0.5155	0.5155	0.5421	0.7223		**70.8**	**97.7**	**103.2**	**103.2**	**97.7**	**70.8**		**344.3**	**31.9**
8	1.2515	0.7276	0.5451	0.5160	0.5100	0.5160	0.5451	0.7276	**70.2**	**97.1**	**103.1**	**104.4**	**103.1**	**97.1**	**70.2**	**347.2**	**31.6**

Active Loop Aerials for HF Reception, Part 2: High Dynamic Range Aerial Amplifier Design

Want to build an effective low-impedance preamplifier? Try an augmented common-base circuit.

By Chris Trask, N7ZWY

The performance of any receiving system is highly dependent on the first few stages, and very often the aerial itself is not given consideration as being a part of that system, let alone being recognized as the stage that determines the minimum noise figure (*NF*) that can be realized. Aerials having poor efficiency or that are not properly matched to the receiving unit can cripple the ability of the operator to receive low-level signals. Electrically small aerials, regardless of their configuration, are especially vulnerable to low efficiencies and hence become the critical element in a receiving system where larger aerials with good efficiency are impractical for any of a variety of reasons. With many radio amateurs and shortwave broadcast (SWBC) listeners living in apartments or subject to property zoning restrictions, small aerials having good performance, both for transmitting and receiving, have become increasingly in demand. This two-part series will describe the theory and practical aspects of a high-performance active receiving loop aerial design.

Sonoran Radio Research
PO Box 25240
Tempe, AZ 85285-5240
ctrask@ieee.org

Loop Aerials—A Brief Review

In the first part of this series, compact aerials for limited space applications were discussed, along with a few options such as short vertical monopoles, short dipoles and loops.[1] Afterwards, the various design aspects of loop aerials were examined using a variety of analytical and simulation methods to evaluate the efficiency, impedance and radiation patterns of single-turn and multiturn loop aerials. A single-turn loop having a diameter of 1 m using 1/4-inch copper tubing was examined in detail both analytically and experimentally, showing that the aerial was usable for frequencies from roughly 5 MHz to 15 MHz. In this, the second and last part of the series, the aerial amplifier, tuner and control unit will be described.

Active Aerials—An Historical Perspective

Electrically small aerials are well known for their low impedance characteristics. The bulk of literature on their design and performance focuses on the preamplifier rather than the aerial

[1]Notes appear on page 48.

element itself since the low resistance of the aerial represents a significant performance limitation.[2] Since reception of signals in the 10 kHz to 30 MHz spectrum is strongly hampered by external atmospheric, man-made and galactic noise, there is little reason to design a receiving system that has a noise contribution far below the received external noise (see Note 2).

It is, however, essential that the active aerial amplifier is designed with the maximum possible dynamic range, which suggests that both NF and IMD performance be considered in the design. Most active aerial amplifier designs tend to focus on the NF performance while giving IMD performance little attention. There are some notable exceptions, such as that proposed by Nordholt and van Willigen.[3]

Aerial Amplifier and Tuner

A complete schematic of the aerial amplifier and tuner is shown in Fig 1. Balun transformer T1 is specifically designed for low impedances. It couples the balanced loop aerial to an unbalanced tuner consisting of varactor diodes D2 and D3 and inductor L1. An augmented common-base amplifier, consisting of Q1 and Q2 and T2 with very low input impedance, a low *NF*, and a high *OIP3* then follows this. This amplifier couples the low-impedance loop aerial to the higher impedance of the coaxial cable by way of a common-base amplifier consisting of Q3, T3 and T4. The voltage regulator U1 provides a stable bias voltage for the amplifier stages while Zener D1 provides a prescribed drop from the supply voltage to the tuner unit, allowing the varactor diodes to have a tuning voltage of approximately 0.5-12 V. The theory and design of the balun transformer and augmented amplifier follow in detail.

Low-Impedance Wide-Bandwidth Transformers

As we noticed in Part 1 of this series, a very low resistance in series with an inductance characterizes the loop aerial impedance. We also learned that it is best to operate the loop aerial with a balanced feed to enjoy the full frequency range available and retain the radiation-pattern nulls that give this compact aerial ideal directivity performance. To maintain this balance, it would be preferable that the antenna be coupled to the tuner by way of a broadband balun transformer before applying any tuning. The reason being that it is both difficult and expensive to go about matching varactor diodes to achieve a balanced tuning capability. Such configurations are best left to motor-driven dual variable capacitors, an even more expensive option that need not be considered for an active receiving aerial. We must also keep in mind that to maintain the efficiency of the aerial, the balun as well as the entire tuning section needs to be designed to minimize loss.[4, 5]

In the design of broadband transformers, several details need to be considered. To begin, the ferrite or powdered-iron material in the core must be appropriate for the operating frequency range. Choosing the wrong material can lead to either insufficient coupling at low frequencies, or excessive core losses at high frequencies. For a broadband transformer being used at low impedances, either of these can prove fatal. Generally, the choices for HF can be cobalt-nickel-zinc ferrites such as Ferronics mix K or a high permeability carbonyl-powdered-iron material such as Micrometals mix 8. For low HF frequencies, nickel-zinc ferrites such as Ferronics mix J or Fair-Rite mix 61 are good choices, while for frequencies below HF, manganese-zinc ferrite materials such as Fair-Rite mix 44 will give good performance. Remember that powdered-iron

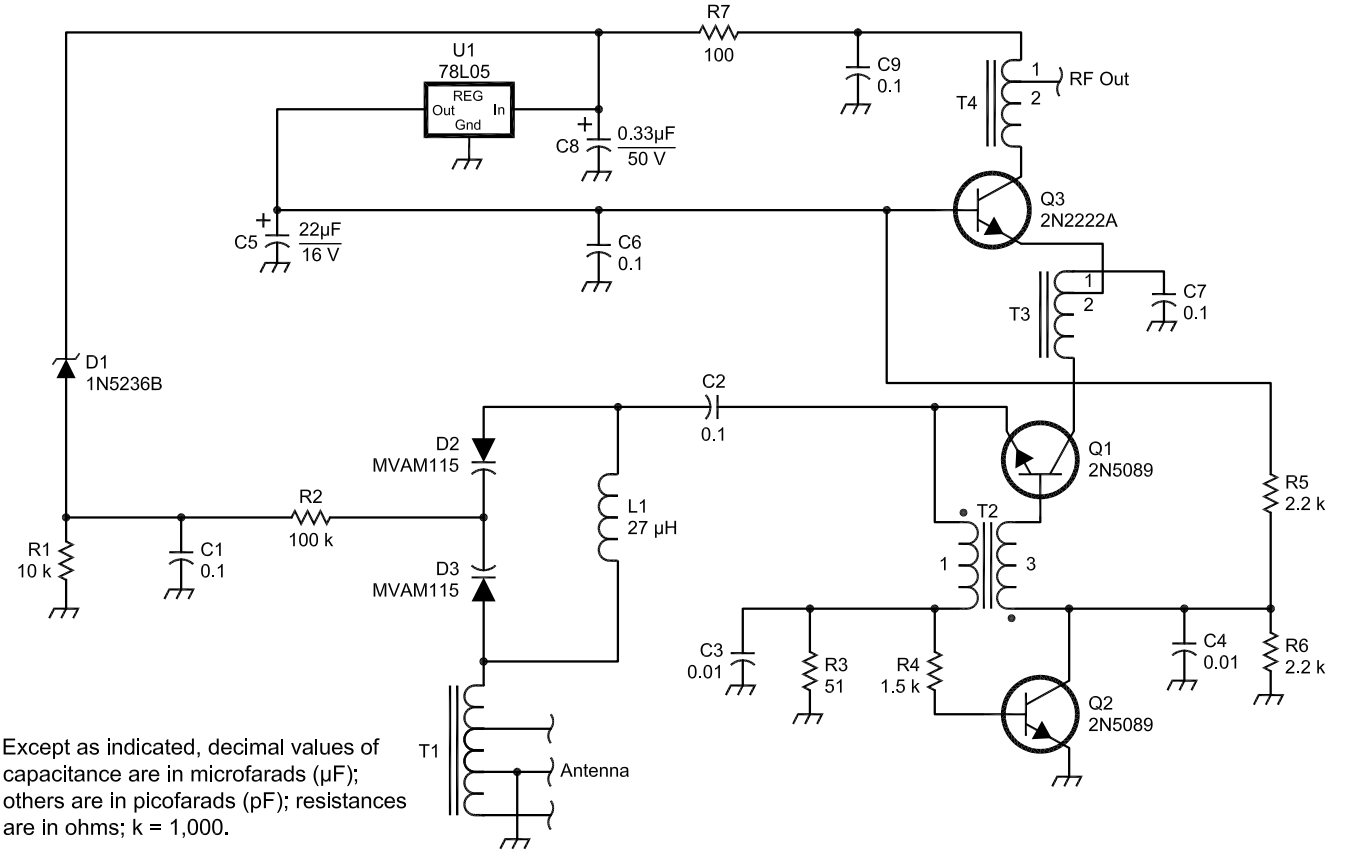

Fig 1—Antenna-amplifier schematic.

materials are "lossier" than ferrites,[6] but they are preferable for broadband transformers at upper HF and beyond.

The shape of the core is also an important factor. Broadband transformers wound on toroidal cores have the highest degree of leakage inductance, which lowers the maximum usable frequency of the transformer and lowers the high end of the aerial's tuning range. The balun (or binocular) core is generally the best shape for all practical purposes. For low frequencies, pot cores give even better performance because their leakage inductance is lowest and they deliver inductors and transformers of much higher *Q*.[7] Not all materials are available in all shapes; this further decreases the options available. The materials mentioned earlier are all available as balun cores, while additional materials are available in the form of toroids and pot cores.

Then there is the matter of the wire. For both good balance and coupling, the wires should all be twisted together. This implies that each strand will be of the same length. Also, the number of wires should be chosen so that the inter-wire coupling is uniform.[8] Fig 2 illustrates the reason for this last statement. In the first case there are only two wires, and obviously the inter-wire capacitance, hence the coupling, is uniform. In the second case, there are three wires, and the inter-wire capacitances are equal between all three wires, again making the coupling uniform between all the wires. In the third case where there are four wires, the capacitances are not equal. For immediately adjacent wires, the inter-wire capacitance is of value *C*, but for the diagonally opposite wires the capacitance is reduced to 0.707 *C*, which means that the coupling is not equal between all four wires.

From this, it should be obvious that for uniform coupling in broadband transformers, the number of wire strands should be limited to either two or three. Since we want to make a balun transformer, this brings our choices down to three wires, for which there are two configurations available, (see Fig 3). In the first case, the balun has a balanced-to-unbalanced impedance ratio of 4:1. Since the loop aerial already has very low impedance, reducing it by a factor of four will make the design of the broadband transformer and the aerial amplifier more difficult. The second balun has a balanced to unbalanced impedance ratio of 1:1, which although it doesn't improve the low-impedance situation, does not make it any worse. In addition, the direct coupling between the unbalanced and balanced terminals of the second case will improve the coupling at lower frequencies, allowing us to use less wire and core materials. This helps in lowering both the resistive losses and the leakage inductance.[9]

Taking all of these details into consideration, balun transformer T1 consists of two turns of trifilar #32 AWG enameled wire, having twelve twists per inch, on a Fair-Rite 2861002402 balun core. The remaining transformers also use this core. T2 consists of two turns and six turns of #32 AWG wire. T3 and T4 each consist of two turns and four turns of #32 AWG wire. With these transformers, the aerial amplifier gives good performance up to 20 MHz, after which increasing core losses cause the *Q* of the tuner to deteriorate. Constructing the transformers using Ferronics K material cores gives good performance up to 24 MHz, but these cores are both difficult and expensive to obtain.

Tuning Section

The tuning section of the aerial amplifier consists of varactor diodes D2 and D3 and inductor L1. The MVAM115 hyper-abrupt varactor was chosen so as to give a wide tuning range. These are difficult to find now, and the NTE618 makes a good substitute. The tuning voltage is derived from the supply voltage passing through the coaxial cable, which is dropped 7.5 V through the 1N5236B Zener diode D1. This drop is necessary because the 78L05 (U1) voltage regulator requires a minimum of 8.0 V to provide adequate regulation for the amplifier 5-V bias. The tuning voltage is applied to the varactors through R2. The dc ground for the varactors is by way of the input balun transformer and L1, the value of which is chosen to provide a parallel-resonant trap for AM-broadcast signals when tuning at the low end of the range.

Carefully choose C2 because it is in series with the antenna and the amplifier input stage, both of which have low impedance. This capacitor should have an exceptionally low equivalent series resistance (ESR) so as to minimize additional losses in the initial stages of the active aerial. Ceramic capacitors made with materials such as Y5V and Z5U will cause the gain, *NF* and tuning *Q* to deteriorate with increased frequency because of their relatively high ESR. Instead, use high quality porcelain capacitors such as the 200B series from American Technical Ceramics (ATC). In a simple test, the performances using a Y5V ceramic disc versus an ATC 200B porcelain chip capacitor were evaluated. The difference was an additional 15 dB of gain and a fivefold increase in the tuning *Q* at 15 MHz.

Augmented Amplifier

Earlier, I mentioned that a major limiting factor in the noise performance of an active aerial is the low antenna resistance, so low that even a theoretical fourfold increase will not offer any significant performance improvement (see Note 2). From this, it is obvious that the burden for designing high-performance active aerials lies in the design of the aerial amplifier itself. The characteristics that define a suitable amplifier include, but are not limited to, low input impedance, low noise figure and low distortion. Most aerial amplifiers answering to these criteria generally fall into the configurations of grounded-grid, common-gate and common-base. Of these,

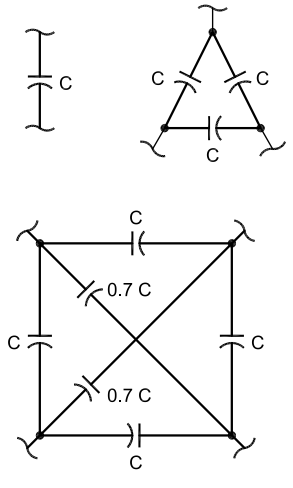

Fig 2—Inter-wire capacitances for twisted-wire transmission lines.

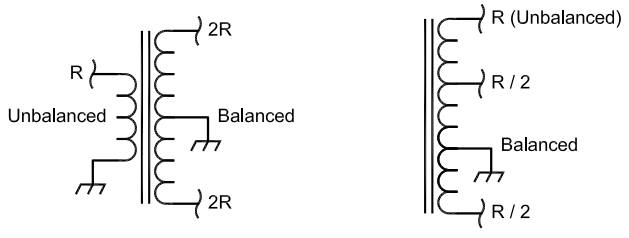

Fig 3—Balun configurations using three twisted wires.

common-base amplifiers offer the best opportunity as they tend to have much lower input impedances than their common-gate counterparts, and a low NF is easily obtained. One drawback, however, is that the input impedance is actually the nonlinear emitter-base junction, which is the primary source of distortion in common-base amplifiers. This nonlinearity problem and the already low input impedance can be substantially improved by the application of linearity augmentation.

Augmentation is a recent entry in the methods available for amplifier linearization.[10, 11] The emitter input impedance of a common-base amplifier is reduced in value and made more linear by detecting the signal voltage at the emitter, and then applying an amplified and inverted signal voltage to the base. Since the emitter signal voltage is a measure of the nonlinear emitter input resistance, connecting the inverted and amplified signal voltage to the base serves to increase linearity of the emitter input resistance as well as decrease it, thus improving the linearity of the common-base amplifier. There are both passive and active forms of augmentation, and in this design both are used in tandem in the input stage of the aerial amplifier. To gain an understanding of the augmentation process, let's begin by considering the emitter input resistance of a common-base amplifier:

$$r_e = \frac{V_E}{I_E} = \frac{V_E}{I_0\, \varepsilon^{\frac{q V_E}{kT}}} \qquad \text{(Eq 1)}$$

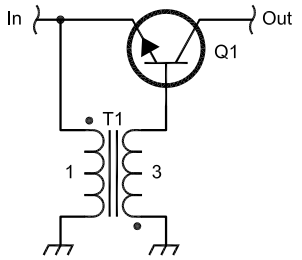

Fig 4—Input stage (high frequency).

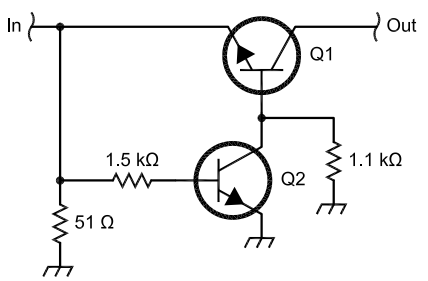

Fig 5—Input stage (low frequency).

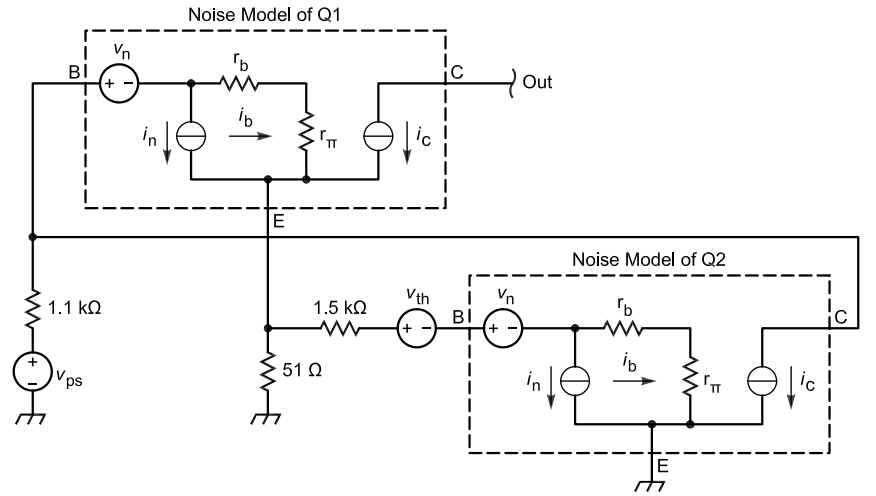

Fig 6—Input stage low-frequency noise model.

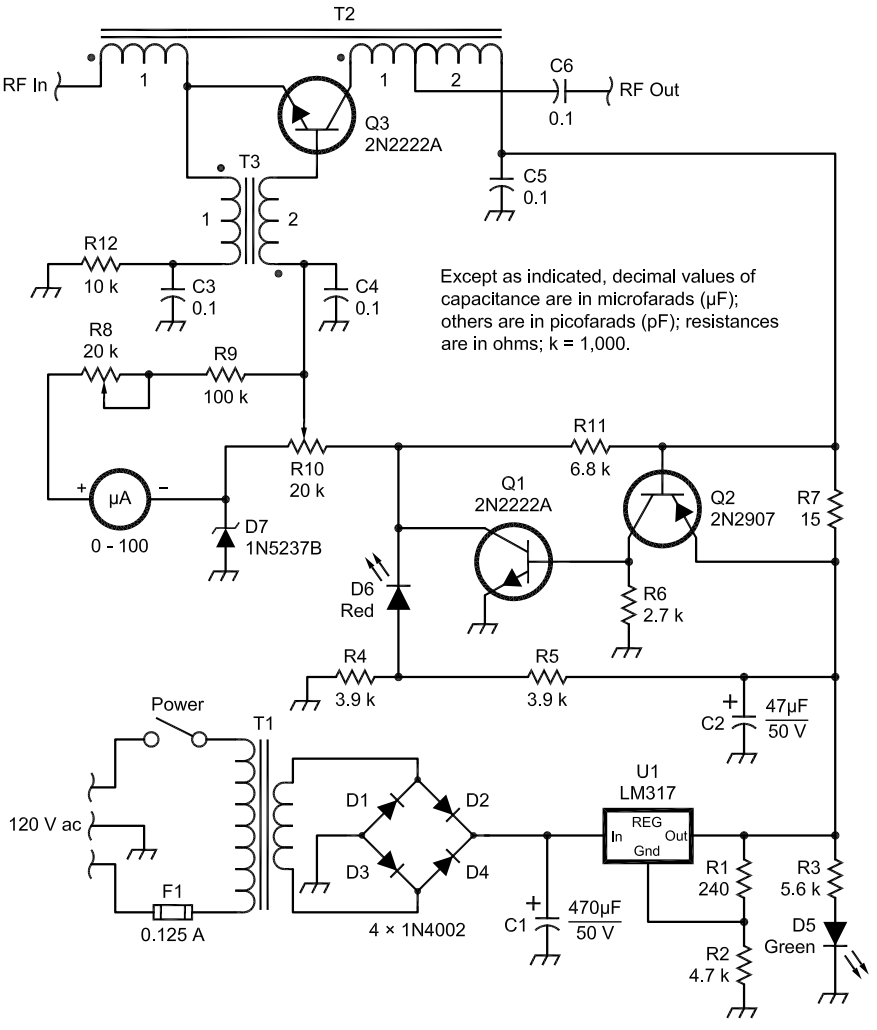

Fig 7—Control-unit schematic.

If we now apply an input signal voltage V_s from a signal voltage source having linear source impedance R_S, the emitter-input current I_E becomes:

$$I_E = \frac{V_S}{R_S + r_e} \quad \text{(Eq 2)}$$

For frequencies in the aerial's range of operation, Q1 and T2 form a passively augmented amplifier, as shown in Fig 4. Here, the signal voltage appearing across the primary winding of T2, which is the emitter signal voltage of Q1, is inverted and magnified by a factor of three at the transformer secondary winding and then applied to the base of Q2. At the same time, signal current from the base of Q1 is magnified and inverted back to the primary of T2, which serves to further reduce the apparent emitter input resistance, which becomes:

$$r'_e = \frac{V_E}{I'_E} = \frac{V_E}{\left(1 - \frac{N}{h_{fe}}\right) \times I_0 \, \varepsilon^{\frac{q V_E (N+1)}{kT}}} \approx \frac{V_E}{I_0 \left(\varepsilon^{\frac{q V_E}{kT}}\right)^{N+1}} \quad \text{(Eq 3)}$$

which shows that the apparent input resistance r'_e of Q1 decreases rapidly as the turns ratio N of T2 is increased. With this lower resistance substituted into Eq 2, the input emitter current becomes:

$$I'_E = \frac{V_S}{R_S + r'_e} \quad \text{(Eq 4)}$$

Since the augmented r'_e of Eq 4 is now much less than the unaugmented r_e of Eq 2, the linear source resistance R_S dominates the determination of the emitter input current and is therefore more linear. This linearization technique decreases the odd-ordered IMD products, such as third (1×2, 2×1), fifth (2×3, 3×2) and so forth, that appear immediately adjacent to the desired signals by as much as 30 dB for a transformer ratio of 1:3

Since the coupling of the augmentation transformer (T2) decreases at low frequencies, the method of passive augmentation loses its effectiveness in addressing the odd-order IMD products, such as second (1×1), fourth (2×2) and so forth, that appear at the lower baseband frequencies. These can disturb the transistor bias conditions and produce further in-band distortion products. For this purpose, active augmentation is applied by way of Q2, as shown in Fig 5. Here, the nonlinear emitter input voltage of Q1 is applied to the base of Q2, which produces a collector current, I_C, which is then applied to the base of Q1. The apparent emitter resistance for the actively augmented amplifier circuit is:

$$r'_e = \frac{V_E}{I'_E} = \frac{V_E}{\left(h_{fe1} + 1 + \frac{1}{h_{fe2}}\right) \times I_0 \, \varepsilon^{\frac{q V_E}{kT}}} \quad \text{(Eq 5)}$$

which is a more substantial reduction in the apparent emitter resistance than Eq 3.

This method of augmentation also has advantages in terms of noise. Referring to the low-frequency noise model of Fig 6,[12] voltage source V_{ps} represents the noise added by U1, and the voltage source V_{th} represents the thermal noise added by the resistors and other passive components. The bias conditions for Q2 are selected in favor of good IMD performance with some consideration given to NF. For Q2, the bias conditions are selected to favor NF, typically less than that of Q1. The values of R4, R5 and R6 are chosen to provide proper source resistance for good NF performance of Q1 and Q2. As the gain of Q2 increases, the output noise of the amplifier becomes that of Q2, which at low frequencies is mostly 1/*f* flicker noise. A method somewhat similar to active augmentation is used to decrease the SSB phase noise of microwave and millimeter-wave oscillators caused by 1/*f* noise.[13, 14]

The output from the input stage is connected to the emitter of common-base amplifier Q3, which serves to isolate the input stage from the varying supply voltage on the coaxial cable. Together with T3 and T4, this stage provides 24.1 dB of signal power gain.

Control Unit

A complete schematic of the control is shown in Fig 7. The power supply starts with the power transformer and continues on to C2, with LED D5 providing a power-on indicator for the front panel. Q1 and Q2, along with R4 to R7 provide current limiting in the event that the coaxial cable to the aerial amplifier is shorted, with LED D6 providing a visual fault indication on the front panel. The current limiter reduces the reference voltage at the top of tuning potentiometer R10, which should be of the 10-turn variety for adequate tuning resolution.

Q3 performs two distinct functions. First, it is the pass device that controls the voltage to the aerial amplifier through the coaxial cable, the voltage being controlled by tuning potentiometer R10. Second, it is the common-base amplifier transistor for the passively augmented loss-less feedback amplifier,[15, 16] which includes T2 and T3 wound on Fair-Rite 2861002402 balun cores. Feedback transformer T2 has windings of 2:2:6 while T3 has windings of 2:6. When constructing this amplifier, be very mindful of the phase orientation of the various windings. This amplifier provides an additional 6 dB of power gain, giving the active aerial system a total gain of about 30 dB.

M1 indicates the tuning of the aerial amplifier. Potentiometer R8 is adjusted for full-scale deflection when the tuning potentiometer is set at maximum.

Synopsis

The active loop aerial described here performs more than adequately for serious DX purposes. The tuning *Q* ranged from 37 at 6 MHz to over 67 at 14 MHz, which decreased above 15 MHz because of the lower *Q* of the loop aerial itself. This makes it obvious that a 10-turn pot should be used for the tuning control. The *OIP3,* as measured at the output of the control unit, was +5 dBm at both 6 and 14 MHz, while the measured *NF* was 1.72 dB at 6 MHz and 1.63 dB at 12 MHz.

Although the aerial will tune down to 5 MHz, remember that the aerial efficiency at that frequency is probably less than 10%, which will add to the *NF* of the aerial amplifier considerably. It would be better to use a 2-meter-diameter 1-turn or a 1-meter-diameter 2-turn loop for the lower bands in order to enjoy the higher efficiency and keep the NF reasonable.

The author uses a variety of active loops for SWBC DXing, including a 2-meter-diameter 1-turn, a 1-meter-diameter 2-turn, a 1-meter-diameter 1 turn and a 0.75-meter-diameter 1-turn loop—all with equally good performance.

Notes

[1]C. Trask, N7ZWY, "Active Loop Aerials for HF Reception Part 1: Practical Loop Aerial Design," *QEX*, Jul/Aug 2003, pp 35-42.

[2]R. A. Sainati, "Active Antenna Performance Limitation," *IEEE Transactions on Antennas and Propagation*, Vol 30, No. 6, Nov 1982, pp 1265-1267.

[3]E. H. Nordholt and D. van Willigen, "A New Approach to Active Antenna Design," *IEEE Transactions on Antennas and Propagation*, Vol 28, No. 6, Nov 1980, pp 904-910.
[4]H. A.Wheeler, "Fundamental Limitations of Small Antennas," *Proceedings of the IRE*, Vol 35, No. 12, Dec 1947, pp 1479-1484.
[5]W. S. Bachman, "Loop Antenna Coupling Transformer Design," *Proceedings of the IRE*, Vol 33, No. 12, Dec 1945, pp 865-867.
[6]C. Trask, "Powdered Iron Magnetic Materials," Workshop on Passive Components for RF Applications, IEEE 2002 International Microwave Symposium (IMS 2002), 4 June 2002, Seattle, Washington.
[7]F. J. Banzi, "Higher Q from Pot Core Inductors," *IEEE Transactions on Parts, Hybrids, and Packaging*, Vol 13, No. 4, Dec 1977, pp 371-377.
[8]G. S. Pandian, "Broadband RF Transformers and Components Constructed with Twisted Multiwire Transmission Lines," Ph D thesis, Indian Institute of Technology, Delhi, Dec 1983.
[9]C. Trask, "Wideband Transformers: An Intuitive Approach to Models, Characterization and Design," *Applied Microwave & Wireless*, Nov 2001, pp 30-41.
[10]C. Trask, "Common Base Amplifier Linearization Using Augmentation," *RF Design*, Oct 1999, pp 30-34.
[11]C. Trask, "Common-Base Transistor Amplifiers with Linearity Augmentation," US Patent #6,271,721, 7 Aug 2001.
[12]K. Hartmann, "Noise Characterization of Linear Circuits," *IEEE Transactions on Circuits and Systems*, Vol 23, No. 10, Oct 1976, pp 581-590.
[13]U. L. Rohde and F. Hagemeyer, "Feedback Technique Improves Oscillator Phase Noise," *Microwaves & RF*, Nov 1998, pp 61-70.
[14]F. Hagemeyer, "Low-Noise Oscillator Circuit Having Negative Feedback," US Patent #5,900,788, 4 May 1999.
[15]C. Trask, "Distortion Improvement of Lossless Feedback Amplifiers Using Augmentation," 1999 Midwest Symposium on Circuits and Systems, Las Cruces, NM, Vol 2, pp 951-954.
[16]C. Trask, "Lossless Feedback Transistor Amplifiers with Linearity Augmentation," US Patent #6,172,563, 9 Jan 2001. □□

A Simple Enhancement for the "Advanced VHF Wattmeter"

A minor modification expands the sweep-measurement capability of a popular homebrew meter

By Bob Kopski, K3NHI

This paper describes a simple modification to the Advanced VHF Wattmeter presented in the May/June 2002 issue of *QEX*. This modification greatly enhances the utility of that instrument.

As presented, the Advanced VHF Wattmeter includes an analog meter, a digital panel meter and an accessory **SIG OUT** port. See Fig 1. The latter has a dc-coupled output voltage proportional to the RF input power level. Its scale factor is 10 mV/dB, and it is intended for use with conjunction with other instruments such as oscilloscopes or recorders. The modification described herein adds considerable utility when used this way. This is accomplished without any changes to

25 W End Dr
Lansdale, PA 19446

Fig 1—The advanced VHF wattmeter includes a digital panel meter for accurate, high-resolution power readings plus an analog meter for trend information. The instrument bottoms out around –76 dBm, but calibration is very good above –70 dBm.

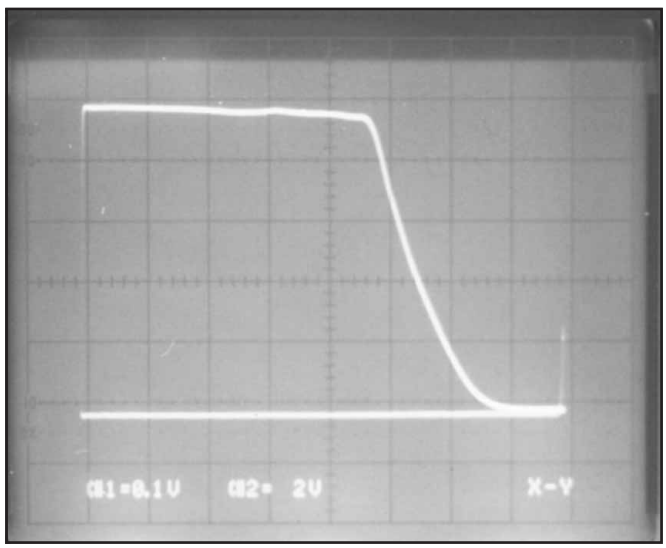

Fig 2—A 120-MHz low-pass filter response as observed via the advanced VHF Wattmeter SIG OUT feature. Sweep width is about 160 MHz, scale factor is 10 dB/division.

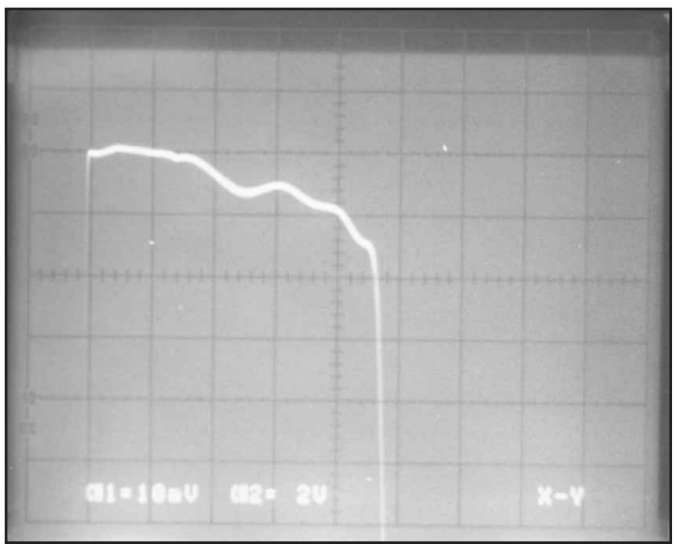

Fig 3—The same filter passband response as seen with a scale factor of 1 dB/division. This enhanced display capability is made possible by the simple Wattmeter modifications described herein.

the front-panel controls or markings on the original instrument.

Figs 2 and 3 show the value of this design enhancement. Both photos display the same swept response of a developmental nine-element 120 MHz low-pass filter as an example. Fig 2 displays the response with the 'scope vertical attenuator set to 100 mV/division. For the 10 mV/dB power-meter output, this is equivalent to 10 dB/division. It is clear that the filter response can be viewed well down on the skirt. This capability is inherent in the operation of the original design.

Fig 3, of the same filter sweep, clearly displays a detailed view of the filter passband ripple. Here the display sensitivity has been increased 10 times, to 1 dB/division. Yet now the filter passband response is in detail view, while the deep skirt of the previous photo is off the bottom of the screen. This test and display versatility was not previously possible.

This extended versatility is achieved by setting the 'scope vertical attenuator to 10 mV/division corresponding to 1 dB/division. Ordinarily, this would put this swept display well off the vertical scale. Now, however, a simple adjustment of the modified instrument's **OFFSET** knob can keep

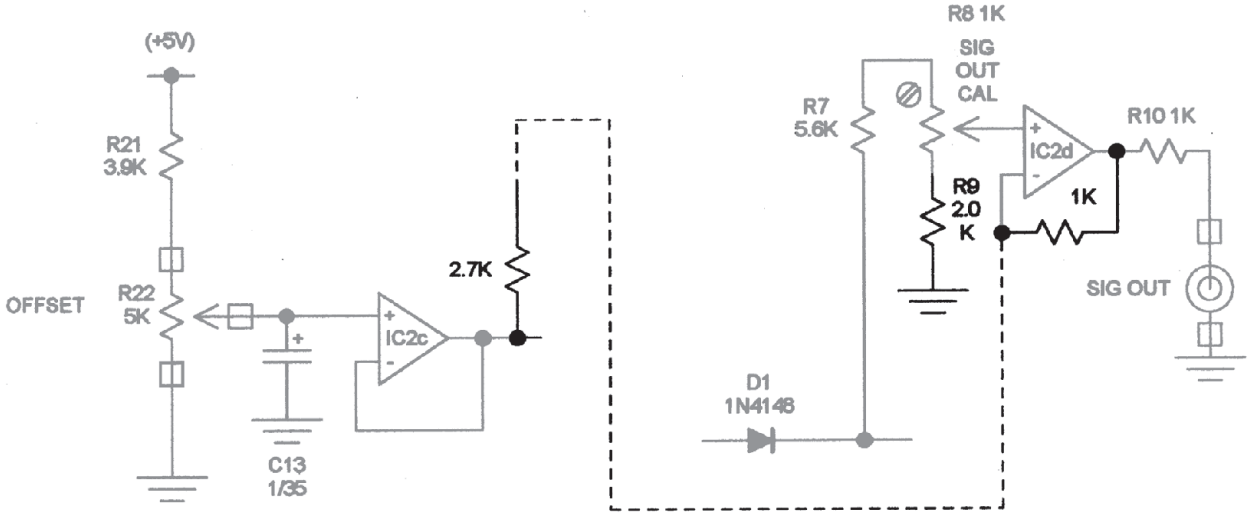

Fig 4—Sections of the original schematic showing changes and additions.

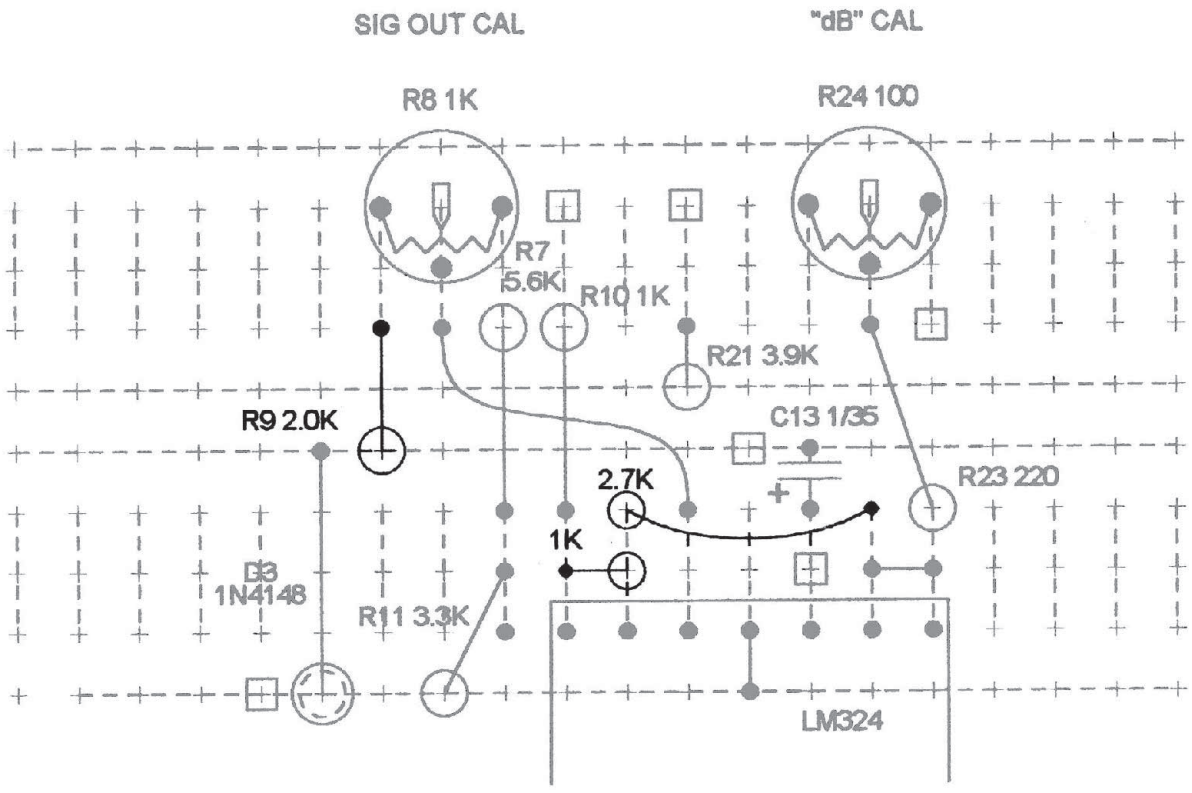

Fig 5—A section of the parts-placement diagram from the original article showing changes and additions.

the desired trace on the screen. This is analogous to using the instrument's analog meter in the "dB" mode as described in the reference article.

It should be noticed here that other 'scope vertical settings can be used as well. For example, vertical-attenuator settings of 50 mV/division and 20 mV/division would result in display factors of 5 dB/division and 2 dB/division, respectively.

The simple circuit modifications needed for this are detailed in the schematic (Fig 4) and the signal processing board assembly drawing (Fig 5). Existing resistor R9 is changed from its original 3.6 kΩ value to a new value of 2.0 kΩ. Two additional resistors, 1 kΩ and 2.7 kΩ, are added to the board. Notice that the 1 kΩ resistor replaces a previously installed jumper wire. After these modifications are in place, the **SIG OUT CAL** trimmer R8 is again adjusted exactly as in the original design for the same output factor of 10 mV/dB. That's all that's needed.

With this modification in place, the original front panel **OFFSET** control (R22) is a "dual use" control. It can offset either the analog meter display (as previously) or (now) the 'scope display as well. In general, this is an "either/or" situation, in that a given control setting will likely not be appropriate for both displays at the same time. This is of no consequence because the analog meter in "dB" mode would normally be used in conjunction with more tedious manual adjustments and measurement, while a 'scope display is most useful for sweep frequency testing. Think of this as having the best of both worlds!

Notice that the *QEX* "Advanced VHF Wattmeter" is itself based on the earlier work of Wes Hayward, W7ZOI, and Bob Larkin, W7PUA, as presented in their paper "Simple RF-Power Measurement" in *QST* (June 2001, p 38ff).

Bob is a recently retired Senior Design Engineer from a major defense contractor. He holds BSEE and BSEP degrees from Lehigh University.

As a lifelong electronics, ham and aeromodeling hobbyist, he routinely combines all three pursuits for the fun of it. His Technician ticket dates to about 1959 when he wanted to homebrew 6-meter radio-control equipment for RC models. He still routinely flies on 6 meters and has also operated fixed and mobile there. He's published an original 6-meter-handheld project in another magazine and the article "An Advanced VHF Wattmeter" in QEX *(May/June 2002, pp 3-8). His broad-based aeromodeling interest dates to the early 1950s, but he has specialized in electric powered RC models for over 25 years. A Contributing Editor to* Model Aviation *magazine for over 20 years, he has a regular monthly column devoted to the electric flying specialty. Additionally, he has published many construction articles covering both model-aircraft design and aeromodeling related electronics. He enjoys it all!* □□

RF

By Zack Lau, W1VT

Harmonic Convergence—Designing Multiple-Conversion Transverters

At the 2002 Microwave Update in Enfield, Connecticut, Sam Jewell, G4DDK, a designer of popular microwave gear for British amateurs, remarked on the difficulty of finding information on the topic of designing dual-band transverters. Here are straightforward procedures for determining the frequencies to use in dual-conversion systems. Often, there are many constraints that significantly limit the design possibilities. Some simple math allows calculation of the best available designs.

Fig 1 shows a typical dual-conversion system. It is often most cost effective to start with a fifth or seventh-overtone crystal around 100 MHz and multiply it to generate local oscillators for both mixers. It is also desirable to minimize the number of multiplier stages, to minimize cost. It is a common technique to use the output of the first multiplier to generate the LO for the second mixer. This reduces the number of possible second-oscillator frequencies, compared to using two entirely separate multipliers. For instance, a design using multipliers of 4 and 15 typically uses more parts than one using multipliers of 4 and 16, because 15 is not divisible by 4. A 16× multiplier can use the 4× output, eliminating a multiplier stage.

The design is further constrained by the second IF. The exact choice of frequency is typically determined by the availability of the second band-pass filter, BPF2. For instance, helical filters are quite popular in Europe, as they are available at reasonable cost. However, they may only be available, in practice, for certain frequencies. For instance, cell-phone filters are probably the cheapest, due to the large quantities produced. Ideally, the frequency you choose would be the nominal frequency of the filter, to minimize the difficulty of filter tuning. Similarly, it may be desirable to reuse a proven printed-circuit-board filter design, rather than go through the exercise of developing a new design. Another consideration for choosing BPF2 is the spectral purity or lack thereof.

Filtering out the image response of the mixer is difficult if the IF is too

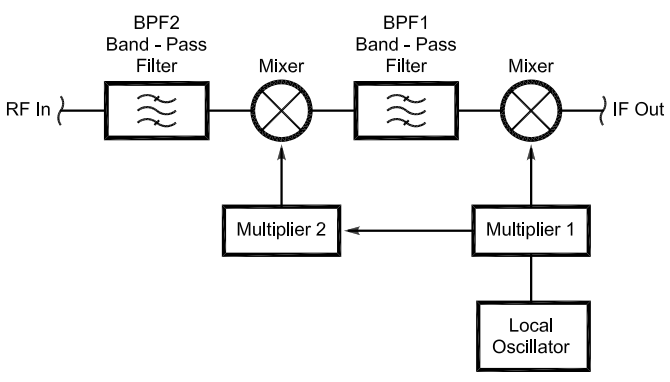

Fig 1—A typical dual-conversion system.

225 Main St
Newington, CT 06111-1494
zlau@arrl.org

low in frequency. The minimum suitable IF is set by the filter technology. Equations on how narrow the bandwidth needs to be are presented in my May 2000 RF column, "A No-Tune 10-GHz Filter." Low-*Q* filters are quite common at VHF and microwaves because of size and cost issues. Low-*Q* printed-circuit-board filters are quite popular—rarely does anyone go through the trouble of machining precision high-*Q* filters out of copper—many hams do not have access to a milling machine or lathe. The low *Q* will set a limit on how narrow a filter you can build before the losses become excessive. A filter is no good if you can't get any signal out of it. This is how one measures unloaded *Q*—you measure the 3-dB bandwidth when the coupling in and out of the resonator is as close to negligible as possible.

If you have a fast Internet connection, you might investigate demonstration programs offered by RF-design companies. It is very possible that demonstration programs can provide all the functionality needed to design basic amateur building blocks, such as simple microstrip filters. I'd look into the offerings by Sonnet Software and Ansoft.[1]

Filters can also have spurious responses—helical filters often have unwanted responses near odd multiples of the desired frequency. This is not terribly surprising—a $^1/_4$-wave resonator also functions as a $^3/_4$-wave resonator. Rick Campbell, KK7B, shows how his 1.0-1.8 GHz extended pipe-cap filter could also be used as a practical 3.5-GHz filter.[2] The harmonic operation makes it easier to couple energy in and out of the resonator. This is very useful with tube cavities, where a quarter wavelength isn't long enough to accommodate the length of the tube. It may also be useful for the higher bands, such as 24-GHz. Peter Rimml, OE9PMJ, published a popular design using two coupled cavities that are large enough for 10-GHz work.[3] Crystals may also have spurious responses—not just overtone responses, but spurious responses near the desired response. Thus, while parallel-connected crystals may look good on a computer, the actual result may not be as desirable, because spurious responses degrade the filter.

The IF cannot be too close to the RF frequency, however, as harmonics and low-order intermodulation products become a problem. For instance, third-harmonic responses are very strong; it is very difficult to build a 146 to 446 MHz transverter. The third harmonic of 146 MHz is 438 MHz, just 8 MHz away from the desired frequency. Intermodulation distortion, or IMD, is also a problem—2×300 MHz – 146 MHz = 454 MHz, also just 8 MHz from the desired frequency. They can be even more troublesome than image responses. While costly, there are often other ways to build better filters that allow low IFs. Filtering out undesirable intermodulation products may be impossible if they sweep across the passband as you tune the frequency.

One rule of thumb, suggested by Rick Campbell, KK7B, is that the IF be 1/10 the RF. "An IF of about 10% of

[1]Notes appear on page 56.

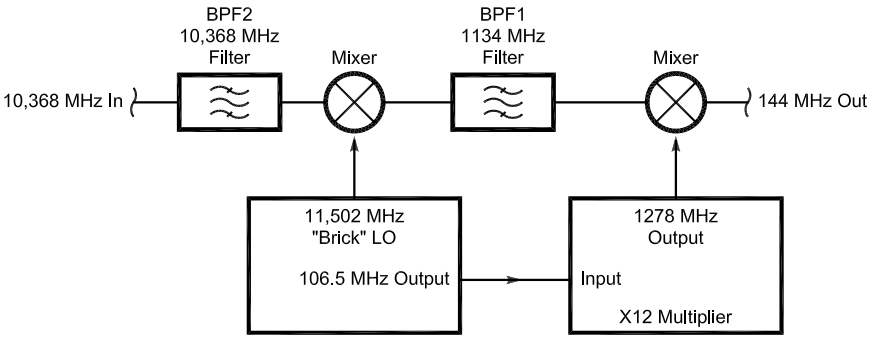

Fig 2—A 10 GHz system using a 96 × 106.5 MHz = 10,224 MHz low-side local-oscillator frequency with 108 – 96 = 12 as the other multiplier. Since both conversions use high-side injection, there was no net sideband conversion.

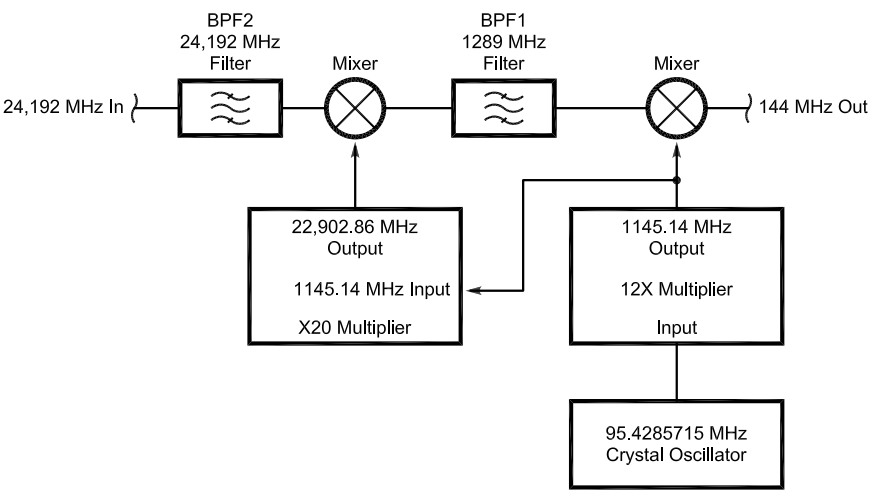

Fig 3—A single-conversion 24,192 to 1296 MHz converter that has been tweaked into a dual-conversion converter to 144 MHz. The crystal is at 95.4 MHz; see text for an explanation of the design process.

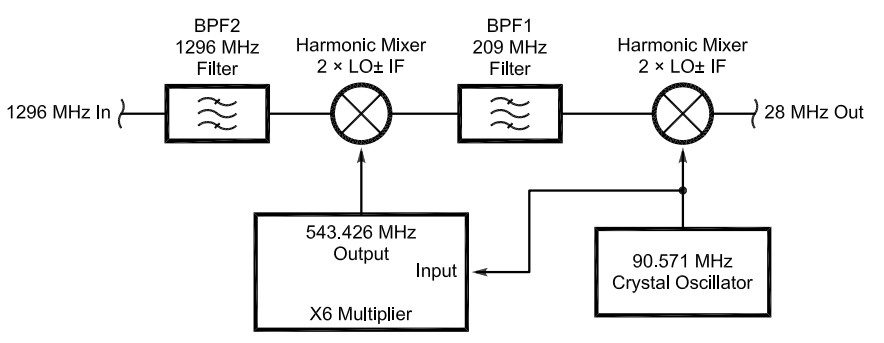

Fig 4—A dual-conversion 1296 to 28 MHz converter using harmonic mixers. See text for an explanation of the design process.

the signal frequency permits good image rejection with a reasonable number of noncritical tuned circuits."[4] Thus, for 24 GHz, the IF should be 2.4 GHz. If the IF is chosen to be much smaller, filtering out the image becomes tougher. A filter with a loaded Q of 100 is often quite a challenge to construct—often requiring machine-shop techniques. The cavities for Peter's 24 GHz filter are made by drilling 18 mm holes in an aluminum block—not exactly a beginner's project. It takes skill to drill many holes that line up properly.

The first step is deciding the input and output frequencies of the system, F_{in} and F_{out}. The radio frequency is usually fixed. There is often more flexibility with the IF. There are different philosophies toward choosing the optimum IF. One school of thought says that it should be a little-used frequency; another, that it should be chosen to simplify logging. For example, let's converting 146.000 MHz to 1296.000 MHz. The last four digits correspond exactly. Two meters is a popular IF for microwave bands, due to the availability of suitable IF rigs. Thus, a 2-meter IF is widely used from 23 cm to 3 cm. You do see more use of 70 cm as an IF for 1.2 cm, because it is difficult to build suitable filters to remove the unwanted image with a single-conversion system. From this, we can calculate a third frequency,

Table 1—Transverter Design Information

F_{con} = 1296 MHz – 28 MHz = 1268 MHz

Crystal Oscillator Frequencies

1268 MHz / 11 = 115.2727 MHz
1268 MHz / 12 = 105.6667 MHz
1268 MHz / 13 = 97.5385 MHz
1268 MHz / 14 = 90.5714 MHz

Dual Low-Side Injection

Netmult = *14* — ***90.571 MHz Crystal***

Design number	*M*	*LO1 (MHz)*	*QR1*	*N*	*LO2 (MHz)*	*IF1 (MHz)*	*QR2*
1	13	1177	10.9	1	91	119	4.2
2	12	1087	6.2	2	181	209	7.5
3	11	946	4.3	3	272	300	10.7
4	10	906	3.3	4	362	390	13.9
5	9	815	2.7	5	453	481	17.7

***Netmult* = 13** — **97.538 MHz Crystal**

Design number	*M*	*LO1 (MHz)*	*QR1*	*N*	*LO2 (MHz)*	*IF1 (MHz)*	*QR2*
6	12	1170	10.3	1	98	126	4.5
7	11	1073	5.8	2	195	223	8.0
8	10	975	4.0	3	293	321	11.4
9	9	878	3.1	4	390	418	14.9
10	8	780	2.5	5	488	516	18.4

***Netmult* = 12** — **105.667 MHz Crystal**

Design number	*M*	*LO1 (MHz)*	*QR1*	*N*	*LO2 (MHz)*	*IF1 (MHz)*	*QR2*
11	11	1162	9.7	1	106	134	4.8
12	10	1057	5.4	2	211	239	8.5
13	9	951	3.8	3	317	345	12.3
14	8	845	2.9	4	423	451	16.1
15	7	740	2.3	5	528	556	19.9

***Netmult* = 11** — **115.273 MHz Crystal**

Design number	*M*	*LO1 (MHz)*	*QR1*	*N*	*LO2 (MHz)*	*IF1 (MHz)*	*QR2*
16	10	1153	9.0	1	115	143	5.1
17	9	1037	5.0	2	230	258	9.2
18	8	922	3.5	3	346	374	13.4
19	7	807	2.6	4	461	489	17.5
20	6	691	2.1	5	576	604	21.6

Dual-Conversion High-Side Injection (both conversions)

***Netmult* = 14** — **90.571 MHz Crystal**

Design Number	*M*	*LO1 (MHz)*	*QR1*	*N*	*LO2 (MHz)*	*IF1 (MHz)*	*QR2*
21	15	1359	20.7	1	91	63	2.2
22	16	1449	8.5	2	181	153	5.5
23	17	1540	5.4	3	272	244	8.7
24	18	1630	3.9	4	362	334	11.9
25	19	1721	3.0	5	453	425	15.2

***Netmult* = 13** — **97.538 MHz Crystal**

Design Number	*M*	*LO1 (MHz)*	*QR1*	*N*	*LO2 (MHz)*	*IF1 (MHz)*	*QR2*
26	14	1366	18.7	1	98	70	2.5
27	15	1463	7.7	2	195	167	6.0
28	16	1561	4.9	3	292	265	9.4
29	17	1658	3.6	4	390	362	12.9
30	18	1756	2.8	5	488	460	16.1

***Netmult* = 12** — **105.667 MHz Crystal**

Design Number	*M*	*LO1 (MHz)*	*QR1*	*N*	*LO2 (MHz)*	*IF1 (MHz)*	*QR2*
31	13	1374	16.7	1	106	78	2.8
32	14	1479	7.1	2	211	183	6.5
33	15	1585	4.5	3	317	289	10.3
34	16	1691	3.3	4	423	395	14.0
35	17	1796	2.6	5	528	500	17.9

***Netmult* = 11** — **115.273 MHz Crystal**

Design Number	*M*	*LO1 (MHz)*	*QR1*	*N*	*LO2 (MHz)*	*IF1 (MHz)*	*QR2*
36	12	1383	14.8	1	115	88	3.1
37	13	1499	6.4	2	230	202	7.2
38	14	1614	4.1	3	346	318	11.4
39	15	1729	3.0	4	461	433	15.7
40	16	1844	2.4	5	576	548	19.6

15 – 2 = 13
15 × 97.5385 = 1463.0775 (167.0775 MHz IF) 1463 / 167 = 8.8
2 × 97.5385 = 195.077 (28 MHz IF) 195 / 28 = 7.0 (may be optimum from a spectral purity point of view)

15 – 3 = 12
15 × 105.667 =1585.0073 (289 MHz IF) 1585 / 289 = 5.5
3 × 105.667 = 317 MHz (28 MHz IF) 317 / 28 = 11

$F_{con} = |F_{in} - F_{out}|$.

We can now calculate the most practical crystal frequencies, which are F_{con}/N, where N is a natural number. It is pretty easy to calculate all of these frequencies with a computer.

It often makes sense to check out the frequencies commonly used with single conversion systems. For instance, 106.5 MHz is often used with 10368 MHz transverters.

F_{con} = 10368 MHz – 144 MHz = 10224 MHz

Netmult = F_{con} / 106.5 MHz = 96

Netmult is a very useful number—it is the multiplier that describes the net effect of all the conversions of the system. Thus, you can add or subtract conversions to the system, and still get the desired input/output conversion, if you vary the multiplier numbers to keep *Netmult* constant. *Netmult* can also be used to calculate the frequency stability of the system—the net drift is *Netmult* × (*crystal drift*). Additional drift is not a problem with multiple conversions, as long as everything is multiplied up from the same reference oscillator.

The two most useful dual aconversion systems are:

Netmult = *Mult3* – *Mult1*

where both conversions are high-side conversions.

Netmult = *Mult3* + *Mult1*

where both conversions are low-side conversions.

By high-side conversion, I mean that the local-oscillator frequency is higher than the RF—conversely, low-side conversion means that the local-oscillator frequency is lower than the RF. It is quite desirable for high-side conversions to occur in pairs, as each high-side inversion inverts the sidebands. This means that the upper sideband appears as lower sideband at the IF. Doing this twice eliminates the inversion. By convention, amateurs use USB on bands at 14 MHz and above and LSB on the bands below 10 MHz. The new 5 MHz band uses USB, as regulatory requirements take precedence over convention and convenience.

It is now possible to calculate all the practical conversions. You may recall the sieve of Eratosthenes, a clever technique used to find prime numbers. A similar technique can be used to find all the useful conversions. First, we calculate all the useful crystal frequencies. Typically, there are only a few that fall in the frequency range of interest. Next, we calculate the net multiplier associated with that frequency. We can now iterate upward from that number to calculate the high-side conversions and iterate downward to calculate the low-side conversions. This is quite easily done with *Mathcad*.[5] It is also a basic exercise for computer programming students—setting up a loop to calculate number arrays.

While there are an infinite number of conversions, only a small number are worth considering. For instance, you may have a PLL brick oscillator already tuned to a particular multiplication factor. Even if you are prepared to re-tune it—there is typically a small number of possible multiplication factors that are practical.

I wanted to use a 106.5 MHz crystal in a dual-conversion 10 GHz system. 106.5 MHz is a popular crystal frequency for 10 GHz transverters. Starting with that, 96 × 106.5 MHz = 10224 MHz, the low-side local-oscillator frequency. I already had a PLL brick oscillator with a multiplication factor of 108. Thus, I could build a dual-conversion system with 108 – 96 = 12 as the other multiplier. Since both conversions use high-side injection, there was no net sideband conversion. The resulting converter is shown in Fig 2.

Another example is a single-conversion 24,192 to 1296 MHz converter—suppose I want to tweak it into a dual-conversion converter to 144 MHz? The crystal is at 95.4 MHz.

24,192 MHz – 1296 MHz = 22,896 MHz

Netmulta = 22,896 MHz / 95.4 MHz = 240

24,192 MHz – 144 MHz = 24,048 MHz

Netmultb = 24,048 / 95.4 = 252.0755

Netmultb – *Netmultb* ≈ 12

Thus, we can use a frequency close to 95.4 MHz with a combination of ×12 and ×240 multipliers. The exact frequency is 24,048/252 = 95.4285715 MHz. Fig 3 shows the resulting system.

Sam was looking for a 1296 to 28 MHz converter. Table 1 lists the conversion data for 40 different designs. Of these, only four have RF/IF ratios greater than 6.0 for both conversions, designs 2, 27, 32 and 37. Design 37 is rather impractical, requiring a multiplication of 13. Design 2 is probably the most practical, with multiplication ratios of 2 and 12. Twelve is a very nice multiplier ratio, factoring into 2 × 2 × 3. Sam mentioned his 2.4 GHz design used a harmonic mixer, which uses half the LO frequency. If harmonic mixers are used in this example, the conversion could be done with just one ×6 multiplier, such as the no-tune LO board designed by Rick Campbell.[6]

The table provides much data that is useful for optimization. For instance, it is often desirable to avoid certain frequencies, to prevent EMI/RFI. It is an easy matter to go through and eliminate the problematic conversions.

Notes

[1]**www.sonnetusa.com/**; **www.ansoft.com/**

[2]R. Campbell, KK7B, "Plumbing Cap and Tubing Filters," North Texas Microwave Society *Feedpoint*, Dec 2002; **www.ntms.org**.

[3]Peter Pauwels, ON1BPS, has dimensional drawings of the filter on his Web page at **home.planet.nl/~alphe078/24ghz4.htm**. Dave Robinson, WW2R, has a more easily read drawing on page 141 of the *Proceedings of the Microwave Update*, 1995.

[4]R. Campbell, KK7B, "Single-Conversion Microwave SSB/CW Transceivers," *QST*, May 1993, pp 29-34.

[5]MathSoft Engineering & Education Inc 101 Main St, Cambridge, MA 02142-1521; tel 617-444-8000, fax 617-444-8001; **www. mathsoft.com/**.

[6]R. Campbell, KK7B, "A Clean, Low-Cost Microwave Local Oscillator," *The ARRL UHF/Microwave Projects Manual* (Newington: ARRL, 1994) pp 5-1 to 5-9 (reprinted from the July 1989 *QST*). □□

Upcoming Conferences

The 2003 AMSAT-NA Annual Symposium, October 17-19, 2003, Toronto, Ontario

AMSAT is a worldwide group of Amateur Radio operators who share an active interest in building, launching and then communicating with each other through noncommercial Amateur Radio satellites. Since its founding nearly 30 years ago, AMSAT has successfully launched over two dozen Amateur Radio communications satellites into Earth orbit.

The Annual General Meeting (AGM) is an opportunity for AMSAT's members, designers and builders to get together and discuss new technologies. The AGM focuses around the presentation of technical papers by its members. These presentations range from new emerging satellite technologies to building receiving antennas from cardboard boxes and aluminum foil!

The symposium and meeting will be held at the Toronto Airport Marriott Hotel, 901 Dixon Rd, Toronto, ON M9W 1J5, Canada; tel 416-674-9400, fax 416-674-8292, toll free 800-905-2811. There's a link from the AMSAT page to the hotel Web site. The hotel has a special AMSAT group rate of $119 CDN (approximately $83 USD) plus applicable taxes for a single or double. The AMSAT room block will be held until September 15. The hotel has free shuttle service from the airport. For pickup, use the hotel courtesy phones located at the terminal exits.

Those who prefer camping may find accommodation at Bronte Creek Camping located between Burlington and Oakville; tel 905-827-6911; **www.ontarioparks.com/english/bron.html**. The campground remains open in October.

Visit the AMSAT Web site at **www.barc. ca/amsat_ca/** for more details and to register for the conference.

Microwave Update 2003

Microwave Update 2003 organizers and the Pacific Northwest VHF Society are joining forces to host a joint conference in the Seattle, Washington, area on September 25-28, 2003. Cost of the registration is $40 prior to September 12th, 2003, for all three days. Single-day or single-event registrations are not available. Late registrations, including at the door, will be $50. Registration forms can be downloaded at **www.microwaveupdate.org.**

Joint conference sessions and the Saturday evening banquet will be held at the Everett Holiday Inn and Conference Center, a short drive north of downtown Seattle.

The Mid-Atlantic States VHF Conference

The Mid-Atlantic States VHF Conference will be held Saturday October 11, 2003, at the Radison, North East Hotel, 2400 Old Lincoln Hwy (at US Rte 1), Trevose, PA 19503-6894. For hotel reservations, call 215-638-8300. Room rates are $99 + 9% tax (mention the block code "Pack Rats"). The 32nd annual Mt Airy Pack Rats Hamarama will follow the conference on Sunday at Middletown Grange Fair Grounds, Penns Park Rd, Wrightstown, Pennsylvania. Watch for more information on the Pack Rats Web site at **members.ij.net/packrats/**. Follow the links to Hamarama and the VHF Conference.

ARRL and TAPR 22nd Annual Digital Communications Conference

The 22nd Annual ARRL and TAPR Digital Communications Conference takes place September 19-21, 2003, in Hartford, Connecticut at the Marriott Hartford Windsor Airport hotel. Updated conference information is available at **www.tapr.org/dcc**.

This is an international forum for radio amateurs to meet, publish their work and present new ideas and techniques. Presenters and attendees will have the opportunity to exchange ideas and learn about recent hardware and software advances, theories, experimental results and practical applications.

The Conference is not just for experts. It is a technically stimulating weekend of fun for all that have more than a casual interest in any aspect of amateur digital communications. Introductory sessions are scheduled throughout the DCC to introduce new technical topics for beginners and experts alike. The introductory seminar topics include WSJT, EchoLink and VoIP, PSK31 and APRS.

Two-Day Conference, Saturday Banquet and Sunday Seminar

Friday: Technical and introductory sessions will be presented Friday and Saturday. The DCC will also host the Seventh Annual APRS National Symposium with expanded coverage both days. There will be a Friday evening social get together.

Saturday: Technical and introductory sessions continue throughout the day. There will be an evening banquet with guest speaker Alex Mendelsohn, AI2Q, followed by a small awards presentation and prize drawing.

Sunday: Each year, the Sunday Seminar features cutting-edge technology in a dedicated four-hour session. This year we are pleased to have again Matt Ettus, N2MJI speaking on the topic of Software Defined Radio. Matt is involved with the GNU Radio project, Hamlib, and others. Matt will give a live demonstration of software defined radio, explain what it is, and how you can design and develop your own projects.

Conference presentations, meetings, and seminars will be held at the Marriott Hartford Windsor Airport Hotel (28 Day Hill Rd, Windsor, CT 06095; tel 860-688-7500, fax 860-688-7509. Please book your room prior to arriving. A special DCC rate of $99/night single or double has been blocked for 50 rooms until September 1st. After that, room rates increase. Transportation to and from the hotel is via shuttle. Please contact the hotel to arrange specific transportation needs.

Register on-line or download the ARRL and DCC 2003 Flier with registration form (from the TAPR Web site **www.tapr.org/tapr/dcc/**) and mail or fax it to the TAPR office: Tucson Amateur Packet Radio, 8987-309 E Tanque Verde Rd #337, Tucson, AZ 85749-9399; tel (972) 671-TAPR (8277), fax (972) 671-8716; **tapr@tapr.org**. □□

Next Issue in QEX/Communications Quarterly

We have a neat piece from Frank Brickle, AB2KT, about experimentation with automatic signal classification in software radios. We have anticipated that the technique, along with adaptive beam forming and other slick new methods, will be a key part of artificial intelligence built into rigs of the future. Be sure to check it out. In addition, Jim Scarlett, KD7O, returns with Part 3 of his series on a state-of-the-art software radio. □□

Out of the Box: Product Review

MICROWAVE PLL CIRCUITS

Hittite (12 Elizabeth Dr, Chelmsford, MA 01824; tel 978-250-3343; **www.hittite.com**) has a line of monolithic VCOs that require no external tuning elements to produce PLL synthesizers for C and Ku bands. The Ku-band ICs contain on-board prescalers. There is also a line of prescaler ICs that are useful for frequency-counter applications and PLL applications. The prescaler ICs come in ÷2, ÷4, ÷8 and count from dc to Ku band. There is also a counter (HMC 394) that can be programmed for ÷2 through 32 with a maximum frequency of 2 GHz. This would allow a ÷10 prescaler up to 5 GHz and a ÷100 prescaler for up to 13 GHz. The prescalers and VCOs are available through Future Electronics (**www.future-active.com**). Prices, in general, are below $10 per piece, but Future has a minimum quantity on most items of 100 pieces. —*Contributing Editor, Ray Mack, WD5IFS;* **rmack@arrl.org** □□

Letters to the Editor

Patents and Relays (Mar/Apr 2003)

Hi Doug,

I recently got the Mar/Apr edition, and as usual, [it is] very interesting. I wish to make two points.

On patents and IPRL: Maybe I'm a bit cynical, but it seems to me that a patent is a license to give money to lawyers! The best use I've found for them is that they look good on your resume. However, these days my employer pays me about $2 k for every one—a far cry from 20 years back when I got $1 for the US rights—so it is worthwhile going through the hassle. How some of mine ever got through and became patents, I don't know, which shows how questionable the whole business can be.

On receivers: I notice that both Jim Scarlett, KD7O, and Sergio Cartoceti, IK4AUY, are using relays for low-level switching of their front ends. One problem with that is that after a little use, relays (unless hermetically sealed, and possibly even then) can give problems when handling very low-level signals from oxidation of the contacts. The classic rig for this trouble is the Yaesu FT-102—it's famous for it—but telephone maintenance technicians of 50 years ago knew all about it. The answer, which I've used with great success in my FT-102 for years, and which G3SBI *et al* used in their CDG2000 design in *RadCom*, is to "bleed" some dc through the contacts. 0.5 to 1 mA from 12 V is quite enough to break down the oxide film.—*Peter Chadwick, G3RZP,* **peter.chadwick@ieee.org**

Energy Conversion in Capacitors (Jul/Aug 2003)

Doug,

I read your really interesting article in *QEX* just yesterday. Thanks. I had never thought about the problem you addressed at the beginning of your article. Last night, I got the idea that it would be interesting to analyze the case where the two parallel capacitors are connected through an actual resistance, rather than simply by the wire you used. Would there still be missing energy?

As you did, assume C_1 is initially charged with a charge Q_1, and assume C_2 is initially uncharged. Then, at time $t = 0$, close a switch connecting the capacitors through R. Let $q(t)$ be the *total* charge transferred from C_1 to C_2 after a time t. Then, the voltages, V_1 and V_2 on C_1 and C_2, respectively, at this time are:

$$V_1 = \frac{Q_1 - q}{C_1} \quad \text{and} \quad V_2 = \frac{q}{C_2} \qquad \text{(Eq 1)}$$

The current, i, from C_1 to C_2 is $i = (V_1 - V_2)/R$. Differentiating once with respect to t and using Eq 1, we obtain:

$$\frac{di}{dt} = \frac{1}{R}\left(\frac{dV_1}{dt} - \frac{dV_2}{dt}\right) = -\frac{i}{RC_S} \qquad \text{(Eq 2)}$$

where C_S is the equivalent capacitance of C_1 and C_2 in series; that is:

$$C_S = \frac{C_1 C_2}{C_1 + C_2}$$

The solution for i is:

$$i = \frac{Q_1}{RC_1} e^{\frac{-t}{RC_S}} \qquad \text{(Eq 3)}$$

We can now evaluate the total energy, W_R, dissipated in the resistance R connecting C_1 and C_2:

$$W_R = \int_0^\infty i^2 R dt = \frac{1}{2}\frac{C_S}{C_1^2} Q_1^2 \qquad \text{(Eq 4)}$$

It is remarkable and quite surprising to me that when I first did this calculation, that the dissipated energy is independent of the actual size of R! That is, no matter how small R is, the energy dissipated in it remains the same.

Is energy conserved in this system? Let's see. Initially ($t = 0$), all the energy in the system, W_0, is stored in C_1. Thus:

$$W_0 = \frac{Q_1^2}{2C_1} \qquad \text{(Eq 5)}$$

At the end ($t \to \infty$), the charge, Q_1, is distributed in the parallel combination of C_1 and C_2, so the energy stored in these two is:

$$\frac{Q_1^2}{2(C_1 + C_2)}$$

But we need also account for the energy dissipated in R. Using Eq 4, we thus obtain for the final total energy, E_1:

$$W_1 = \frac{Q_1^2}{2(C_1 + C_2)} + \frac{C_S Q_1^2}{2C_1^2} = \frac{Q_1^2}{2}\left[\frac{1}{C_1 + C_2} + \frac{C_2}{C_1(C_1 + C_2)}\right] = \frac{Q_1^2}{2C_1} \qquad \text{(Eq 6)}$$

Thus, we see that $W_1 = W_0$. In other words, energy is conserved in this system, and this remains true no matter how small R becomes. There is no need to invoke radiation or any other mechanism to explain where any missing energy has gone. There will be some radiation loss, but that will be accounted for by adding to R the radiation resistance of the system.

How does this result square with your result? You considered C_1 and C_2 connected together and showed that (when $C_1 = C_2$) the energy stored finally in the parallel combination of C_1 and C_2 was only one-half of the energy stored initially in C_1. My analysis shows that the energy lost is all in any residual resistance of the connection between the two capacitors. This is consistent with your statement that "Radiation and heat are the only forms known for the other half."

What if we connected the two capacitors together with perfectly conducting wires and ignored radiation losses? For example, we might make the circuit very small. The implication of these assumptions is that when we close the switch connecting C_1 and C_2,

an infinite pulse of current would instantaneously redistribute the charge between the two capacitors. This means that $di/dt = \infty$ at switch closing, which means in turn that the residual inductance of the wires connecting the two capacitors, no matter how small, would be important.

In other words, in this circuit, the energy would always begin oscillating between the capacitor and the residual inductance, and it would thus be conserved. No energy would disappear. In a real system, this oscillating energy would be ultimately dissipated, a phenomenon that would be accounted for by the appearance of a series resistance, whether it were a radiation or ohmic resistance.

I thought very interesting your discussion of efficiency, and how high efficiencies could be obtained using bridges and other means to minimize the difference in potential between two capacitors when transferring charge from one to the other. I had never really thought about this issue, but I am sure that you are right.

While reading this discussion, I did think of the elementary derivation of the energy stored in a capacitor that I learned in freshman physics. Consider a capacitor, C, with a charge q on its plates. The work, dW, needed to add an additional charge dq is the work needed to move dq through the potential V between the plates of the capacitor. In other words:

$$dW = Vdq = \frac{qdq}{C} \qquad \text{(Eq 7)}$$

Integrating leads to the standard formula for the energy stored in a capacitor.

Here, we clearly assume that the efficiency of the process that charges the capacitor is 100%. That is, we assume all the work we do ends up as stored energy in the capacitor. Is this consistent with the results of your paper?

To do this experiment in practice, we would need to connect a source of electromotive force with a variable output voltage to the capacitor. We would start the source at 0 V and very slowly (to eliminate radiation and other resistive losses) raise the output voltage. The voltage across the capacitor would rise in lock step with the voltage from the source, so the voltage difference between the two would always be near 0, the condition you showed is needed to get 100% efficiency.—*Bill Kaune, W7IEQ, 111 Piper Ct, Richland, WA 99352;* **w7ieq@arrl.net**

Dear Bill,

Thanks for your fine comments and for the derivations. You are right that energy conversion in charging a capacitor is independent of the resistance in the charging path and of the time taken to do the charging. At first, I deplored that result; but in the finish, I embraced it. Please note that my equations contain neither R nor t.

Many prominent readers wrote me about how placing an inductor in the charging path would eliminate the energy conversion I discussed. That seems to do what you describe by minimizing the potential difference between source and capacitor as the capacitor is charged. Yet without waveform control, that still does not do the job when the charging voltage is a step function. This is so because as the capacitor reaches its intended voltage, half the energy is in the capacitor and the other half is in the inductor. So, I have learned that a step function cannot achieve more than 50% efficiency.

I should emphasize that 50% efficiency applies only to charging a capacitor from zero to some positive potential energy using a step function. Controlling charging current as you suggest in fact does minimize losses; and as N. Sokal[1] and F. Heinrich[2] have shown, energy conversion may vanish. Thanks for your insight!—*Doug Smith, KF6DX;* **kf6dx@arrl.org**

Notes

[1]N. Sokal and R. Redl, "Control Algorithms and Circuit Designs for Optimal Flyback-Charging of an Energy-Storage Capacitor (eg, for Flash Lamp or Defibrilator)," *IEEE Transactions on Power Electronics*, Vol 12, No. 5, Sep 1997.

[2]F. Heinrich, "Entropy Change when Charging a Capacitor: A Demonstration Experiment," *American Journal of Physics*, Vol 54, pp 742-744, 1986. I. Fundaun, C. Reese and H. Soonpaa, "Charging a capacitor," *ibid*, Vol 60, pp 1047-1048 (1992).

Special Properties of 45° (λ/8) Networks (Jul/Aug 2003)

Dear Editor:

I read with considerable interest the article "Special Properties of 45° (λ/8) Networks" by Grant Bingeman, KM5KG. Some aspects of the subject could be explained in more detail.

The network design procedure used by the author is the procedure for designing a network having image impedances of R_{load} and R_{in} and a propagation constant of jB, using Bingeman's nomenclature. Such networks are electrically equivalent to a section of matched transmission line of electrical length b in series with an ideal transformer having an impedance ratio of R_L/R_g or the inverse, depending on whether the transmission line is matched to R_{in} or R_{load}.

The phase properties of this equivalent circuit are entirely dependent on the transmission line. So, to simplify analysis, the ideal transformer can be ignored and attention focused on the transmission line, which is matching R_{in} to R_{in} or R_{load} to R_{load}. Numerically simplified, the line matches an immitance of $1 + j0$ to $1 + j0$. For an eighth-wave network with a propagation constant of –135°, the elements, as reactances for a **T** network, are

$$X_3 = -j\sqrt{2} \qquad \text{(Eq 8)}$$

$$X_1 = j\left(1+\sqrt{2}\right) \qquad \text{(Eq 9)}$$

$$X_2 = j\left(1+\sqrt{2}\right) \qquad \text{(Eq 10)}$$

For a π network, the susceptances are identical to the reactances of the **T** network. The same equations apply to either network configuration.

For a **T** or π network used to match an antenna to a transmitter, Bingeman asks whether a specific propagation constant can simplify adjustment by eliminating or reducing the interaction between the end elements, X_1 and X_2 or the π equivalents. He answers yes, the propagation constant of the network should be an odd multiple of 45°, preferably negative to provide a low-pass network.

Looking at the effect of X_2, it is evident that if the load has a reactive component, that component can be canceled by adjusting X_2 so that the resulting X_2' is

$$X_2' = X_2 - X_L$$

where X_L is the reactance of the load. If X_1 and X_3 of the network are correct for the resistive component of the load, this adjustment has no effect on the load resistance, and after being made, the impedance seen at the generator end of the network is $R_g + j0$. No adjustment of X_1 is required. This is true regardless of the propagation constant of the connecting network. Notice, however, the restrictive conditions

Considering the effect of a change in the load resistance, the situation is more complex. However, consider a Smith chart. In the region very near the center of the chart, the lines of constant resistance and constant reactance are very near orthogonal. If the load resistance is changed slightly, the line is no longer matched and an SWR circle surrounds the origin. By proceeding an odd multiple of 45° towards the generator, the transformed impedance seen at the generator becomes 1

+ $j\Delta X$. Adding a reactance of $-j\Delta X$ to the network reactance X_1 brings the impedance to the original $1 + j0$. This adjustment has no effect on the transformation of the load and does not require any adjustment of X_2.

If the network impedance-transformation equation is solved for X_{in}, the result is:

$$X_{in} = Z_0 \frac{R_{load} - R_{in}}{R_L \tan B} \qquad \text{(Eq 11)}$$

The reactance at the generator end of the network caused by the change in load resistance for a network with a propagation factor of an odd multiple of $j45°$ is thus

$$\Delta X = X_{in} - Z_0 \frac{\Delta R_{load}}{R_{load}} \qquad \text{(Eq 12)}$$

provided that the change in R_L is small.

If the change in load resistance is not small, the lines on the Smith chart can no longer be considered orthogonal and the impedance seen at the generator can no longer be returned to $1 + j0$. Bingeman suggests a limiting case corresponding to an SWR at the load of 2.62 or load immitances of $2.62 + j0$ and $0.382 + j0$ relative to a nominal load of 1.0. With a load of 2.62, the immitance seen at the generator end is $0.6667 + j0.7454$. The SWR is still 2.62. If X_1 is reduced by $j0.7454$, the real component remains 0.6667 but the imaginary component is reduced to zero. The SWR is now 1.5. It is not possible to match the generator by adjustment of only X_1.

In fact, it is impossible to achieve an immittance seen at the generator of $1 + j0$ if X_3 remains fixed. The best that can be done is an immittance of $0.7639 + j0$, which requires adjustment of both X_1 and X_2, which both must be $j\sqrt{2}$. The two controls interact. The resulting SWR is 1.309. In a practical sense, achieving an SWR of 1.5 may be satisfactory.

In Tables 9 and 10 of the article, the π networks matching reactive loads are quarter-wavelength networks—not eighth wavelength. Do these networks share the desir-able properties of the eighth-wavelength networks? The answer is yes and no.

The ability to compensate for load reactance with X_2 without interaction with X_1 is present. As explained, this property is independent of the network propagation constant.

However, if these networks must also match a resistive load of 100 Ω to a generator impedance of $50 + j0$, there is a problem. The network transforms a 100-Ω resistive load to 100 Ω, and no adjustment of X_1 changes this to 50 Ω. However, by adding $j100$ Ω to the load by adjusting X_2, the 50-Ω generator can be matched. For resistive loads other than 100 Ω, this is not possible. The network simply inverts the load impedance, so that a 262-Ω load is transformed to 38.2 Ω. The SWR at the generator remains at 2.62, higher than is possible with an adjusted eighth-wavelength network. The fact that these π networks give a current phase shift of an odd multiple of 45° is a consequence of the 45° phase shift associated with the load and the 90° phase shift caused by the network. This result, associated with a specific load, is not significant in how the network responds to adjustments of the end elements.

Resistive loads can be matched, but this requires adjustment of both X_1 and X_2. If the central element is retained at $j100$ Ω, to match a load of 262 Ω X_1 and X_2 become $-j47.35$ and $-j82.49$. These are significant changes and the controls interact while the adjustment is in process. The propagation constant becomes –60.93°. *—Bert Weller, WD8KBW*

On a Double-Balanced Mixer with the FST3125M

After our Mar/Apr 2003 *QEX* article about a high-level accessory for the HF amateur bands, my father, I4FAF, has been quite busy developing a broadband HF amplifier. It is a high-gain 300 W PEP/CW, high-voltage (100 V) unit using low-cost power MOSFETs.

We faced some reliability problems. We already have and enjoy very much our tetrode linear amplifiers built around the rugged 4CX800A (I added new photos to my Web site). So we decided instead to dedicate our free time to evaluating the high-level H-MODE mixer with the FST3125M (Fairchild IC) having three-balun (trifilar-winding) transformers and a simpler version presented by I7SWX (April, 2003 *Radcom* on p 82), which has only two baluns.

We have produced with EAGLE CAD a small evaluation board. The original version has three binocular transformers (Amidon BN-43-2402, 4 trifilar turns, #29 AWG), a 74HC86 two-channel squarer, an H-MODE FST3125M IC and all other parts. We tested it: It works as specified by G3SBI (see CDG2000 Web site), but with these bonuses:

- A single 5 V supply (without any need—with good decoupling for noise—to split the supply for the squarer and with 7 V for the FST3125M),
- With 74HC86/74AC86 you do not need to put your LO at twice frequency to achieve the desired IF, that is, 9 MHz; but you get extremely high IP3 (over + 40 dBm) and conversion loss around 5.5 dB. We measured LO-IF isolation in our practical circuit at around 40 dB (with adjustment of a balance trimmer in the squarer circuit). We tested the LO range from 10.8 MHz to 39 MHz (that is, IF at 9 MHz) and measured isolation ranging from 42 dB to a worst-case figure of 34 dB at the IF port;
- Isolation at RF-IF port is much more adjustment-balance-trimmer sensitive and we have measured values ranging from 55 dB (at RF of 1.8 MHz) to 24 dB worst-case at a frequency of 30 MHz (best case was at 14 MHz with 60 dB);
- LO power level is only a 0-dBm sine wave at the squarer input.

We have successfully tested the LO frequency range from 10.8 to 39 MHz. The PC board is small, well behaved and shielded.

The best following circuits are a diplexer and a roofing filter like those already presented at the CDG2000 Web site, as found in *Radcom* magazine, about CDG2000 (June 2002 to December 2002) and in *Experimental Methods in RF Design* (Newington: ARRL) pp 6.49-6.53.

Today I discovered from a Google Web search on H-MODE mixers that JA9TTT, Mr Takahiro Kato has put on his Web site a very complete article with plenty of spectrum-analyzer (an ADVANTEST TR4171) photos of performance tests of both the H-MODE FST3125M versions. It includes the W7AAZ-G3SBI three-balun version and Giancarlo, I7SWX's version with only two baluns, both of which have fundamental frequency input at the local-oscillator side.

JA9TTT has done a very nice job with a lot of photos, well documenting the performances that we also have verified. We already have experienced an on-air test of it with a full receiver chain with very favorable first impressions: a very clean receiving experience. We placed the mixer unit after our *QEX* (Mar/Apr 2003) front-end unit. We added a 9-MHz, 2.4-kHz crystal filter and a W7AAZ IF-AGC with AD600 ICs and a product detector with audio amplifier.

I just wanted to inform you and your readers about JA9TTT's work and the well documented reports available on his Web site at **www.ksky.ne.jp/~t-kato/hamf/hamhome.html**. Click on the translator option for Japanese to English. It is not a perfect translation but it is useful. I will put the circuit-board templates on my Web site at **www.qsl.net/ik4auy/**.*—Sergio Cartoceti, IK4AUY;* **sergio.cartoceti@tin.it** □□

ARRL Resources for RF, DSP, and Design

Your Communications Journey Begins Here!

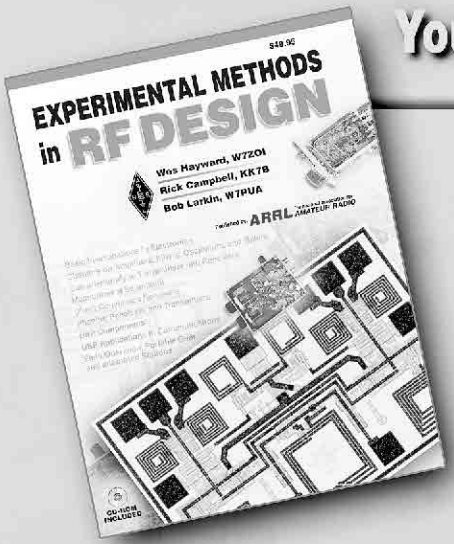

Experimental Methods in RF Design
ARRL Order No. 8799 ..... **$49.95***

Successor to the widely popular *Solid-State Design for the Radio Amateur.*

Immerse yourself in the communications experience by building equipment that contributes to understanding basic concepts and circuits. Explore wide dynamic range, low distortion radio equipment, the use of direct conversion and phasing methods, and digital signal processing. Use the models and discussion to design, build and measure equipment at both the circuit and the system level. Laced with new unpublished projects and illustrated with CW and SSB gear.
CD-ROM included with design software, listings for DSP firmware, and supplementary articles.

Contents:

Basic Investigations in Electronics
Chapters on Amplifiers, Filters, Oscillators, and Mixers
Superheterodyne Transmitters and Receivers
Measurement Equipment
Direct Conversion Receivers
Phasing Receivers and Transmitters
DSP Components
DSP Applications in Communications
Field Operation, Portable Gear and Integrated Stations

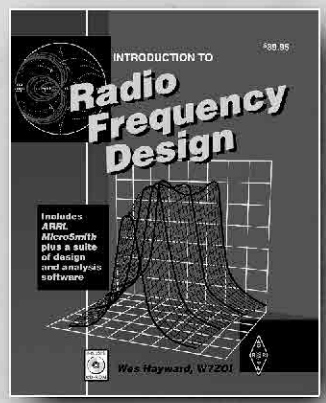

Introduction to Radio Frequency Design, includes software. ARRL Order No. 4920..... **$39.95***

The fundamental methods of radio frequency design using mathematics as needed to develop intuition for RF circuits and systems. Simple circuit models are used to prepare you to actually design HF, VHF and UHF equipment. Book includes a CD-ROM with ARRL MicroSmith Smith® Chart simulation software, and a suite of design and analysis software (for IBM PCs and compatibles).

First ARRL Edition, third printing, © 1994-2000.

Contents:

Low Frequency Transistor Models
Filter Basics
Coupled Resonator Filters
Transmission Lines
Two-Port Networks
Practical Amplifiers and Mixers
Oscillators and Frequency Synthesizers
The Receiver: an RF System

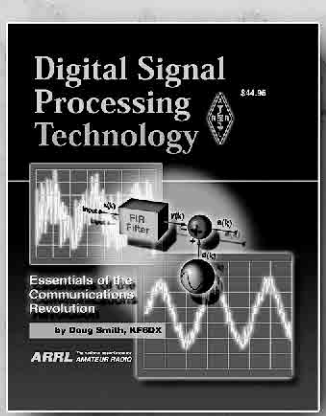

Digital Signal Processing Technology—Essentials of the Communications Revolution,
ARRL Order No. 8195 ..... **$44.95***

A comprehensive, readable work for anyone interested in Digital Signal Processing (DSP). The book begins with basic concepts, details digital sampling including fundamental and harmonic sampling, aliasing and mechanisms at play in real data converters, digital filter design, mathematics of modulation and demodulation, digital coding methods for speech and noise-reduction techniques, digital transceiver design, and other current topics. Sufficiently analytical for the advanced engineer or experimenter (with a working knowledge of algebra), while simultaneously affording an understandable picture of this exciting technology.

Contents:

Introduction to DSP
Digital Sampling
Computer Representations of Data
Digital Filtering
Analytic Signals and Modulation
Digital Coding Systems for Speech
Direct Digital Synthesis
Interference Reduction
Digital Transceiver Architectures
Hardware for Embedded DSP Systems
DSP System Software
Advanced Topics in DSP.....*and more*

***Shipping and Handling charges apply. Sales Tax is required for orders shipped to CA, CT, VA, and Canada.**

Prices and product availability are subject to change without notice.

ARRL *The national association for AMATEUR RADIO*

SHOP DIRECT *or call for a dealer near you.*
ONLINE WWW.ARRL.ORG/SHOP
ORDER TOLL-FREE 888/277-5289 (US)

QEX Subscription Order Card

ARRL
225 Main Street
Newington, CT 06111-1494 USA

For one year (6 bi-monthly issues) of **QEX**:

In the US
☐ ARRL Member $24.00
☐ Non-Member $36.00
In the US by First Class mail
☐ ARRL Member $37.00
☐ Non-Member $49.00
Elsewhere by Surface Mail
(4-8 week delivery)
☐ ARRL Member $31.00
☐ Non-Member $43.00
Canada by Airmail
☐ ARRL Member $40.00
☐ Non-Member $52.00
Elsewhere by Airmail
☐ ARRL Member $59.00
☐ Non-Member $71.00

QEX, the Forum for Communications Experimenters is available at the rates shown at left. Maximum term is 6 issues, and because of the uncertainty of postal rates, prices are subject to change without notice.

Subscribe toll-free with your credit card **1-888-277-5289**

❑ Renewal ❑ New Subscription

Name_____ Call _____

Address_____

City_____ State or Province _____ Postal Code _____

❑ Payment Enclosed to ARRL

Charge:

❑ MasterCard ❑ VISA ❑ AMERICAN EXPRESS ❑ DISCOVER

Account # _____ Good thru _____

Signature_____ Date_____

Remittance must be in US funds and checks must be drawn on a bank in the US.
Prices subject to change without notice.

06/01

ARRL Marketplace!

These publications have been added to the ARRL Library... so you can add them to yours!

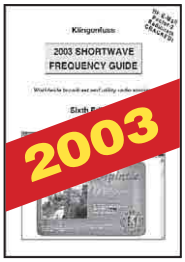

2003 Shortwave Frequency Guide

Schedules of clandestine, domestic, and international broadcast stations worldwide! Quickly find frequencies and a superb alphabetical list of stations. Includes another 10,078 entries for utility stations (Red Cross, United Nations and more).

ARRL Order No. 8663—**$39.95**

2003 Super Frequency List on CD-ROM

Includes all shortwave broadcast stations worldwide, plus all utility stations from 0 to 30 MHz. Nearly 40,000 entries! Find the latest schedules of clandestine, domestic and international broadcasting services compiled by top experts in this field.

ARRL Order No. 8841—**$24.95**

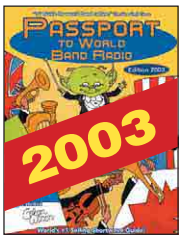

Passport to World Band Radio 2003 edition

Use this popular shortwave guide to zero in on news, sports and entertainment from the world over. Includes a channel-by-channel guide to World Band Schedules.

ARRL Order No. 8833—**$19.95**

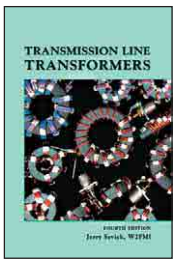

Transmission Line Transformers 4th Edition

Tremendous coverage of the subject of broadband transmission line transformers. Guanella and Ruthroff as well as hundreds of real transformers.

ARRL Order No. TLT4—**$39**

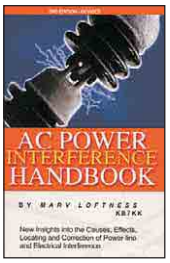

NEW!

AC Power Interference Handbook

New insights into the causes, effects, locating and correction of power-line and electrical interference. Easy to read, and practical for hams and EMI investigators. 2nd edition, revised.

ARRL Order No. 9055—**$29.95**

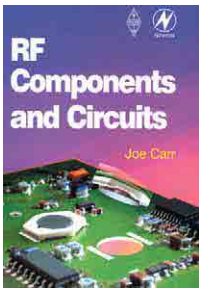

RF Components and Circuits

A comprehensive introduction to understanding, designing and building RF circuits, including fault-finding and use of test equipment.

ARRL Order No. 8759—**$37.99**

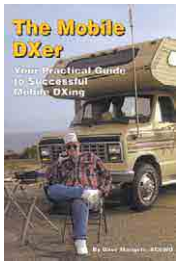

The Mobile DXer

A practical guide to successful mobile DXing. Learn how to select and install mobile gear and pick antennas. Understand propagation, mobile DX operating tips, and making the most of portable operating.

ARRL Order No. TMDX—**$12.95**

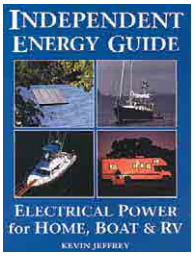

Independent Energy Guide —Electrical Power for Home, Boat & RV

Covers fixed, portable, and mobile energy systems; DC charging sources and AC power systems, solar, wind and water power, battery chargers, inverters, and more.

ARRL Order No. 8601—**$19.95**

Understanding, Building, and Using Baluns and Ununs

Theory and practical designs for the experimenter. Includes new balun and unun designs not included in the previous edition, and crystal clear explanations of how and why they work.

ARRL Order No. 8982—**$19.95**

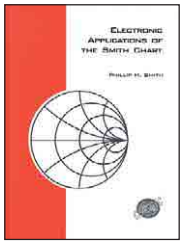

Electronic Applications of the Smith Chart

How the chart is used for designing lumped element (inductors and capacitors) and transmission line circuits (coaxial, waveguide, stripline or microstrip lines). Includes tutorial material on transmission line theory and behavior, circuit representation on the chart, matching networks, network transformations and broadband matching.

ARRL Order No. 7261—**$59**

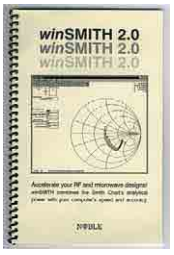

winSMITH 2.0

An easy-to-use, flexible computerized Smith Chart. Accelerate your RF and microwave designs! Unlock a greater understanding of transmission lines and simple matching problems. 3.5-inch installation diskette. Requires Microsoft *Windows*.

ARRL Order No. 7946—**$80**

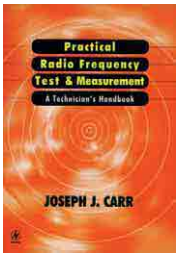

Practical Radio Frequency Test & Measurement

Learn the basics of performing tests and measurements used in radio-frequency systems installation, proof of performance, maintenance, and troubleshooting. Provides immediate applications, test set-ups, procedures, and interpretation of results.

ARRL Order No. 7954—**$39.99**

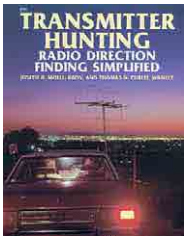

Transmitter Hunting —Radio Direction Finding Simplified

Covers equipment and techniques for HF and VHF radio direction finding. Locate jammers and other sources of malicious interference, engage in sport hunting, even help search-and-rescue groups!

ARRL Order No. 2701—**$24.95**

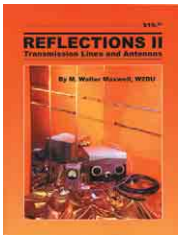

Reflections II —Transmission Lines and Antennas

by M. Walter Maxwell, W2DU. An in-depth treatment of transmission lines, standing waves, antenna matching, reflected power and antenna tuners. Second edition.

ARRL Order No. REF2—**$19.95**

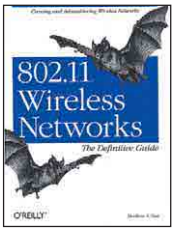

Wireless Networks: The Definitive Guide

Creating and administering wireless networks. Offers a full spectrum view of 802.11®, from the minute details of the specification, to deployment, monitoring, and troubleshooting.

ARRL Order No. 8884—**$44.95**

- **Build Your Own Test Equipment** #8604 ..... **$31.95**
- **Communications Receivers** #CR3E **$74.95**
- **DXpeditioning—Behind the Scenes** #DXBS **$28**
- **DX World Guide** #7199 ..... **$25**
- **The Electronics of Radio** #ERAD **$44.95**
- **Filter Design by Transmission Zeros (CD-ROM)** #8782 ... **$99**
- **HF Radio Systems & Circuits** #7253 ..... **$75.00**
- **Hiram Percy Maxim** #7016 ..... **$19.95**
- **International Microwave Handbook** #8739 ..... **$39.95**
- **Power Supply Cookbook** #8599 ..... **$39.99**
- **Q from A to Z (CD-ROM)** #8773 ..... **$79**
- **Radio-Electronic Transmision Fundamentals** #RETF **$75**
- **Radio Receiver Design** #RRCD **$89**
- **Radio Receiver Projects You Can Build** #8620 ..... **$24.95**
- **The NEW Shortwave Propagation Handbook** #7636 ..... **$19.95**
- **Wind Power for Home and Business** #8867 ..... **$35**
- **Yellowstone Farewell** #8944 ..... **$18**
- **33 Simple Weekend Projects** #7628 ..... **$15.95**

Order Toll-Free
1-888-277-5289
www.arrl.org/shop

Shipping: US orders add $5 for one item, plus $1 for each additional item ($10 max.). US orders shipped via UPS. International orders add $2.00 to US rate ($12.00 max.). Orders are shipped via surface mail. Other shipping options are available. Please call or write for information. **Sales Tax** is required for shipments to CT (including S/H), VA 4.5% (excluding S/H), CA (add applicable tax, excluding S/H) and Canada (excluding S/H).

ARRL *The national association for AMATEUR RADIO*

225 Main Street • Newington, CT 06111-1494 USA

tel: 860-594-0355 fax: 860-594-0303 e-mail: pubsales@arrl.org www.arrl.org/

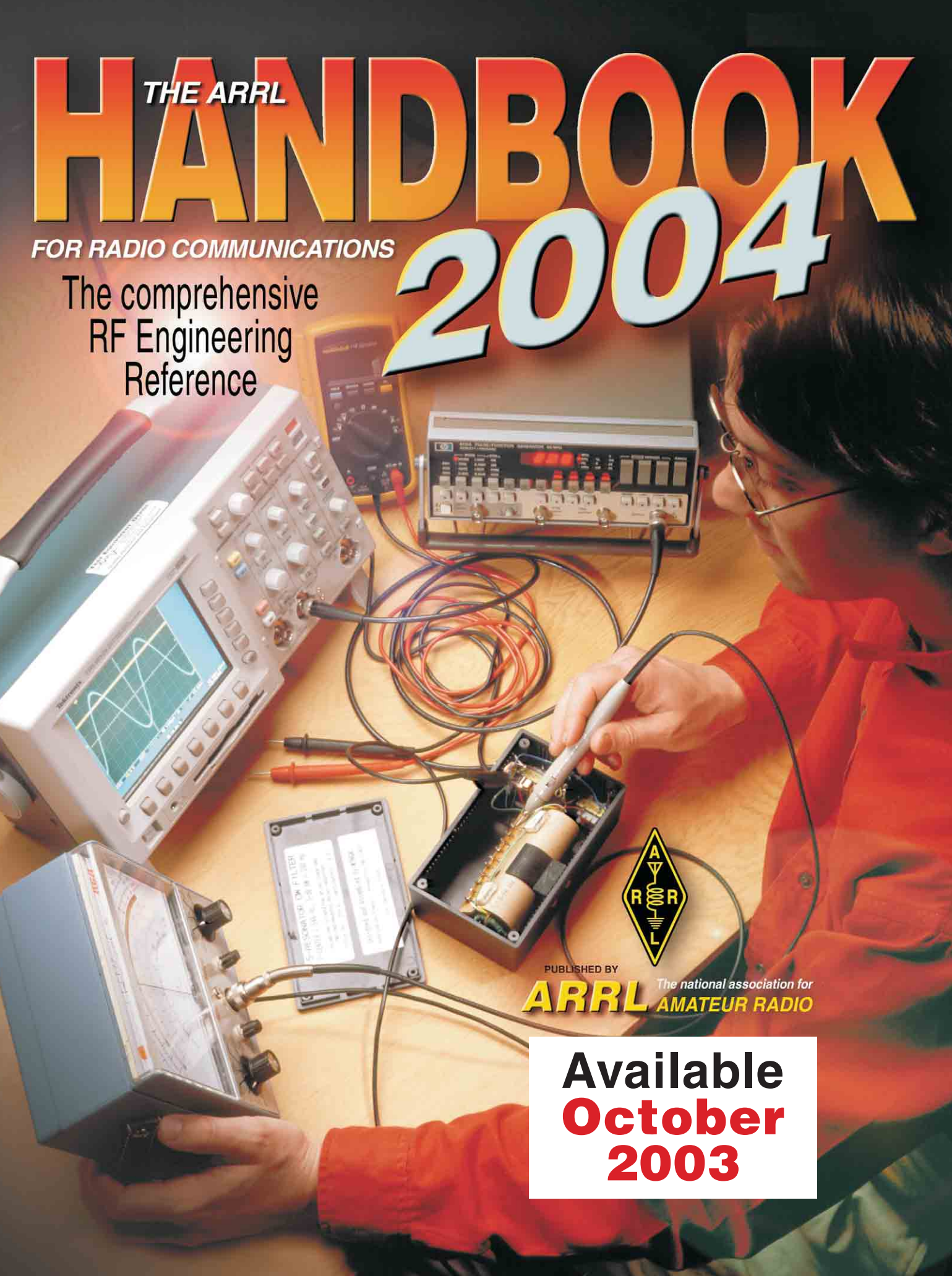
THE ARRL
HANDBOOK
2004
FOR RADIO COMMUNICATIONS
The comprehensive
RF Engineering
Reference
PUBLISHED BY
ARRL
The national association for
AMATEUR RADIO
Available
October
2003